AN ELECTRONIC SCANNING TECHNIQUE FOR CONTINUOUS TRACKING OF HUMAN EYEBALL MOVEMENTS

BY

KENNETH RICHARD PEAL

B.Eng., McMaster University, 1964

A THESIS SUBMITTED IN PARTIAL FULFILMENT OF

THE REQUIREMENTS FOR THE DEGREE OF

MASTER OF APPLIED SCIENCE

in the Department of

Electrical Engineering

We accept this thesis as conforming to the standards required from candidates for the degree of Master of Applied Science

Members of the Department
of Electrical Engineering

THE UNIVERSITY OF BRITISH COLUMBIA

November, 1967

Department of Electrical Engineering

The University of British Columbia
Vancouver 8, Canada

Date November 1967

ABSTRACT

The design of a system for studying human eyeball movements is presented. The system output provides eyeball location and pupil size in the form of step-wise voltages which are up-dated a minimum of 4000 times per second. Eye movements up to $\pm$ 45 degrees in two dimensions can be tracked. The frequency response of the system ensures continuous tracking of all eye movements including the fastest saccades.

The method employed is a photoelectric scan which uses feedback to lock onto the pupil and follow its movements. In the final system, this is performed by a scanning photomultiplier tube which electronically dissects an optical image of the eye.

To check the feasibility of the proposed system before the scanning photomultiplier is purchased, the work is performed in two parts: first the circuitry required to perform the scan is developed and tested without the use of a scanning photomultiplier tube; then an experiment is performed which simulates the scanning photomultiplier and enables the over-all system performance to be evaluated.

In the first part, a system is constructed which performs similarly to the final system except that the electronic dissection of the image is performed using an oscilloscope in conjunction with a simple photomultiplier instead of the scanning photomultiplier. This "flying-spot system" is used to test the circuitry required to perform the scan: the circuitry proves to be entirely satisfactory.

In the second part, the simulation enables the signal-to-noise ratio of the scanning photomultiplier to be predicted. On the basis of this, a recommendation is made to purchase the scanning photomultiplier and to construct the complete system.

TABLE OF CONTENTS

Page

LIST OF ILLUSTRATIONS

ACKNOWLEDGEMENT

Acknowledgement is gratefully given to the National Research Council of Canada for the financial support received under grant 67-3350 and for a bursary received in 1965-66 and a studentship in 1966-67.

I would like to thank my supervisor, Dr. J.S. MacDonald, for his continuous support and guidance, and for his many helpful suggestions freely given through the course of this research.

I would like to thank Professor F.K. Bowers for carefully reading the final draft and for making many valuable comments.

Acknowledgement is also given to my wife for her assistance in preparing the final draft and many of the drawings, to Mrs. R . Wein for the typing, and to my friends and colleagues for the proofreading.

CHAPTER 1

Introduction

1.1 Movements of the eye

The human eyeball is continuously in motion. There are many types of movement varying in amplitude from those measured in seconds of arc up to some that are greater than 50 degrees in extent. When a person is viewing a scene, these movements permit various points of interest to be selected for detailed viewing. This is performed by placing the image of each point of interest successively on the fovea or centre of sharpest vision on the retina (see figure A.1 appendix A). The person is said to have his gaze fixated on each point in turn. In examining any scene the eye performs a series of fixations interspersed with movements from one point of interest to the next.

In the literature, these and other eye movements are categorized as follows (from references 1, 2, 3, 4, 5).

Saccades are fairly large fast jumps which effect a voluntary change in fixation points. They may be larger than 50 degrees with velocities as high as 600 degrees/second for the large excursions. Typically, a 10 degree saccade may take 0.1 second.

Pursuit movements are those with which the eye follows a moving object in its field of view. They are involuntary and cannot occur without a moving object. Limiting speed is about 30 degrees/second.

Vergence movements are those in which the eyes move independently in order to permit binocular vision of a near object or a far object. Range is about 15 degrees and speed up to 10 degrees/second.

The eyes also turn with a rolling or torsional motion about the line of sight. This motion is slow and involuntary. These movements are quite small and are not considered in this work.

Nystagmus refers to oscillatory or unstable eye movements. Optokinetic and vestibular nystagmus are two types which can be induced in a subject by appropriate motion of the subject relative to his field of view. Spontaneous nystagmus on the other hand may be a sign of certain disorders.

Finally there are the three classes of miniature movements (less than 1 degree) which occur during attempted fixation. Tremor consists of very small fast movements which are caused by the balanced muscular system which controls the eye. Their frequency is in the range from 30 to 70 Hz. and the amplitude is measured in seconds of arc.

Drift movements are larger, very slow, apparently aimless movements. They are apparently due to instability in the oculomotor system and are measured in minutes of arc.

Flicks or small saccades are apparently correcting for the drift movements in order to keep the eye fixated on the desired target. They are normally from 2 to 10 minutes of arc and last approximately 0.02 second.

1.2 The need to measure eye movements

Measuring a subject's eye position tells what part of a scene he is looking at. From this, information can be deduced about what the subject actually sees. This is useful in psychological experiments such as studies of reading, studies of how information is taken from scenes and how people solve problems, and studies of man-machine interface situations.

Several medical applications exist. In examining a patient's field of view it is necessary to know automatically and accurately his point of fixation. Eyeball position information can also be used in simulating the conditions of certain eye diseases (tunnel vision for example). In addition, the movements of the eye are of interest medically since ocular disorders may be indicated by abnormalities in these movements. Finally, physiologists are interested in how the various movements are related to the mechanism of vision.

A related subject is that of measuring pupil size and reflexes. These are essential in dark-adaption studies and are also useful as indicators of disorders.

Bioengineers are interested in studying the control systems which control pupil size and eye position. In these applications, information is required about the normal eye movements, their velocities and accelerations. Also useful is information about how the eye behaves when an image is stabilized on the retina, and in order to achieve this, the direction of gaze must be accurately measured.

1.3 Survey of methods of measuring eye movements

Most of the commonly used methods fall into one of five general categories: photographic, corneal reflection, contact lens, electro-oculography, and photoelectric.

1.3.1 Photographic methods

Originally the eye itself was photographed then later a piece of bright material was placed on the eye and this alone was photographed. Another application used photography of the corneal reflection[6]. The most serious objections to these methods are: (a) a great deal of film is used to obtain relatively little information; (b) the film has to be developed and laboriously examined after the test so there is no possibility of working in real time.

1.3.2 Corneal-reflection method

This method results from the fact that a light shone near a human eye causes a highlight to appear on the cornea. This highlight is easily seen by an observer or an optical system. When the eye turns as the subject changes his direction of gaze, the corneal reflection moves. This movement is used to measure eye movements.

The corneal-reflection method is attractive since it measures movements in two dimensions, does not interfere seriously with vision,and is suitable for use with large numbers of subjects. Also, it is suited for use in real-time experiments[7] and can supply information directly for computer analysis[8]. However, it is limited in accuracy by the irregularities on the surface of the cornea, and in extent by the irregularities near the edge of the cornea. For good accuracy the centre 10 degrees should be used[6] but it can be used up to ± 12 degrees[1]. Another objection to this method is that head movements introduce relatively large errors into the measured eye movements[9].

1.3.3 Contact-lens methods

Various methods involving scleral or corneal contact lenses are accurate for very small eye movements (down to 10 seconds of arc). Usually a mirror or light is mounted on the lens and the light from this goes into an optical system. This method is fairly insensitive to head movements[9]. However in order to reduce slippage, the lens must be tight-fitting and hence be carefully custom-fitted. This means that it may be uncomfortable to wear and that a limited number of subjects can be used. Also, the attachment prevents binocular vision and will likely affect the movements it is designed to measure. Finally, it is suspected that for saccades greater than 5 degrees, slippage does occur[1].

1.3.4 Electro-oculography

It has been found that small electric-potential changes are associated with eye movements. By placing electrodes on the skin around the eye, it is possible to record two-dimensional eye movements of amplitude varying from 1 degree up to 90 degrees. This is known as electro-oculography. However, the potentials are very small and are in the presence of large muscle-action potentials. Also, their variation with the position of the eye is nonlinear. In addition, the necessity of placing electrodes on the subject is sometimes undesirable.

1.3.5 Photoelectric methods

A photoelectric technique has been developed[10] which causes a bright light to scan across the optic disk (part of the retina). On this area there are several blood vessels and these absorb more light than the surrounding surface. The different amount of reflected light is sensed by a photocell, and by synchronization with the scanning signal accurate measurements of small movements are obtained. Since the shape of the blood vessels is important, the subjects used must be screened for suitability to the method. It is useful for horizontal movements only, and in fact, vertical movements can cause errors.

Another photoelectric technique[11] focuses the spot from a cathode ray oscilloscope onto the limbus (boundary between iris and sclera), and by means of a feedback system moves the spot as the eye moves so that the spot stays on the limbus. Thus, the deflection signals generated by the system to move the spot are a measure of the eye position. This requires operation in a darkened room and is not easily adaptable for two-dimensional measurements. It is linear for movements of 0.1 to 10 degrees. It is limited to the range for which the limbus remains visible.

A variation of this technique has been described[12] in which the relative movement of the limbus and the corneal reflection is measured to determine eye movements. This relative movement should be zero for translational eye movements (i.e. head movements) but finite for rotational eye movements. In fact, this method reduces the effect of head movements by a factor of five from the original method but is still subject to the same limitations.

In another photoelectric technique[13], the differential reflectivity of the sclera and the iris is used by focusing the light reflected from the eye through a slit onto a phototube. As more or less of the sclera appears through the slit, more or less signal is obtained from the phototube. In this way, accurate eye movements are measured subject to the limit that the limbus must be visible. In this reference, the system was suspended from a stationary counter-weight, which restricts head movements.

A scheme has been developed[14] which mounts a light and photocells on "motorcyclist's goggles". The light is effectively infra-red so the subject's vision is not disturbed by it. It is shone centrally on one eye and the photocells measure differentially the amount of light reflected to obtain a measure of eye movement. A variation of this method[15] using two lights is linear over the range $\pm$ 15 degrees. However, this is limited to horizontal movements and permits essentially monocular vision.

Another variation[16] of this idea uses an axial filament lamp and optics to produce two sharply focused light bars on each eye. One bar is bisected by the temporal and one by the nasal limbus of each eye. The reflected light is sensed by solid-state photodetectors to yield a measure of horizontal eye movements. The sensitivity is 2 minutes of arc and the output is linear to ± 5% for horizontal movements of ± 20 degrees.

In a recent system under development[17], a type of television camera tube is used with a specialized scan which locks onto certain features of the eye to track its movements. The features used are the pupil-iris boundary and a special corneal reflection. This system is expected to be useful for movements up to ± 20 degrees with little interference from head movements. Because of the application for which the system was designed (military: visual control system[18]) the subject is required to look monocularly through a telescope. There are then two light sources shining on the eye.

The circuitry required to implement this scheme is fairly complex due to the complex scan and light system used. This in turn is required by the necessity of tracking the pupil as well as the corneal reflection. The purpose of tracking the corneal reflection is to reduce the effect of the head movements on the measurements (reference 18 appendix A).

1.4 Requirements for the present study

It can be seen from the above survey that each of the methods described has a particular range or type of movements for which it is best suited. Also, very few are useful and accurate for large eye movements. One of the requirements for the present system was that it measure very large eye movements (up to $\pm$ 45 degrees) and yet be capable of measuring some of the miniature movements as well.

Since the applications for the system were expected to be in clinical medicine as well as in research, it was desirable that it be designed for use with many different subjects and that it should present as little visual and physical hindrance to the subject as possible in order that the responses be measured under natural conditions. This includes the requirement that the system be capable of working in daylight.

One of the important applications of the system was to be the measurement of velocities and accelerations of the eyeball movements. In order to achieve this, the eye position output should be continuous, or if sampled, it was estimated that the rate should be in excess of 4 KHz.

It was required that the system output be in real time and consist of eyeball position in two dimensions. It was also recognized that a valuable asset would be a measure of the pupil size as another output.

1.5 Choice of the method

The method chosen was a photoelectric scan of the eye. The X and Y outputs of the system are voltage levels which are linearly proportional to the location of the centre of the pupil. The origin in the X-Y plane* is represented by zero volts and the extreme positions by some maximum positive and negative voltage. The basic component in the system is a memory element which samples the voltage representing the pupil position and holds this value as the output until a new sample is taken. The rate at which these samples are taken is variable from 4 KHz. to 8 KHz.

The basis for the operation of the system is that the pupil reflects less light than the iris. Thus a photoelectric scan can use this difference to locate and track the pupil-iris boundary. The especially attractive feature of the pupil is that it is visible to an observer (and hence usable by a tracking system) in all positions where the subject can see. Thus, a system which tracks the pupil over its whole range of movement can measure all useful eye positions. (This neglects the possibility of measuring eye movements during sleep. In this case all methods fail except electro-oculography.) In addition, it is possible to measure the size of the pupil with this method.

---

*Since the eyeball is essentially a sphere, the pupil does not move in a plane. The conversion to angular eye movements can be performed with simple trigonometry.

Since the system tracks the pupil, any visible light that is used would be seen by the subject. For this reason, the use of near infra-red illumination is proposed. In order not to interfere with dark adaption, the wavelength should be longer than 6500 Å. However, to be entirely invisible, it should be longer than 7600 Å. References 19 and 20 indicate that good pupil-iris contrast exists under infra-red illumination. Experiments in the present study (see section 5.6) confirm this conclusion.

1.6. Comparison with other methods

Other photoelectric methods which track the position of the limbus are practically limited to measuring horizontal movements only. This is so because under normal conditions, most of the top and bottom of the limbus is covered by the eyelid. It is possible to prop the lid open during tests but this was rejected on the grounds that it would be a serious hindrance to the subject. Also for very large horizontal movements this method fails because the limbus is covered by the eyelid.

Electro-oculography and the contact-lens methods were rejected mainly because they prevent natural response by the subject. Further, the contact-lens methods are useful only for small eye movements.

There are two serious drawbacks to the corneal-reflection method. First, it has a practical limitation to movements in the range of $\pm$ 12 degrees. Second, it is more seriously affected by head movements than the method of tracking the pupil[9].

1.7 Limitations of the method

Some of the problems are due to positioning and are common to all methods: for example the presence of the forehead, nose, and eyelashes and the fact that the exact details of these features vary from one subject to another. It is obvious that the eyelids and eyelashes can partially or totally block visibility of the pupil for short periods. Thus, a truly continuous system output is not possible. However, high-speed electronics and automatically attained output in the system minimize the total no-output period.

If a concentrated source of light is used to illuminate the eye, a corneal reflection will be created. Since the system responds to differences in light level (between iris and pupil), this represents a serious potential source of noise. This can be avoided by using a sufficiently diffuse source of light or by carefully positioning a non-diffuse light source (see section 5.4).

Finally, minor errors exist even if the centre of the pupil is accurately tracked. One reason is that the pupil is observed through two refractive media: the aqueous humour and the cornea. Another reason is that as the eye turns, the pick-up device receives a foreshortened image of the pupil. The effect of the foreshortening on the apparent centre of the pupil is nil while the effect of the refraction is quite small. Scale drawings of the situation show that the combined effect of the two factors is as follows: the pupil diameter appears larger than its actual size when viewed from a position normal to its surface (13% for a 7mm. pupil) but smaller when viewed from a position at larger angles to the surface (11% for a 7mm. pupil); the maximum error in centre position is 1.5% of its full range of movement. If it is desired to use the pupil diameter as an accurate system output, a correction curve should be computed and applied to the pupil-diameter information from the system. The error in the centre position is neglected in this work.

CHAPTER 2

The scan method and its realization

2.1 The scan system

As explained in section 1.5, the system operation is based on the fact that the pupil reflects less light than the iris. The photoelectric scan system uses a voltage sweep which effectively causes light to sweep across the eye. The differing amounts of reflected light caused by the different reflectivities of the pupil and the iris cause a change in the signal in the transducer. The sweep voltage at which this change occurs represents the location of the pupil-iris boundary. Since the pupil is a circle, four such locations can be used to compute its centre. This is the desired system output.

It is important that an efficient and simple scan system be chosen. Figure 2.1 shows a simple method to locate the centre of a circle. Using this method, the cardinal points

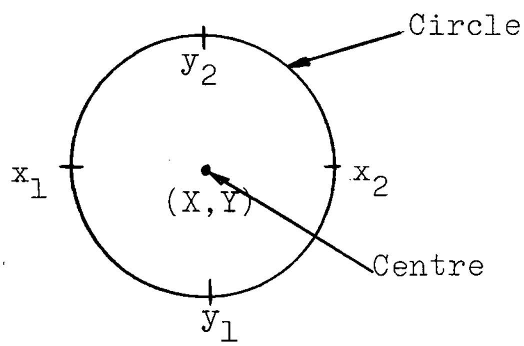

Centre location

$$X = \frac{x_1+x_2}{2}$$

$$Y = \frac{y_1+y_2}{2}$$

Figure 2.1
The centre of a circle

on the pupil-iris boundary are located. That is, x_1 and x_2 are located vertically at the pupil's vertical centre location Y, and y_1 and y_2 are located horizontally at the pupil's horizontal centre location X. In this case, it is a simple matter to compute the pupil diameter, viz. $D = x_2 - x_1 = y_2 - y_1$. The scan system used inthis work locates the four points shown in figure 2.1 and thus yields the pupil diameter as well as the pupil centre. It is described below.

The scan system consists of four short sweeps. One is located at each of the four cardinal points of the pupil as shown in figure 2.2. Each sweep starts at a voltage which is a small value (ε) below the previous value for the respective cardinal point. In the system ε is adjustable. It must be less than the pupil diameter and it has a maximum value of 0.5 cm. The sweep moves towards the previous location of the cardinal point. As soon as the boundary is located, the new voltage representing its location is stored and the sweep is stopped.

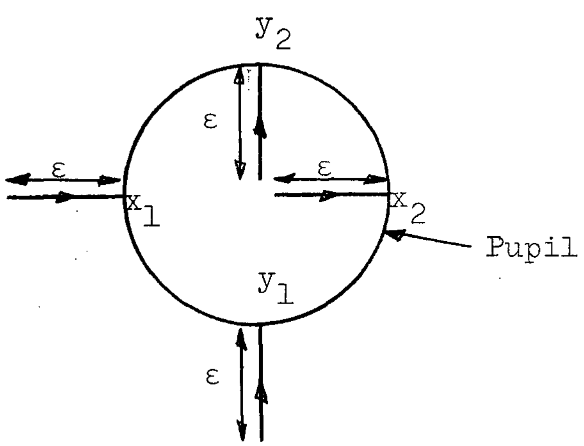

Figure 2.2
The four-sweep scan system

This is performed at each of the four points in turn. Then the four new values are used to compute the new value for the centre of the pupil and the pupil diameter. This new information is used to position the sweeps in the next cycle of the four-sweep scan. This whole procedure is repeated continuously to yield a constantly up-dated estimate of the pupil centre and the pupil diameter.

When the eye is in motion, the various boundaries are encountered earlier or later on each of the sweeps. The four sweeps are generated by one circuit which also generates an alarm if the maximum sweep voltage (2ε) is achieved without encountering a boundary. This signifies that the system has failed to locate one of the four cardinal points on the pupil. Occurrence of an alarm condition initiates a full-raster search which approximately locates the pupil so that the tracking scan can be re-initiated. The sweep length and speed are adjusted so that eye movements alone should not cause an alarm. However, this alarm-and-search provision is necessary to re-attain meaningful output after blinks and during system set-up and calibration.

2.2 Comparison with other scan systems

A normal television-type raster has a repetition rate near 60 Hz. In this application however, each full frame yields only one estimate of the eye position. Thus, it would be necessary to have a frame repetition rate of the order of 4 KHz. This is not possible with normal television pick-up tubes. More important however, this full-raster scan is very in-efficient since during most of the raster, no useful information is being obtained.

Another type of scan uses feedback to avoid scanning areas which contain no information. There are two general types of such scans. The first is a reduced-area rectangular scan which adjusts the positions of the horizontal and vertical scans to follow the image (figure 2.3). The second is a non-rectangular tracking scan which locks onto the image of the pupil and follows it (figure 2.4). One type of the latter is a small-spiral curve-tracing scan (figure 2.4(a)) and another is a variable-size circle scan which is placed on the pupil (figure 2.4(b)). This could possibly be a spiral scan which automatically adjusts to fit the pupil when contact is made.

While both types of non-rectangular scans are capable of yielding considerable information about the shape of the curve, they are much less efficient than the four-sweep scan (figure 2.2) in locating the centre of the pupil. Also, it is apparent that the rectangular tracking scan of figure 2.3 is less efficient than the four-sweep scan.

2.3 Realization

In considering the method of realizing the scanning process, flying-spot systems are impractical when studying eye movements in two dimensions. The reason for this is the presence of the corneal reflection. In a one-dimensional problem, it is

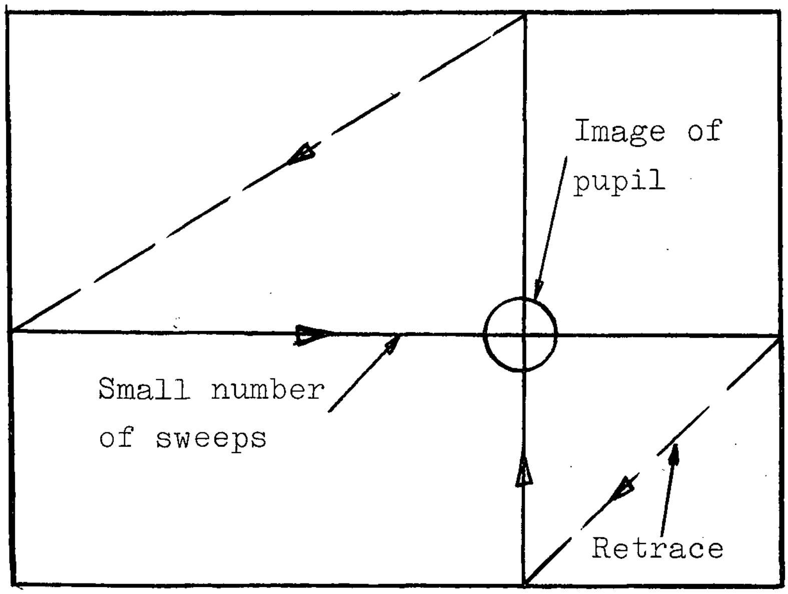

Figure 2.3
Rectangular tracking scan

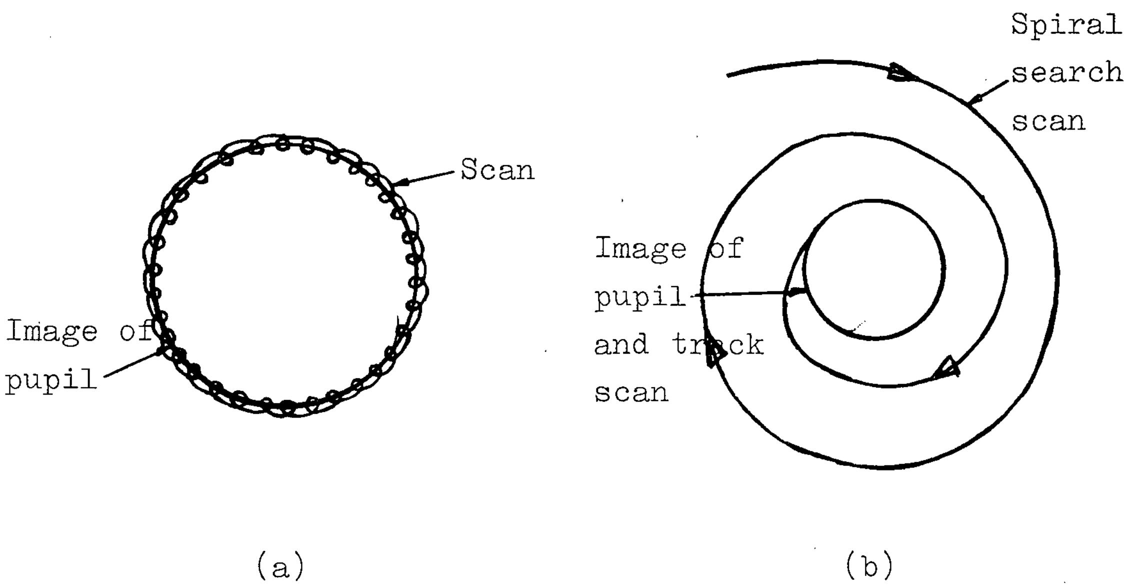

Figure 2.4
Non-rectangular tracking scan

possible to position the pick-up element so that the corneal reflection never encounters it. When two-dimensional eye movements are considered however, this is not possible. It was considered advisable to prevent this corneal reflection at the outset by using a static light source to illuminate the eye. Another advantage of this scheme is that the incident light level can be varied independently of the other system parameters to adjust the signal level and thus the signal-to-noise ratio. In flying-spot systems other parameters such as spot size and raster rate must also be adjusted when the light level is changed.

Normal television tubes are not suitable for use with the type of scans described. Vidicons have a relatively high dark current so single-line scanning will result in an extremely low signal-to-noise ratio. Also, characteristics such as lag and sensitivity will vary across the target depending on how frequently each particular section of the target has been scanned. But, the fundamental problem is that of speed of response. The lag in response to a light-to-dark or a dark-to-light change is about 0.2 second for 90% of the change. This is due partially to inherent photoconductor lag and partially to the inability of the electron beam to cancel small charges at the target.

A tube which is useful in this application is the image dissector. This is essentially a scanning photomultiplier tube. As in the standard photomultiplier, there is a photoemissive cathode usually maintained at some high negative potential. In an image dissector, instead of continuously gathering all the photoelectrons into the multiplier structure, electrons from one small portion of the cathode are gathered into the multiplier at any one time. The small portion which is thus examined can be varied electronically and thus the image on the photocathode is dissected. The means for performing this dissection is shown in figure 2.5. The subject is optically imaged onto the photocathode which then emits an electron image corresponding to the optical image. By means of a focus coil this image is focused onto the plane of the aperture. Thus, only those electrons which fall on the aperture enter the multiplier and create the video output. In addition to the focus coil, there are two deflection coils which deflect the electron image in order that the electrons from any point on the cathode may enter the aperture.

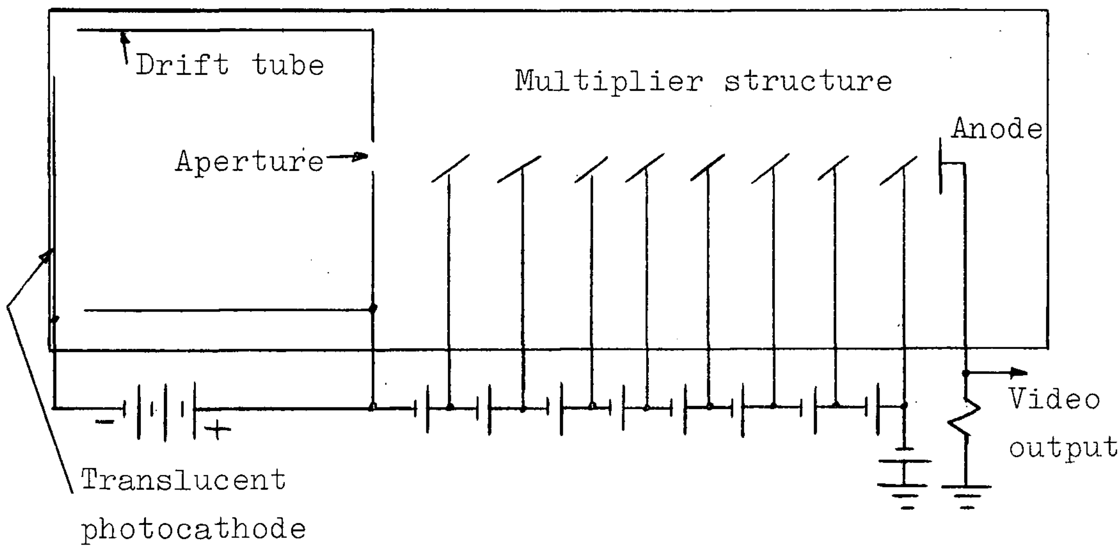

Figure 2.5
Image dissector

Since there is no charge storage, the image dissector is not suitable for low light-level operation, but if enough signal can be obtained, this tube has several advantages over normal television tubes. The most notable advantage is that literally any type of scan is permissible with no adjustment in the video level. It is thus possible to search the photosensitive area for the information required and then use a different type of scan to examine one part of the area in detail. This second scan can be a reduced-area scan, a single-line scan, or even a "stopped scan".

Because the photoemission process has a wide linear range, these tubes also have a wide range. With suitable multipliers, they can achieve operation over five orders of magnitude. Finally, they are available with S1 photocathodes which yield good response in the near infra-red.

It is thus apparent that an image dissector is ideally suited to the present application. While they are commercially available from at least two sources (ITT Industrial Laboratories, Fort Wayne, Indiana, and CBS Laboratories, Stamford, Connecticut), they are very expensive (approximately $3000). Before such a tube was purchased, it was decided to perform a careful feasibility study to predict the final performance of the system.

There are two parts to this feasibility study. One is the development and testing of the electronics to perform the scanning and computation. Because of the similarity between the image dissector and the standard photomultiplier, it was possible to do this development using a standard photomultiplier.

The procedure is described in section 2.4. The other part of the study is predicting the operation of the image dissector itself in this application. This process is described in sections 5.2 to 5.7.

2.4 The final system and the flying-spot system

Figure 2.6 shows the photoelectric interface as proposed for the final configuration. Here the eye is illuminated and focusedonto the photocathode of the image dissector. As described in section 2.3, this tube scans the electron image of the eye and the video signal is used to control the scan so that it tracks the pupil.

Figure 2.7 shows a configuration which performs essentially the same function as that in figure 2.6. The three signals involved may have different levels but they are otherwise identical. In figure 2.7, the spot from the oscilloscope is focused onto the "eye" and the light which is reflected from the "eye" is picked up by the photomultiplier. Thus,by scanning the oscilloscope spot, the "eye" is scanned so the light received at the photomultiplier is a dissected image of the eye. It is thus possible using this flying-spot system to test an electronic system which will be useful in the final configuration. This is the system which was constructed and which is described in chapter 3. There is one important limitation however. It is not possible to use a real eye in this configuration because of the corneal reflections caused by the spot. Instead, a flat model of the eye was used to give a

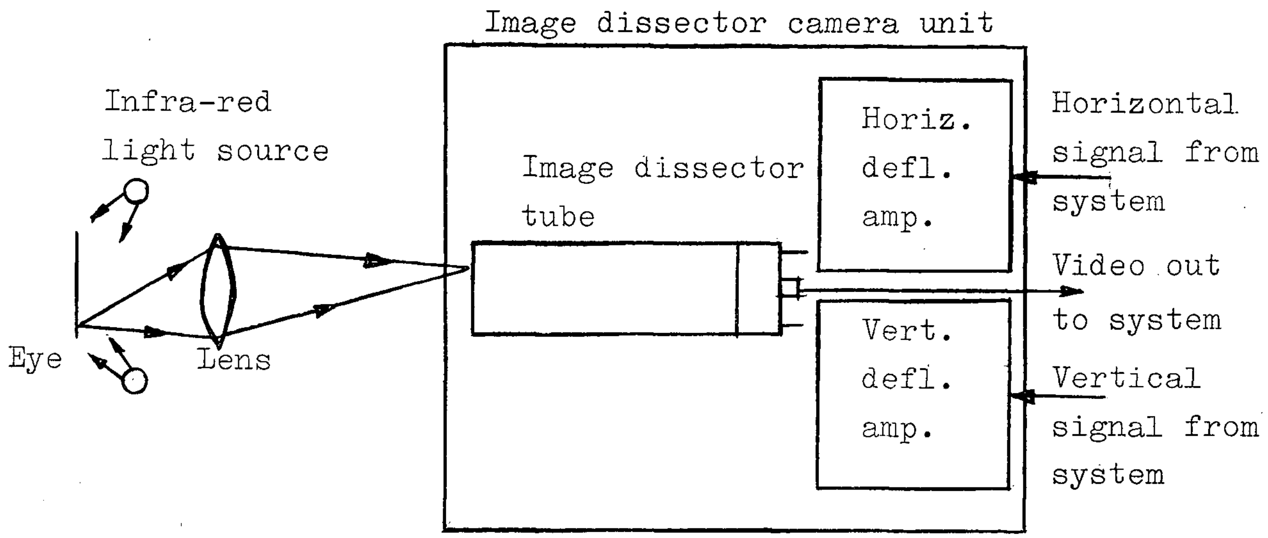

Figure 2.6
Final configuration

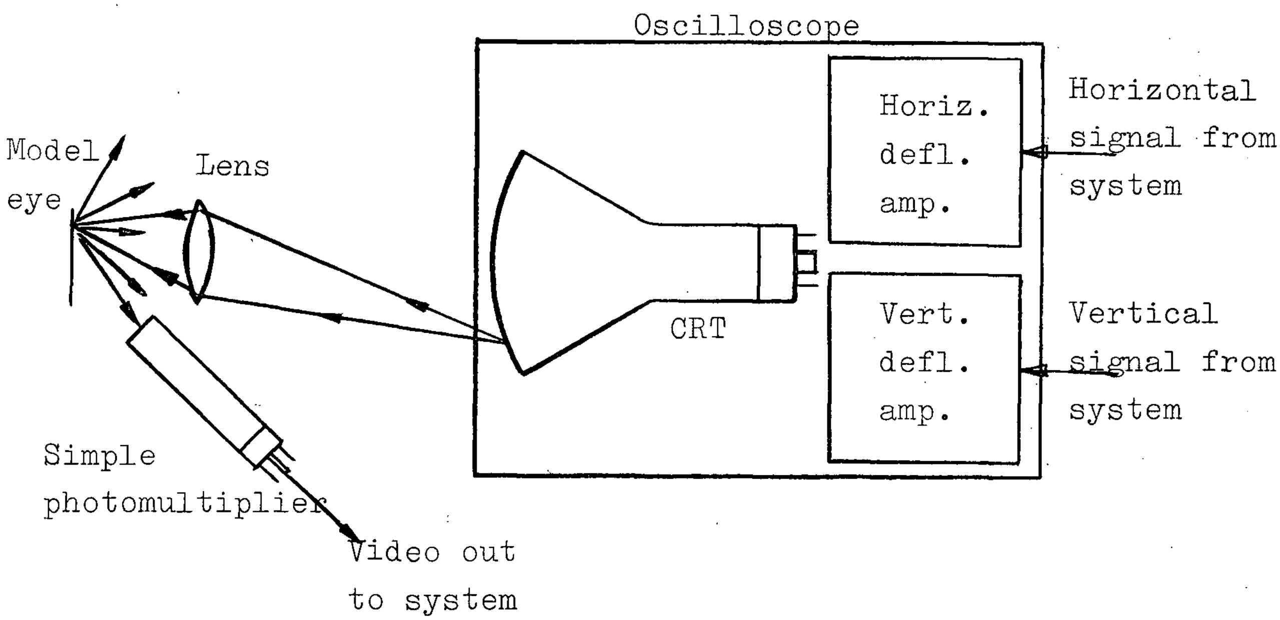

Figure 2.7
Flying-spot configuration

pupil-iris boundary without corneal reflections.

From figure 2.8, it is possible to calculate the projected area covered by the pupil for eye movements of ±45 degrees. Providing for a maximum pupil diameter of 1 cm.:

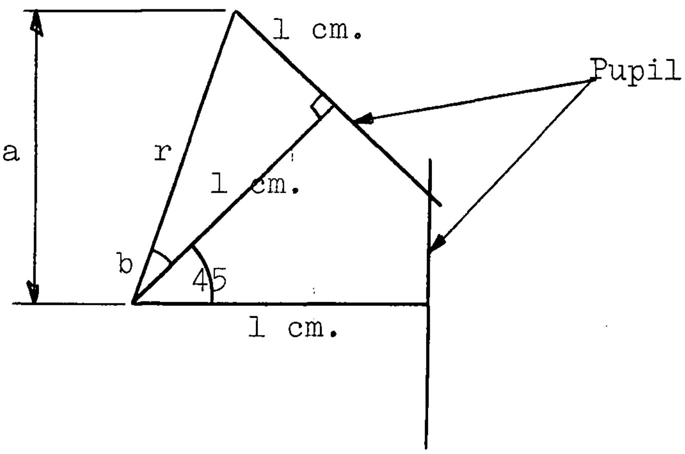

Figure 2.8
Projected area of the pupil

$$r = \sqrt{0.5^2 + 1^2} = 1.12 \text{ cm.}$$

and $$b = \text{arc tan } 0.5 = 26.5 \text{ degrees.}$$

Then $a = r \sin (b + 45) = 1.06$ cm. Thus, the area covered by the pupil is a square 2.12 cm. on the side.

During the track sweep, additional area must be allowed since the sweep can extend beyond the pupil a maximum distance of ε. This is permitted to be as large as one-half the maximum pupil diameter, i.e. $\varepsilon \leq 0.5$ cm. Then the total area at the eye which must be scanned is a square with sides of length $2.12 + 0.5 + 0.5 = 3.12$ cm.

On the oscilloscope face (in the flying-spot system) an active area of 8 cm. square is used to scan this required area.

Thus, the optical magnification from the eye to the oscilloscope face is 2.56. In the system, the maximum deflection signal is ± 5 volts. The oscilloscope amplifier sensitivity then is 1.25 volts/cm. Thus, the conversion factor from measurements at the eye (in cm.) to voltage changes in the system is 3.2 volts/cm. The oscilloscope used was a Tektronix type 561 with a short-persistence phosphor. The lens used was a 55 mm. f/2 Pentax (Super Takumar) and the photomultiplier was a Philips 150 AVP. The S11 cathode material was chosen to match the spectral distribution of the light from the oscilloscope phosphor (P16).

CHAPTER 3

Operation of the electronic system

3.1 General

The electronic section of the system is largely common to the image-dissector realization and the flying-spot system. The minor differences involved are discussed in section 4.3. The system was constructed for use in the flying-spot configuration on $4\frac{1}{2}$" plug-in circuit cards. The complete system required 14 such cards in addition to the video detection and blanking circuits mounted on the photomultiplier. Circuit diagrams for each card appear in the appendices. The Roman numerals in figures 3.1 and 3.2 signify the card number where the element is found. The circuit diagrams can be located in the appendices from table 3.1.

Card No.	Video	I	II	III	IV	V	VI	VII
Figure No.	E.2	E.3	E.4	E.5	E.6	E.7	B.1	D.1
Card No.	VIII	IX	X	XI	XII	XIII	XIV	
Figure No.	C.2	B.1	B.1	B.1	B.2	C.3	C.1	

Table 3.1

There are two modes of operation in the system: search and track. In the former, a television-type raster is generated which approximately locates the pupil. Then,in track mode, the four-sweep scan described in chapter two accurately tracks movements of the pupil. In both cases system operation is based upon locating the pupil-iris boundary. The mechanism for performing this can be explained with the help of figure 3.1. The video circuits on the photomultiplier are designed to detect only two video levels - light and dark. The light level corresponds to the oscilloscope spot being located on the sclera or iris. The dark level corresponds to the spot being on the pupil. When a deflection signal moves the spot from one region to the other, the video section generates a boundary signal. This causes the control logic to send a load signal to one section of the analog buffer. This is a sample and hold circuit which loads the voltage level of the deflection signal corresponding to the location of the pupil edge.

During the four-sweep scan (i.e. in track mode) this occurs regularly at each of the four cardinal points of the pupil. These four voltages are used in the output-computation and memory sections to generate voltages corresponding to the X and Y location of the pupil centre and to the pupil diameter.

As shown in figure 3.1 additional "scan information" is computed to be used in conjunction with the track sweep to produce the four-sweep scan which in turn generates continuously up-dated output information. In this mode the control logic generates: video blanking signals during spot repositioning; load signals at boundaries and after computation; and signals to control the track sweep generator. Not shown in figure 3.1 are three additional sets of switches. Two are in the output section to allow time-sharing of components and the other is in the scan-computation section to permit

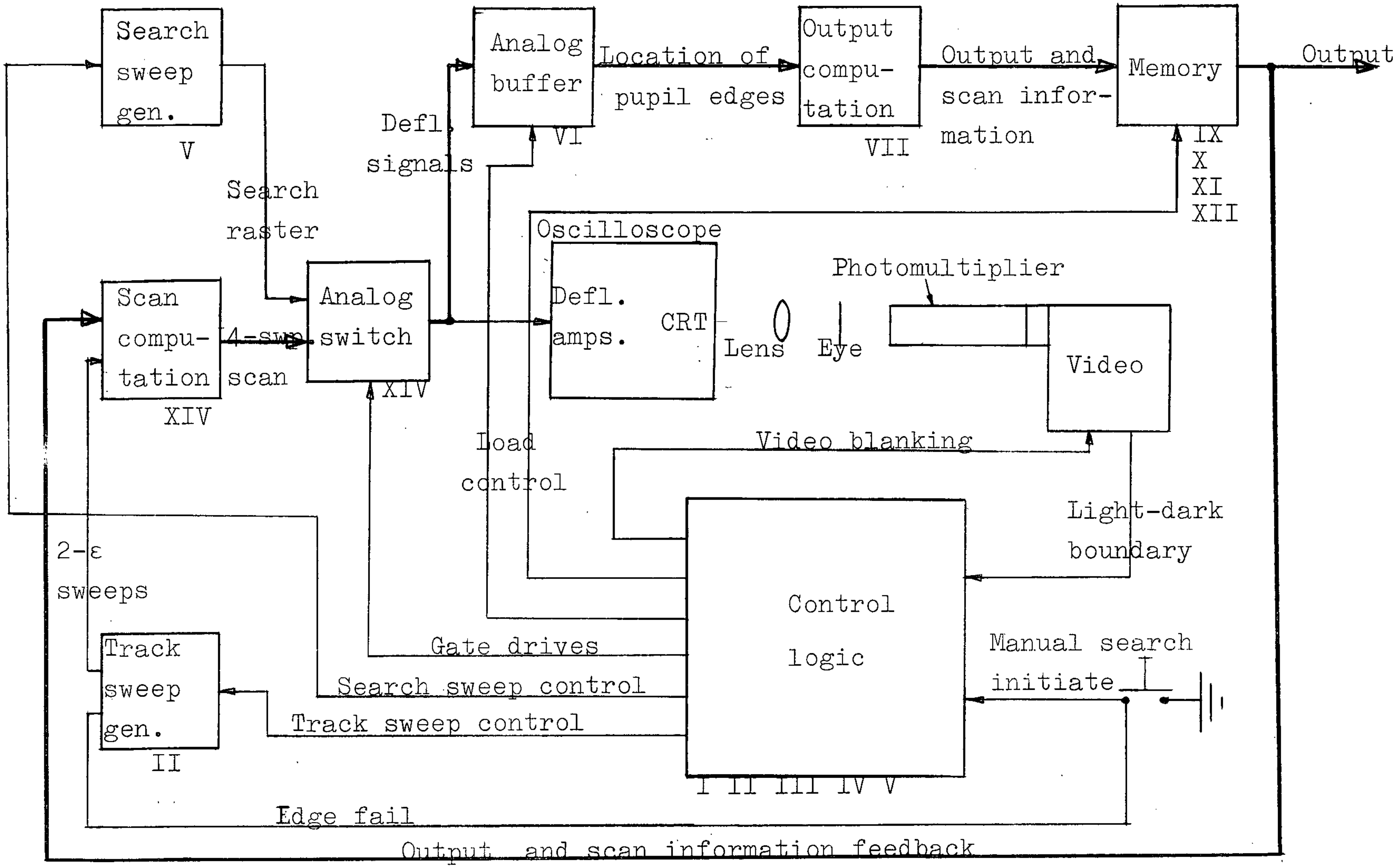

Figure 3.1 General block diagram

successive selection of the feedback information. The control logic also generates gate-drive signals for these switches. (These are the counter-controlled switches on figure 3.2).

If one of the pupil boundaries is not located, then the track sweep generator will achieve its maximum value (2ε) causing an edge-fail signal to be generated. This resets the logic and generates a search-initiate signal. The gate drives to the analog switch are also changed so that the search raster is applied to the oscilloscope deflection amplifiers. When this raster locates the pupil, the control logic switches again to the four-sweep scan.

Figure 3.2 is a more detailed diagram showing the functional details of each block in figure 3.1. The following description of the operation is based upon figure 3.2.

3.2 Initialization

If the manual search button is pressed, the system is initialized and the search procedure begins regardless of the previous state of the system.

The initialization consists of setting the two search mode flip flops, resetting the track mode flip flop, and presetting the sample and hold number 9 to zero volts (zeroing the pupil diameter signal for search). During this period, video blanking is performed to prevent false edge detection (not shown on figure 3.2; see figure E.4).

As a consequence of the initialization: (a) the two-bit counter is preset to 00 (by the "set/clear" input to the counter);

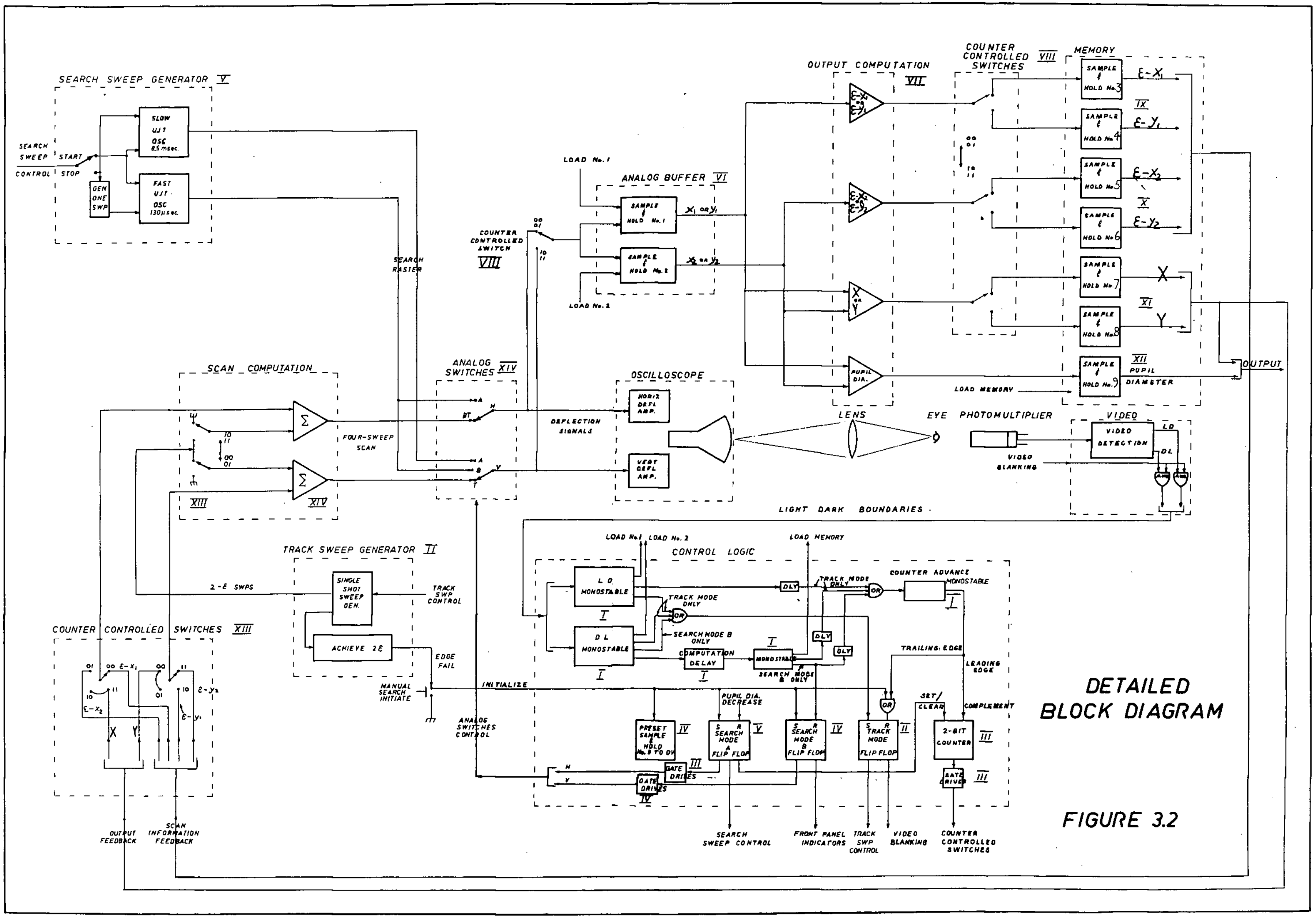

DETAILED BLOCK DIAGRAM

FIGURE 3.2

(b) the two unijunction sweep oscillators are turned on; (c) the analog switches are both set to position A. As a consequence of this, the oscillator outputs are fed via the analog switches to the horizontal deflection amplifier ("fast sweeps" - 130 μsec. per sweep) and the vertical deflection amplifier ("slow sweeps" - 8.5 msec. per sweep).

After a fixed period of time, video unblanking occurs and the search procedure becomes active.

3.3 Search mode A

In this mode, the video detection circuits are active. When a transition from the light to the dark level occurs, the video detection circuit triggers the LD monostable which generates a load signal for sample and hold number 1. When a transition from the dark to the light level occurs, it causes the generation of a load signal to sample and hold number 2. In all cases, the occurrence of this second load signal means that the pupil has been crossed so both edges (x_1 and x_2) have been located. After the computation delay (to allow for the slewing rate of the operational amplifiers in the computation section), a load-memory signal is generated for sample and hold numbers 3, 5, 7, and 9 (the mechanism for selection of sample and holds is described in appendix E). This means that a first estimate of the x-parameters is available. These are $\varepsilon - x_1$, $\varepsilon - x_2$, X, and pupil diameter. This process occurs during each horizontal sweep of the search raster that encounters the pupil.

Since counter complementing does not occur in this mode, the switches do not change and repeated estimates of the same information are obtained. However, as the search raster progresses past the centre of the pupil, the pupil-diameter signal which was formerly increasing starts to decrease. Circuits in the control section which monitor the pupil-diameter signal, detect this decrease and reset the search mode A flip flop (see figure E.7). This stops the two unijunction oscillators, thus terminating the television-type raster.

3.4 Search mode B

In addition to stopping the search mode A raster, resetting the mode A flip flop sets the counter to 11, the analog switch V to position B, and switch H to position BT. The latter two settings connect the fast sweep generator to the vertical deflection amplifier and one side of the scan computation section to the horizontal deflection amplifier. As a consequence of the new counter setting, the various counter-controlled switches assume appropriate settings. In the scan computation section this means that the DC level representing the estimate of X obtained in A (held in sample and hold number 7) is applied to the horizontal amplifier.

When the search sweep control moves to "stop", there is a delay (to allow for switching) followed by the triggering of one fast sweep. (Video blanking is performed during the delay.) The realization of these functions appear in figure E.7. This sweep is applied to the vertical deflection amplifier. Because it is located horizontally at the voltage X, the sweep will intersect the pupil near its cardinal points and thus load fairly accurate estimates of the y-parameters. Due to the settings of the counter-controlled switches, these will be loaded as follows: $\varepsilon - y_1$ into sample and hold number 4; $\varepsilon - y_2$ into number 6; Y into number 8; and a new more-accurate pupil-diameter signal into number 9.

Figure 3.2 shows that following the DL boundary in this mode, the "search mode B only" signal performs three functions (realization of these functions is described in appendix E and figure E.3). First, the track mode flip flop is set. This zeros the track sweep and blanks the video. Then the search mode B flip flop is reset. This sets analog switch V to position T and indicates "track" mode on the front panel. Finally, the counter-advance monostable is triggered. The results of this are discussed in the next section.

At this point, both search mode flip flops are reset and they stay in this condition as long as the system stays in track mode. Thus, the following functions are fixed throughout track mode: the two-bit counter is a simple complementing counter; the analog switches are in positions T and BT; the video blanking is controlled by the state of the track mode flip flop; both unijunction oscillators are off.

3.5 Track mode

In this mode, the system operates in a cyclic manner continuously repeating the fou -sweep scan. The procedure for this is as follows.

As stated above, the counter-advance monostable was triggered. The leading edge of the pulse it generates complements the counter. Since it was last in state 11 it now assumes state 00 and the counter-controlled switches change accordingly. This means that the oscilloscope spot is located vertically at the value of Y obtained in search mode B and horizontally at $x_1 - \varepsilon$ obtained in search mode A. Also, the switches in the output section are set to up-date the x-parameters.

Whenever the track mode flip flop is set, the video is blanked. This is necessary in this mode to avoid false signals caused by switching and zeroing of the track sweep generator both of which occur while this flip flop is set. At the end of the switching delay, the track mode flip flop is reset. This unblanks the video and triggers the track sweep. This is a single-shot sweep generator which sweeps from zero to a maximum of 2ε volts. Due to the scan computation, this sweep is added to the $\varepsilon - x_1$. Accounting for the inversion in the operational amplifier, this causes the oscilloscope spot to sweep from $x_1 - \varepsilon$ to a maximum of $x_1 + \varepsilon$.

During the course of this sweep, the spot crosses from the light (iris and sclera) to the dark (pupil). Thus the video detection circuits cause sample and hold number 1 to load (in this case an up-dated x_1). In track mode, additional functions are performed: (a) the track mode flip flop is set, thus blanking the video and zeroing the sweep and (b) the counter-advance monostable is triggered. Again this monostable complements the counter (which now becomes 01) causing the switches to follow. This means that the oscilloscope spot is located vertically at Y (as before) and horizontally at $x_2 - \varepsilon$. Once again, the trailing edge of the monostable resets the track mode flip flop which unblanks the video and triggers the track sweep. This causes the oscilloscope spot to sweep from $x_2 - \varepsilon$ to a maximum of $x_2 + \varepsilon$.

In this case, the video detects a change from dark to light, so sample and hold number 2 is loaded (with an up-dated x_2). As in the first case, the track mode flip flop is then set with the same results. In this case however, a computation delay is triggered instead of the counter-advance monstable. After the delay, newly-computed information is loaded into sample and hold numbers 3, 5, 7, and 9 (see figure E.3) and then the counter-advance monostable is triggered. This sets the counter to 10 so the oscilloscope spot is located horizontally at X and vertically at $y_1 - \varepsilon$. In this case, the switches are set to up-date the y-parameters. The two short sweeps are positioned and performed in an analogous manner to that for the x-case just described. When the counter has reached 00, the cycle begins again.

3.6 Automatic search initiate

Each time one edge of the pupil is detected, the track sweep is stopped as stated above by setting the track mode flip flop. Thus, the track sweep should never achieve its maximum value of 2ε volts. In fact if this does occur, the system generates an edge-fail signal which performs the same function as the search-initiate button on the front panel. This initializes the system and starts the search procedure again. Thus, an automatic search is initiated when track mode fails.

3.7 Performance of the flying-spot system

3.7.1 Static performance

The photographs in figure 3.3 show the features of the various modes of operation.

Figure 3.3(a) shows the pupil diameter signal and the horizontal and vertical deflection signals as the system changes from search to track mode. Initially the pupil-diameter signal is set to zero and the search raster is being performed. The first non-zero pupil-diameter signal shows where the pupil is first encountered. As the centre of the pupil is passed and the diameter signal decreases, search mode B is performed (single sweep on the lower trace). Then track mode is achieved. The jitter on the pupil-diameter signal during track mode could be due to two factors: (a) the photomultiplier was set at an angle to the simulated eye so the pupil appeared foreshortened; (b) a consistent inaccuracy exists in one or more of the sample and holds (see appendix B).

Figure 3.3(b) shows the actual search raster. Again, mode A, mode B, and track mode are visible. The overlapping of the two sweeps in track mode is caused by the large value of ε used (see figure 2.2). A smaller value is used in figures 3.3(c) and (d).

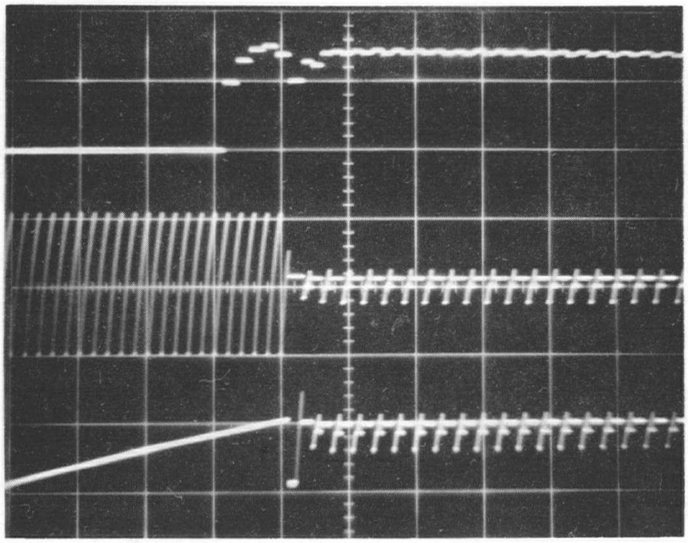

(a)

Horiz. sens.: 0.5 msec./div.

Vert. sens.: top trace 1 v./div.

lower traces 5 v./div.

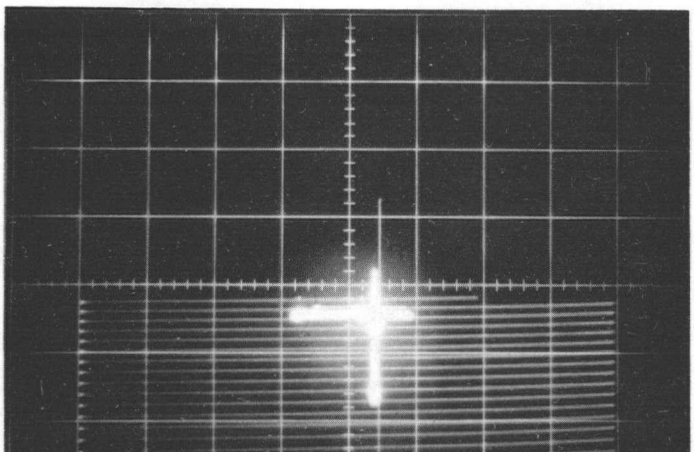

(b)

Horiz. and vert. sens.: 1.25 v./div.

Figure 3.3

Waveform photographs

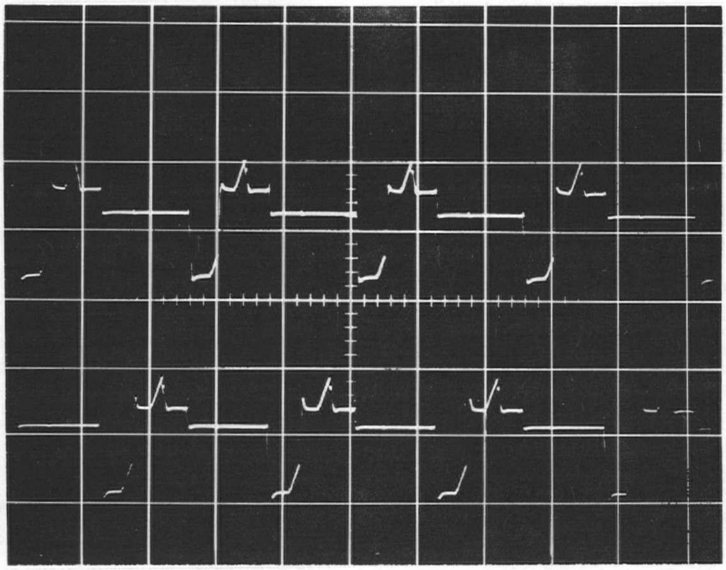

(c)

Horiz. sens.: 50 μsec./div.

Vert. sens.: 1 v./div.

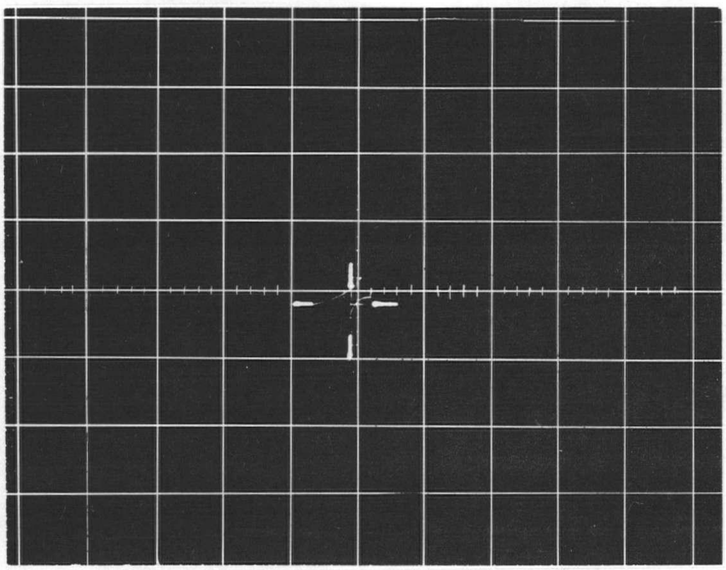

(d)

Horiz. and vert. sens.: 1.25 v./div.

Figure 3.3

Waveform photographs (continued)

Figure 3.3(c) shows the system continuously in track mode. The traces show the vertical and horizontal deflection signals when the four-sweep scan is continuously repeated. The period of each cycle of the scan indicates that the sample rate is 8 KHz. Figure 3.3(d) shows the actual scan this generates.

System operation was achieved for various values of the parameters at all speeds from 4 KHz. to 8 KHz. Measurements indicate that the resolution of the system is equivalent to eye movements of the order of 10 minutes of arc.

3.7.2 Dynamic performance

In order to test the dynamic operation of the system, consideration was given to designing a mechanical apparatus to move the model eye (figure 2.7). However, a much more flexible method was devised. The simple deflection amplifiers in the oscilloscope were replaced with differential amplifiers. A function generator output was then applied to the second input of each amplifier. This signal was subtracted by the amplifier from the system-generated deflection signal thus acting as a disturbance which caused the various pupil boundaries to be encountered earlier or later on each sweep. For the electronics of the system, this is identical to pupil movement. It was thus a very simple matter to adjust the function generator to simulate any pupil velocity.

To simulate the maximum pupil velocity of 600 degrees per second or 33.6 volts per second (see section 3.9), a triangular wave of peak-to-peak amplitude 6.8 volts should be set to 5 Hz. In these tests, two such generators were used (one for horizontal and one for vertical) so that the relative drift would ensure that all of the active area of the oscilloscope face was used.

The analysis in sections 3.8 and 3.9 indicates that the values of k_1 and k_2 are approximately unity at this maximum pupil velocity. It was thus anticipated that the system should track velocities far in excess of this maximum value. With the function generator set to 6.8 volts, the maximum frequency which the system would track was determined. For all sample rates this value was in excess of 70 Hz. Thus, the system is capable of tracking velocities far in excess of those which the eye can achieve.

Figure 3.4 illustrates the dynamic performance of the system. The disturbances are 80 Hz. triangular waves from two signal generators. The second and fourth traces show the step-wise output: the offset of the output from the input is deliberately caused in the oscilloscope amplifier. Figure 3.5 shows system recovery after an eye-blink. This was simulated for the photograph by blanking the CRT, thereby causing the system to initiate the search procedure. The square wave shown in the upper trace is differentiated and applied to the CRT grid to cause temporary blanking only. Thus, the photograph indicates that the system recovers in about 4 msec.

3.8 Time relations in track mode

In considering the operation of the system it is instructive to study the horizontal and vertical deflection

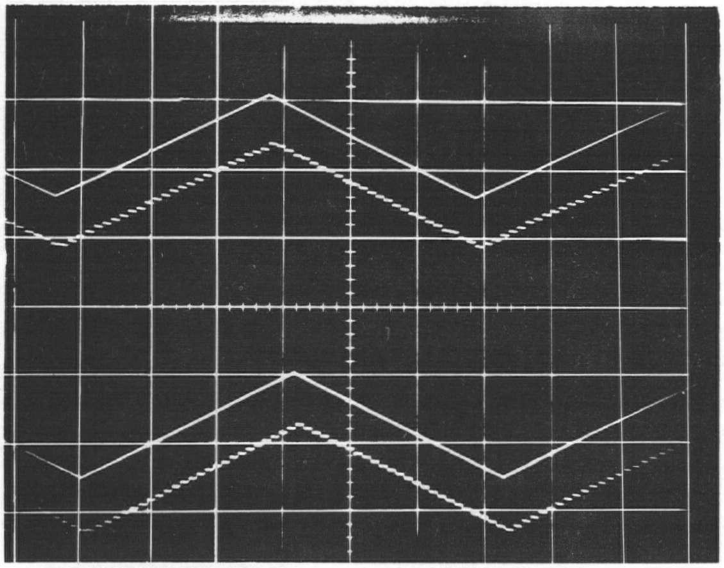

Y disturbance

Y output
(vert. sens.: 0.2 v./div.)

X disturbance

X output
(vert. sens.: 0.5 v./div.)

Horiz. sens.:
2 msec./div.

Figure 3.4
Dynamic performance

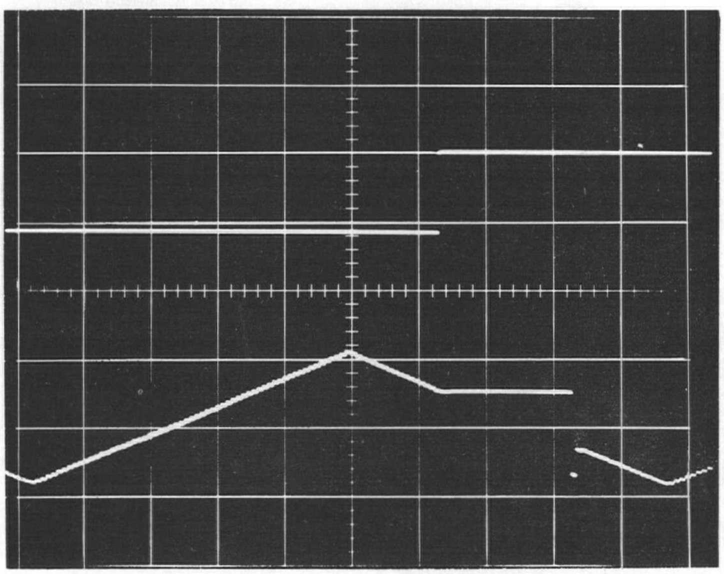

Vert. sens.:
5 v./div.

Vert. sens.:
0.5 v./div.

Horiz. sens.:
2 msec./div.

Figure 3.5
System recovery after eye-blink

signals. One cycle of the scan consists of four short sweeps, two of which appear on the horizontal deflection signal and two on the vertical deflection signal.

Between each of these sweeps there is a delay. As pointed out in section 3.5, the counter-advance monostable is triggered after every edge encounter. The pulse length is approximately 17 μsec. This delay allows for the slewing of the operational amplifiers in the scan-computation section before the scan is begun. In addition to this delay, it is necessary after the second of each pair of edges (i.e. after x_2 and y_2) to insert a computation delay to allow for the slewing rate of the operational amplifiers before the newly computed information is placed in memory. The delay is 16 μsec. and the load pulse is 2 μsec. so the total delay is 18 μsec. These delays are marked on the deflection signals shown in figure 3.6. The period of the counter-advance monostable is marked as CA. The period of the computation delay is marked as D. The values k_{11}, k_{12}, k_{21}, k_{22} are defined as the portion of the 2ε sweep that occurs at each position. Since the maximum value for the sweep is 2ε, they are constrained to be between 0 and 2.

To determine the time required for each of the four sweeps, it is necessary to consider the type of pupil movement that is occurring. As drawn in figure 3.6, no pupil movement is occurring since $X' = X$ and $Y' = Y$. This is because $x_1' = x_1$, $x_2' = x_2$, etc. (i.e. $k_{11} = k_{12} = k_{21} = k_{22} = 1$). However, if movement were occurring, $X' \neq X$ and $Y' \neq Y$. In this case, $X' =$

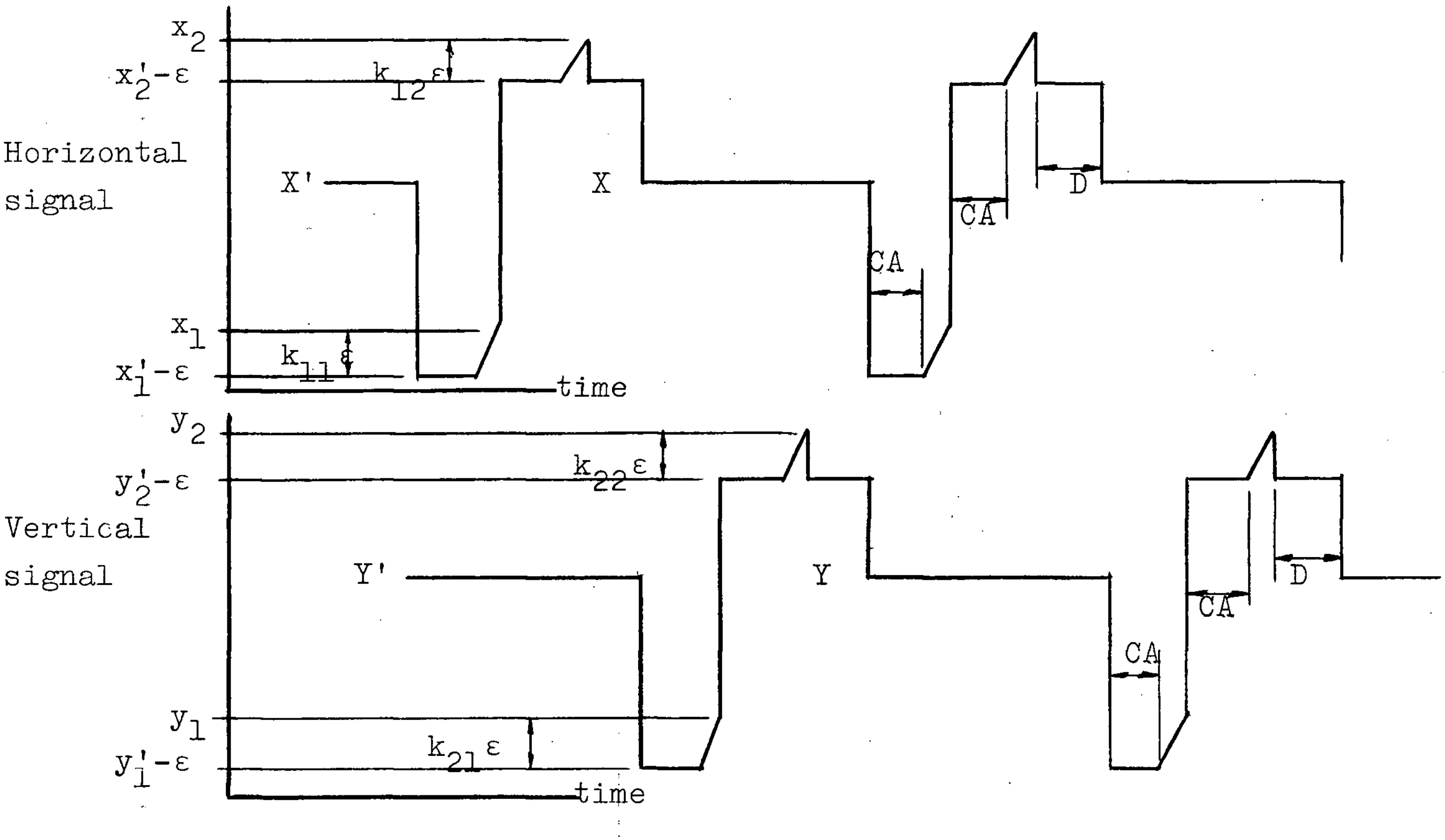

Figure 3.6
Deflection signals in track mode

$\frac{x_1' + x_2'}{2}$ and $X = \frac{x_1 + x_2}{2}$ etc. i.e. the primed variables are the previous values and the unprimed variables are the up-dated values. If the pupil moves at constant velocity, it is assumed that the sample rate is a constant (see appendix F). In this case, $k_{11} = k_{12} = k_1$ and $k_{21} = k_{22} = k_2$ since the pupil moves the same distance in the x direction during each period of the scan and the same distance in the y direction during each period of the scan. Since each of the four sweeps is performed by the same sweep generator, each will be at the same speed v_s. The time required for each horizontal sweep is $\frac{k_1 \varepsilon}{v_s}$ sec. and for each vertical sweep is $\frac{k_2 \varepsilon}{v_s}$ sec.

Thus, the period of the four-sweep scan for the condition of constant pupil velocity is

$$T = \frac{k_1 \varepsilon}{v_s} + CA + \frac{k_1 \varepsilon}{v_s} + D + CA + \frac{k_2 \varepsilon}{v_s} + CA + \frac{k_2 \varepsilon}{v_s} + D + CA$$

or

$$T = \frac{2\varepsilon}{v_s}(k_1 + k_2) + 2D + 4CA. \qquad \ldots .3.1$$

Since the output information is up-dated once each cycle of this scan and it is required that this information be up-dated at least S times per second (from section 1.5 this is 4 to 8 KHz.), the period T must be less than $\frac{1}{S}$. The condition of slowest sample rate (i.e. largest T) is $k_1 = k_2 = 2$ therefore

$$\frac{1}{S} \geq \frac{8\varepsilon}{v_s} + 2D + 4CA.$$

Inserting values for D and CA this becomes

$$\frac{8\varepsilon}{v_s} \leq (\frac{1}{S} - 104)\ \mu\text{sec.} \qquad \ldots.3.2$$

This is the requirement on the system parameters in order to satisfy the output sample rate requirement of S KHz.

Consider equation F.1 (appendix F):

$$v_s t_n = v(CA + t_{n-1} + DLY + t_n) + \varepsilon.$$

Also by definition $v_s t_n = k_r \varepsilon$ where $r = 1, 2$. In equation F.1, the term in parentheses is the sample period (which is in the range 125 to 250 μsec.) and v is the pupil velocity (maximum value is 33.6 volts/sec. - see section 3.9) thus equation F.1 becomes

$$v_s t_n \approx 33.6 \times 200 \times 10^{-6} + \varepsilon.$$

For the range of ε used in the system (~1 volt) this becomes

$$v_s t_n \approx \varepsilon,$$

which means that in all cases $k_1 \approx k_2 \approx 1$. Thus equation 3.1 indicates that the sample rate is approximately constant and in practice the sample rate can be set at zero pupil velocity.

3.9 Limitation set by pupil velocity

During one cycle of the scan, the pupil moves $(k_1 - 1)\varepsilon$ in the x direction and $(k_2 - 1)\varepsilon$ in the y direction. The pupil velocity in the x direction then is

$$v_{px} = \frac{(k_1 - 1)\varepsilon}{T} \qquad \ldots.3.3$$

and in the y direction it is

$$v_{py} = \frac{(k_2 - 1)\varepsilon}{T} \qquad \ldots.3.4$$

Studying these two equations it is apparent that the direction of pupil movement is indicated by the values of k_1 and k_2. If both k_1 and k_2 are greater than 1, both v_{px} and v_{py} are positive so this represents velocities in the first quadrant in figure 3.7. In the figure, $k_1 = 1$ represents the $v_{px} = 0$ axis and $k_2 = 1$ represents the $v_{py} = 0$ axis. Similarly, the other quadrants are as shown in the figure. However, the system cannot track velocities over the whole of the v_{px} vs. v_{py} plane. It is constrained to those velocities for which k_1 and k_2 are between 0 and 2. On this plane, a figure will be formed by plotting v_{px} vs. v_{py} for various combinations

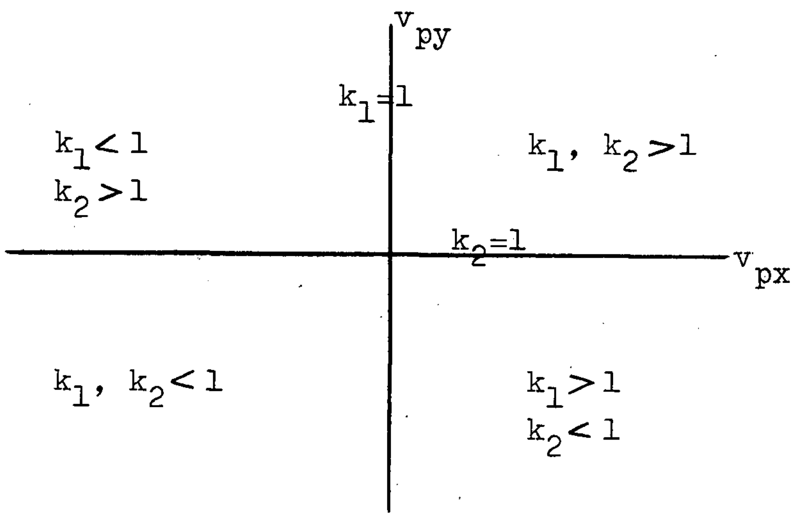

Figure 3.7
Direction of pupil movement indicated by k_1 and k_2

of k_1 and/or $k_2 = 0$ or 2. This figure represents the maximum velocities in the various directions that the system is capable of tracking. The purpose of this section is to find the smallest of these velocities and ensure that it is larger than any velocity the human eye can achieve.

From section 1.1, the maximum velocity for the eye is 600 degrees per second. For movements of the eye about the straight-ahead position, figure 3.8 gives

$$a = \sin \phi$$

thus

$$\frac{da}{dt} = \cos \phi \frac{d\phi}{dt}$$

$$= \frac{600}{180} \pi \cos \phi \text{ cm./sec.}$$

$$= 10.5 \cos \phi \text{ cm./sec.}$$

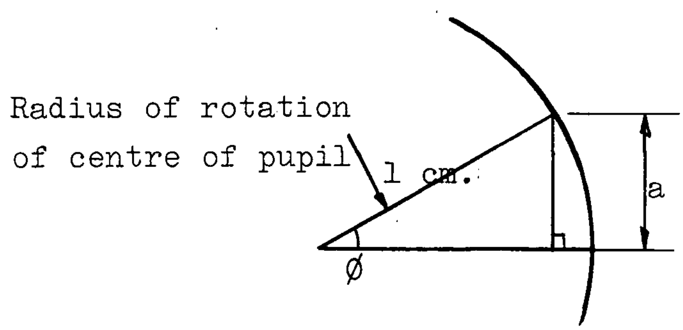

Figure 3.8
Determination of maximum linear pupil velocity

Thus, the maximum pupil velocity may be taken as 10.5 cm./sec. or, in the system this is equivalent to 10.5x3.2 = 33.6 volts/sec.

To find the velocity-limiting figure on the v_{px} vs. v_{py} plane, it is necessary to plot the velocities for the following combinations of k_1 and k_2:

(1) $k_1 = 0 \qquad 0 < k_2 < 2$

(2) $k_1 = 2 \qquad 0 < k_2 < 2$

(3) $k_2 = 0 \qquad 0 < k_1 < 2$

(4) $k_2 = 2 \qquad 0 < k_1 < 2.$

In each case, the velocity expressions (equations 3.3 and 3.4) are of the form

$$v_1 = \frac{b}{at + e}$$

$$v_2 = \frac{ct}{at + e}$$

where t is the k which is varying (parametric equations). Solving v_1 for t and substituting for t in v_2 yields

$$v_2 = \frac{cb - cev_1}{ab} = \frac{c}{a} - \frac{cev_1}{ab}$$

which is of the form $y = mx + b$. Thus, the four combinations of k_1 and k_2 listed above yield four straight lines with common end points. Thus, the figure is closed and has four straight sides. Figure 3.9 shows the $\frac{v_{px}}{\varepsilon}$ vs. $\frac{v_{py}}{\varepsilon}$ plane with two such figures plotted on it. From these figures, the smallest limits are 4650 for S = 4000 and 8250 for S = 8000 or the smallest velocity limits are 4650ε and 8250ε. In all cases, this must exceed the maximum pupil velocity of 33.6 volts/sec. This sets a limit on the parameter ε according to the minimum sample rate:

$S = 4000 \qquad \varepsilon \geqslant 7.25$ mv.

$S = 8000 \qquad \varepsilon \geqslant 4.16$ mv.

This condition is satisfied for all practical values of ε.

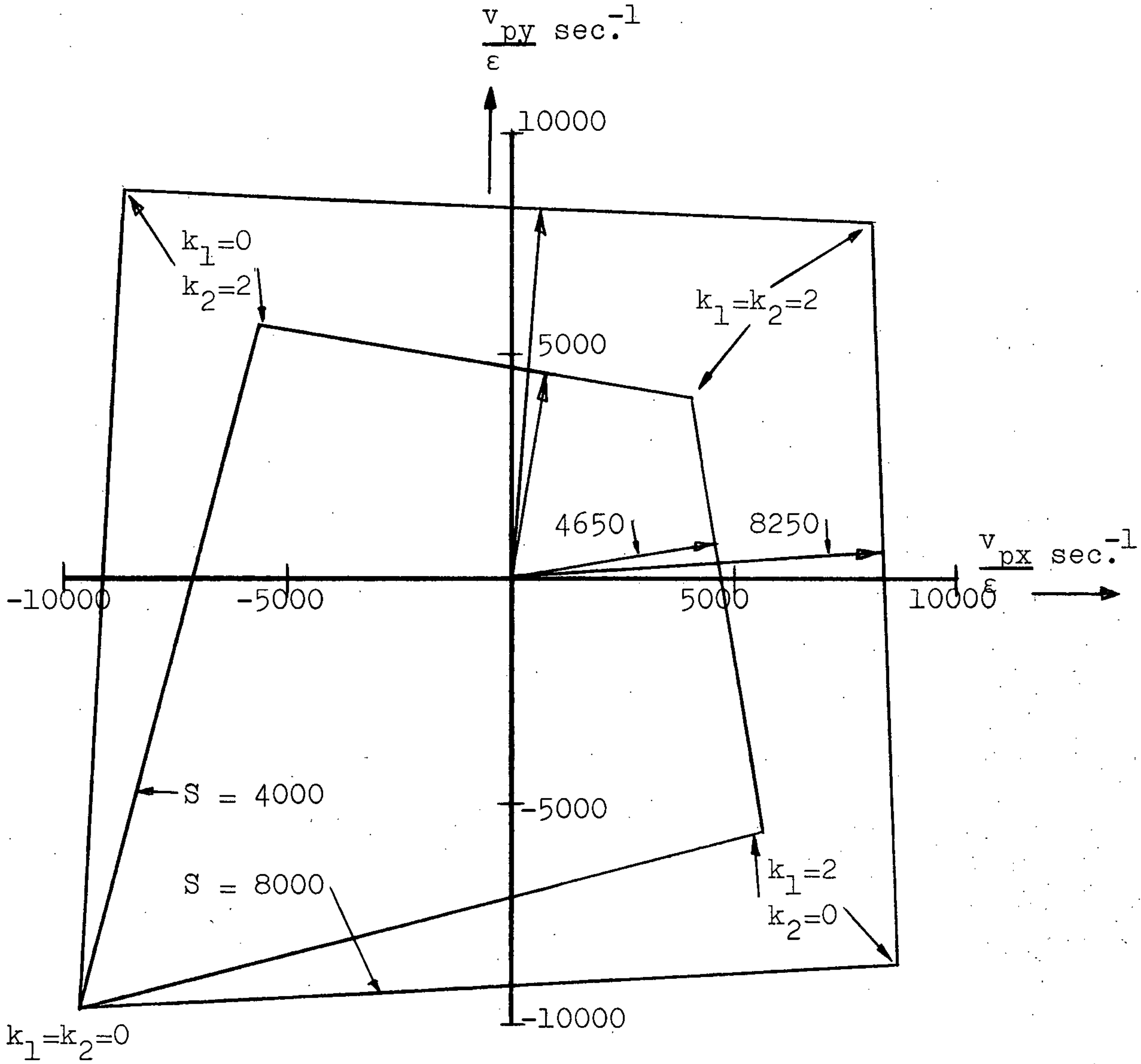

Figure 3.9

Limitation on system parameters set by maximum pupil velocity — velocity-limiting figures on the $\frac{v_{px}}{\varepsilon}$ vs. $\frac{v_{py}}{\varepsilon}$ plane for two values of output sample rate S

CHAPTER 4

Details of the final system

4.1 Physical layout of the system components

For applications where the eye movements themselves are being studied, it is convenient to measure them relative to the subject's head. If the measuring instrument is firmly fixed to the head, the movements of the head (if permitted) do not interfere with the measurements of the eye movements.

However, small movements of the head relative to the measuring instrument will still remain. These are mainly due to pulse, and their influence can be made as small as if the head were clamped to a fixed object. A practical means of achieving this is to use a head cap with a bite bar and a skull strap[21]. In this case, the pick-up elements of the system are mounted on a cap which the subject wears. An adjustable strap which is firmly fixed to the head cap, fits around the top of the subject's head. This prevents back-and-forth and some rotational movement of the instrument relative to the head. A dental impression is also mounted firmly on the cap so that the subject can bite firmly on it. This prevents up-and-down and further limits rotational motion of the cap.

It is important that the weight of the cap plus the equipment on it be kept to a minimum. Also, some provision for adjusting the centre of gravity of the device is necessary. In this case, the image dissector tube with focus and deflection coils, the optics, and the illumination means must be mounted on the cap.

The total weight of the tube, coils, and optics will be approximately 22 ounces (tube 6, coils 6, and optics 10 ounces). The material used to mount the lens system should be light in weight. Finally, the light-source weight will depend on the configuration used (this is discussed in chapter 5).

The optical system must produce an image of one eye on the photocathode of the image dissector. Figure 4.1 shows the means for performing this. The half-silvered mirror is necessary since the subject must be able to see. However, this permits

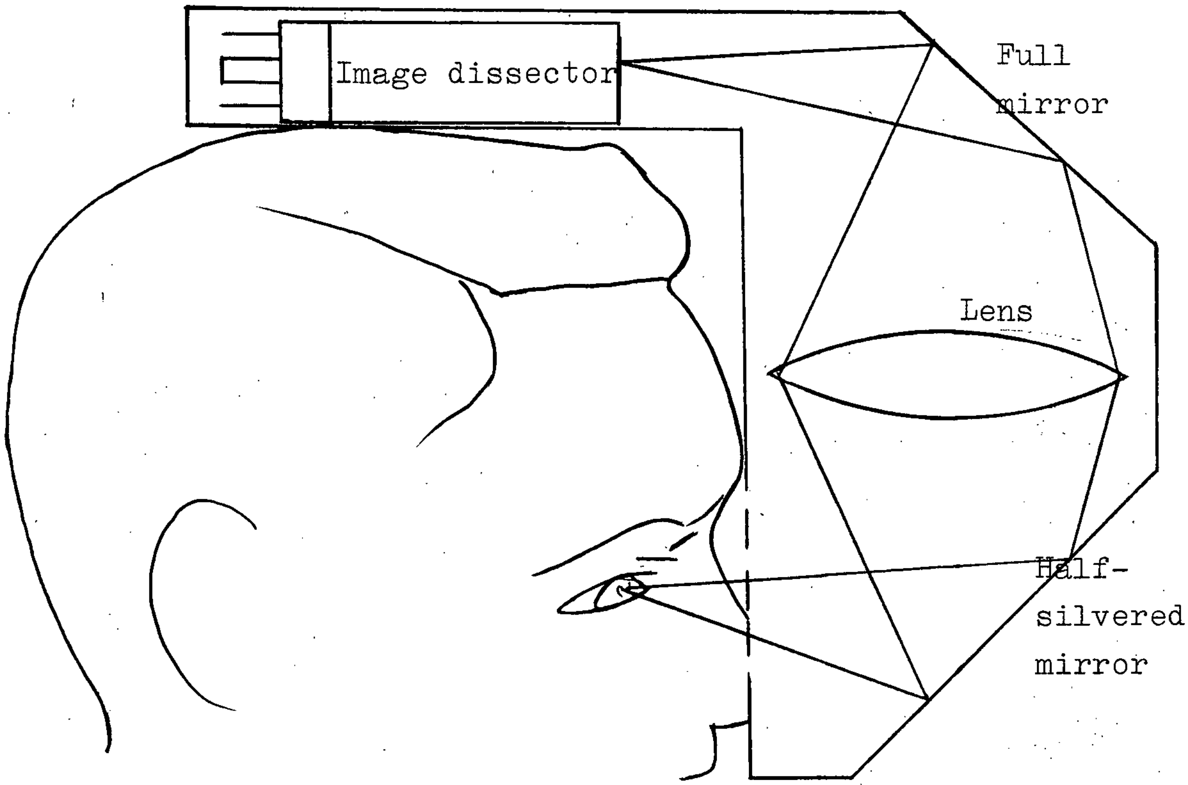

Figure 4.1
Optical system

considerable stray light to enter the optical system. This problem can be overcome most easily by using mechanical chopping of the illuminating light and synchronous detection of the video signal. In addition, since the image of the eye is formed with infra-red light, an infra-red filter may be used in front of the image dissector to prevent stray visible light from saturating the tube. This will only slightly decrease the radiant power in the image.

Finally, it is found that there is some problem in positioning a light source to illuminate the eye. Measurements of the nose and brow, and scale drawings indicate that the movement of the subject's line of sight must be limited vertically to approximately +20 to -48 degrees from the straight-ahead position. The limits horizontally are 30 degrees nasally and 62 degrees temporally. This allows for an oval light source about 1.5 cm. wide at a distance of 2 cm. from the eye. Figure 4.2 illustrates the

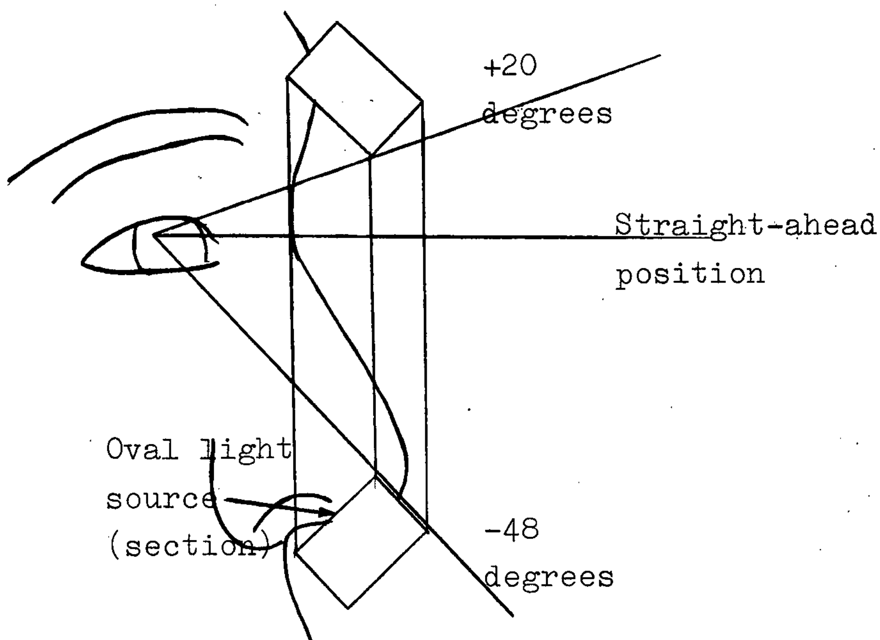

Figure 4.2
Possible lighting configuration

situation. If a more conventional shaped light source is used, larger angles may be achieved by properly positioning the source.

4.2 Optics

Assuming a $1\frac{1}{2}$ inch image dissector (eg. ITT F 4011), the maximum useful photocathode diameter is 1.1 inch. It would be possible to use the entire area of the photocathode. Actually, as stated in section 2.4, the scanned area at the eye is a square (with sides 3.12 cm.). Thus, it would be necessary to inscribe a square within the 1.1 inch diameter of the cathode.

However, the entire area was not considered for two reasons. First, other workers[17] have found that the photocathode of a similar tube was extremely non-uniform, sensitivity near the edge of the "useful area" dropping to about 1/10 of its value for the centre area. (The centre area was fairly uniform.) No uniformity data were obtainable for this tube, so an arbitrary assumption had to be made. Secondly, by using a smaller area of the cathode, a higher concentration of radiant power in the image is achieved, thus yielding more potential signal (the question of resolution is dealt with in section 4.4). The arbitrary assumption made was that the approximately uniform area of the photocathode was 0.75 inch diameter. Thus a square inscribed in this area has a side of $\frac{0.75}{\sqrt{2}}$ inch or $\frac{0.75}{\sqrt{2}} \times 2.54 = 1.35$ cm. Thus the magnification from the eye to the image dissector cathode is $\frac{1.35}{3.12} = 0.432$.

It was found that using a 55mm. focal-length lens to achieve this magnification, the object-to-lens and lens-to-image distances (u and v respectively) were convenient. In this case $\frac{v}{u} = 0.432$, and since the focal length $F = \frac{uv}{u + v}$,

$$55 = \frac{0.432u^2}{1.432u};$$

thus $u = 182$ mm.

and $v = 78.5$ mm.

For a maximum pupil size of 1 cm. and for eye movements of ± 45 degrees, a scale drawing indicates that a depth of field of approximately 7.5 mm. is required. In order to calculate the f-stop required to achieve this, the hyperfocal distance (H) must be calculated. This is defined as the near limit of the depth of field when the lens is focused on infinity. From reference 22 :

$$H = \frac{F^2}{f x d} = \frac{F x D}{d}$$

where
F = focal length of lens ,

f = f-stop of lens ,

d = diameter of acceptable circle of confusion ,

D = diameter of the lens diaphragm ;

and near limit of

$$\text{the depth of field} = \frac{H x u}{H + (u - F)} \; ; \qquad \ldots.4.1$$

and far limit of

$$\text{the depth of field} = \frac{H x u}{H - (u - F)} \; . \qquad \ldots.4.2$$

An estimate of a useful value for d was arrived at as follows. In the operation of the flying-spot system as described in chapter 3, the oscilloscope spot size was approximately 1 mm. while the scanned area of the oscilloscope face was a square 80 mm. on the side. To maintain this ratio in the final system, the aperture size would be $\frac{13.5}{80} = 0.17$ mm. Taking this as the approximate value of d, the hyperfocal distance $H = 8500$ mm. Using equations 4.1 and 4.2 , this yields a depth of field of

6 mm. at f/2.0 and 7.5 mm. at f/2.8.

To summarize, the optical imaging of the eye onto the image dissector is performed with a 55 mm. lens set at f/2.8 positioned 182 mm. from the eye and 78.5 mm. from the dissector photocathode. The magnification from the eye to the cathode is 0.432.

4.3 Electronics

The electronics section of the system remains unchanged from that detailed in chapter 3 and related appendices except for the following.

As explained in section 2.4, the two photoelectric interfaces involve signals which are identical except for possible level differences. Indeed, the video signals from the image dissector may well be different from those from the photomultiplier. However, since the video is clipped to two levels by the comparator (see figure E.2), it is a simple matter to arrange the bias and resistors to achieve this with the new signals. In the case of the horizontal and vertical deflection signals, the difference in the two configurations is slightly more important. In the "flying spot configuration", these signals are voltage levels which drive the oscilloscope amplifiers directly. In the "final configuration", since the image dissector is magnetically deflected, it is necessary to insert current drivers controlled by the voltage levels from the system. (These can also be obtained from ITT as part of their F 5005 vidissector camera unit).

It is also possible to make changes in the system parameters ε, sweep speed, and sample rate. The parameter ε is changed by adjusting the potentiometers on cards II and VII (see figures E.4 and D.1). The sweep speed is changed by changing the capacitor C on card II (figure E.4). The sample rate is set by these values of ε and sweep speed according to equation 3.1.

Since it is desired to measure eyeball accelerations as well as displacement and velocity, the sample rate should be set as high as possible. Measurements on the system however, indicate improved resolution at the lower sweep speeds. Since the track sweep generator is stopped as soon as the required boundary is located, the variation in the voltage at which it is stopped is a measure of the resolution. Figure 4.3 is a sketch of the output of the track sweep generator. The magnified portion shows the end of one of the sweeps for repeated crossings of the same edge of the pupil (for zero pupil velocity). In the sketch, three different stopping points are indicated. This shows three different voltages (v_1, v_2, and v_3) which are used to represent the same edge of the pupil. Thus the resolution in volts is approximately $r = v_3 - v_1$.

Figure 4.4 shows three photographs of this magnified sweep for system operation at 4, 6, and 8 KHz. In these photographs, there are many transients instead of just three but their spread can be used as in figure 4.3 to measure the voltage resolution. The results appear in table 4.1.

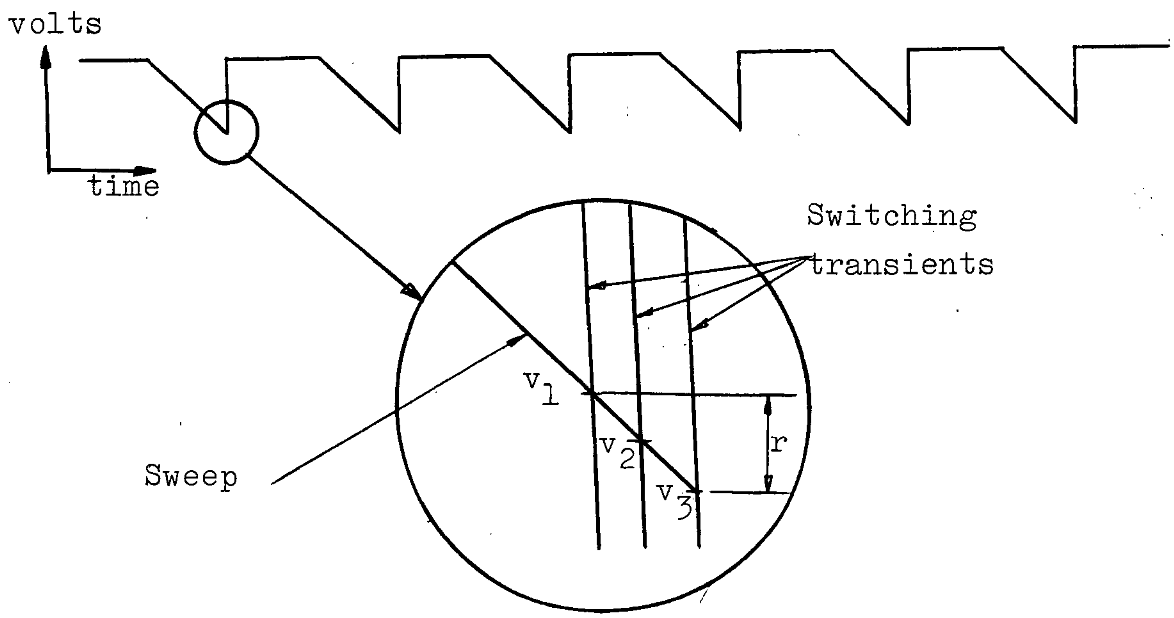

Figure 4.3
Resolution measured from the track sweep generator

Sample rate (KHz.)	4	6	8
Sweep capacitor (μF.) (C, figure H.4)	0.7	0.32	0.13
Resolution (mv.)	8	12	15

Table 4.1

It is apparent from table 4.1 that there is a trade-off between the sweep speed (which determines the sample rate) and the resolution. However, the variation in sweep-stopping voltage measured in figure 4.4 (i.e. resolution) is a secondary factor since this voltage (i.e. the edge location) is actually determined by the time that the video signal crosses the threshold level. When there is noise on the video signal, repeated crossings of

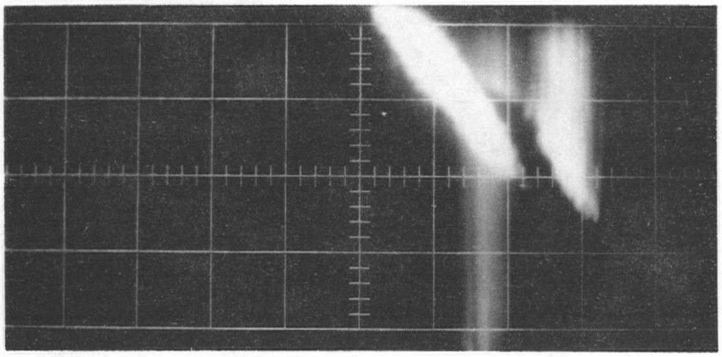

(a) 4 KHz.

Horiz. sens.: 500 nsec/div. Vert. sens. : 10 mv./div.

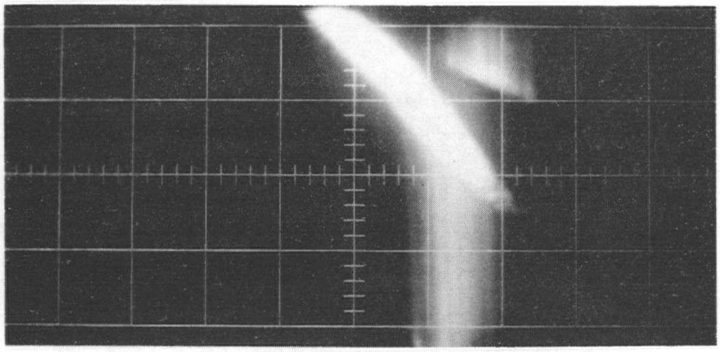

(b) 6 KHz.

Horiz. sens.: 200 nsec/div. Vert. sens.: 10 mv/div.

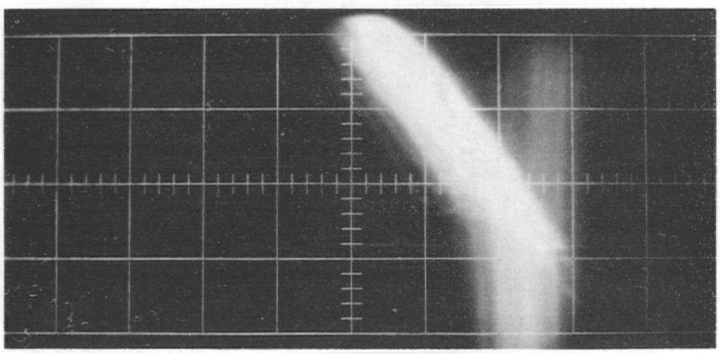

(c) 8 KHz.

Horiz. sens.: 100 nsec/div. Vert. sens.: 10 mv/div.

Figure 4.4

A magnified portion of the track sweep generator output the same boundary yield slightly different times for the crossing of the threshold level. As shown in figure 4.5, this

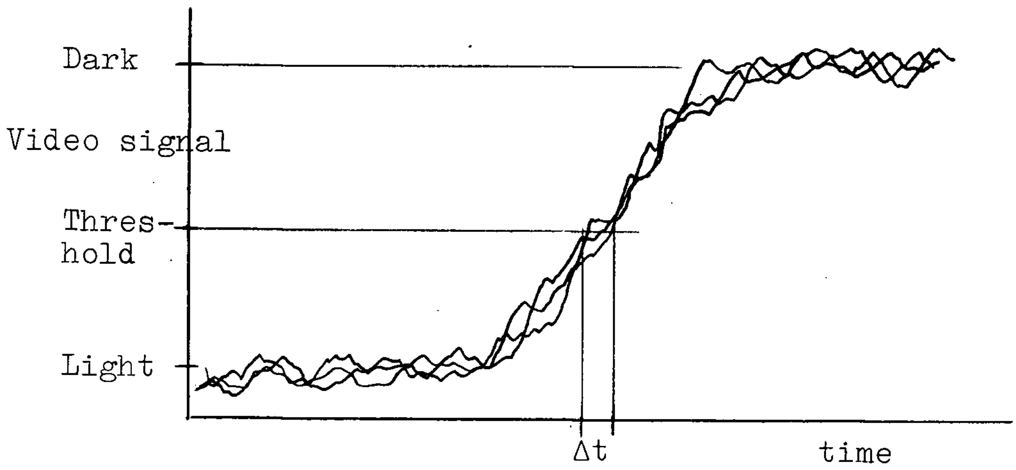

Figure 4.5
Time uncertainty at the threshold

creates an uncertainty in time Δt, within which the actual threshold crossing occurred. This uncertainty causes the voltage variation which limits resolution. Good system resolution depends upon obtaining a consistent estimate of this actual crossing time. This can be approximately achieved by low-pass filtering the video signal. This is performed by the components R and C in figure E.2*. Originally these components were necessary because the noise caused multiple triggering of the comparator at each transition of the video signal. This prevented operation of the system at the slower sample rates.

*This assumes that the common base and emitter follower stages between the photomultiplier and this RC filter perform negligible band limiting themselves. With the transistor types used this is justified for the bandwidths occurring in this case (of the order of hundreds of kilohertz).

In the final system, RC is chosen to minimize the uncertainty shown in figure 4.5 (see section 4.5).

However, in figure 4.4, this video filter was not changed. The reason for the poorer resolution at higher speeds is as follows. The resolution is the product of the sweep speed and the time-domain uncertainty Δt. At the higher speeds, the video risetime at the threshold is shorter so the uncertainty is reduced (see figure 4.10). However, in increasing the sample rate, the sweep speed must be more than proportionately increased. This is due to the fact that a considerable portion of each cycle is taken up with delays between the sweeps. The final effect of the reduction in time uncertainty and the increase in sweep speed is poorer resolution at the higher sample rates.

4.4 Effect of aperture size and shape on resolution

In an image dissector, the aperture size determines the size of a picture element (in tubes where the magnification is unity from the cathode to the plane of the aperture, the size of a picture element and the aperture are equal). For the tube being considered (ITT F 4011), the aperture can have almost any shape and the size can range from 0.0005 inch to 0.350 inch. In normal television-type applications, the aperture size and shape determine the resolution.

However, in the present application, the video is an entirely different type of signal. It is clipped to produce a two-level signal and the only information extracted from it is the point in time at which it crosses an intermediate threshold level when changing from one level to the other. The system uses this information to sample the sweep voltage at this point. Then, if the edge being observed by the system is straight and the video signal is clean, the resolution is essentially determined by the accuracy of the sampling procedure.

The situation being considered is as follows. An aperture is being scanned over a field of interest, part of which is dark and part of which is light. The boundary between the two parts is stationary, straight and at right angles to the aperture velocity. The light in each region is uniform. As the aperture crosses the boundary from dark to light, the output from the tube is proportional to the area of the aperture which sees the light region. Figure 4.6 illustrates the result. This is drawn for a square aperture so the response curve is linear. However, the

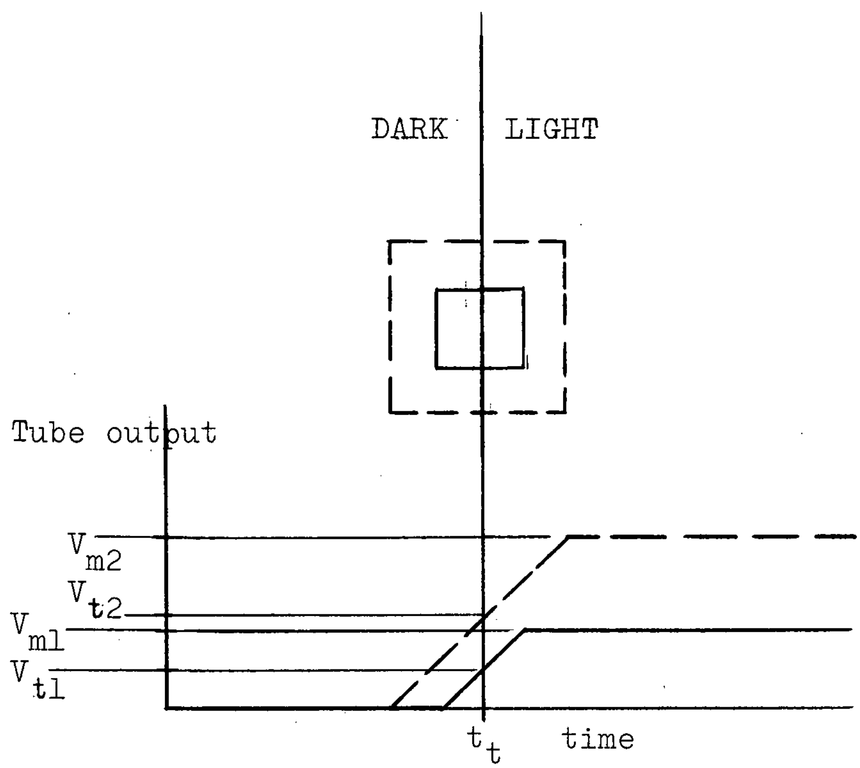

Figure 4.6

The effect of aperture size on the video threshold result is true for any symmetrical aperture (see figure 4.9). The dotted lines show the effect of using a larger aperture. This aperture sees the edge sooner and for a longer time but, since it is symmetrical, the half-way level in the output (V_t) occurs at the same point in time. It is apparent then that for a stationary boundary, the resolution is independent of the aperture size.

The error due to a non-stationary boundary is caused by the sample and hold load pulse. During this pulse (length 2 μsec.) the aperture continues to move and the actual position loaded in the sample and hold is the aperture position at the end of the pulse. This represents a consistent offset in the direction of aperture movement. However, the pupil could be moving in this direction or the opposite direction at its maximum velocity of 33.6 volts/sec. so this represents an error of

$$2 \times 2 \times 10^{-6} \times 33.6 = 0.1 \text{ mv.}$$

Note, however, that for zero pupil velocity, the delay due to this pulse does not cause an error because the offset it produces is consistent and is thus eliminated by calibration.

An increase in aperture size yields an increase in anode current in the image dissector. The principal noise in this output current is assumed to be shot noise (see section 4.6), so the rms noise current is proportional to the square root of the DC anode current. Thus, the noise current increases more slowly than the signal current, so an increase in aperture size yields an increase in signal-to-noise ratio.

The upper limit on the aperture size is set by the requirement that the edge being observed by the system be straight. The edge in this case is the pupil-iris boundary of the eye. Figure 4.7 shows a problem that occurs when the aperture is too large. In this figure, the areas shown shaded are related by $A_1 = A_2 + A_3$. The aperture is effectively one-half on the pupil and one-half on the iris. Thus, the tube output is at the threshold level so the pupil edge is recorded as being located at position 1 rather than 2 as it should be.

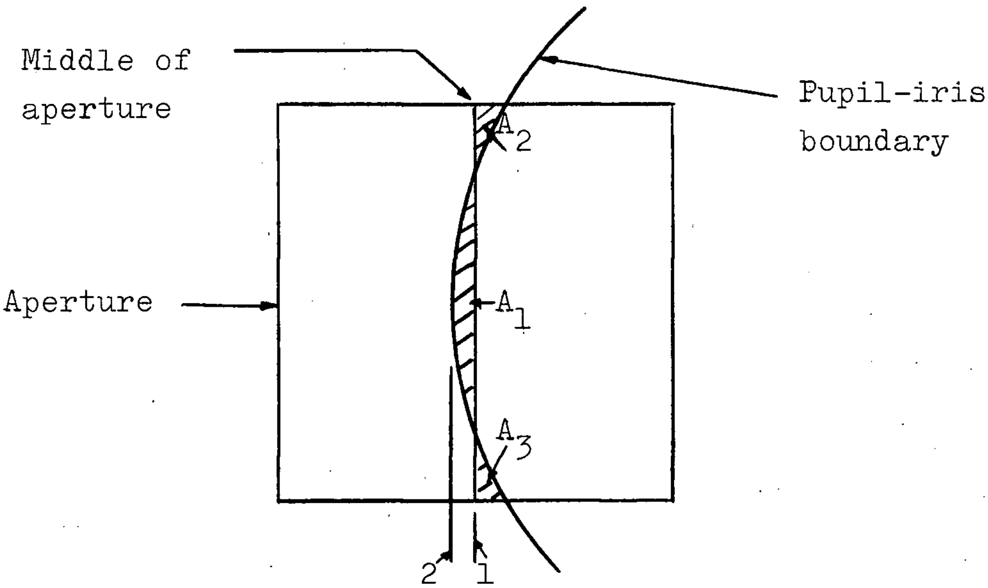

Figure 4.7
The effect of aperture size on the edge location

A symmetrical error occurs at the opposite pupil-iris boundary yielding a value of pupil diameter which is too small. Even more important, the amount of this error varies in time due to variation in the curvature of the pupil.

To estimate the effect of this limit, consider figure 4.8. The aperture has size a, the extent of the departure from a

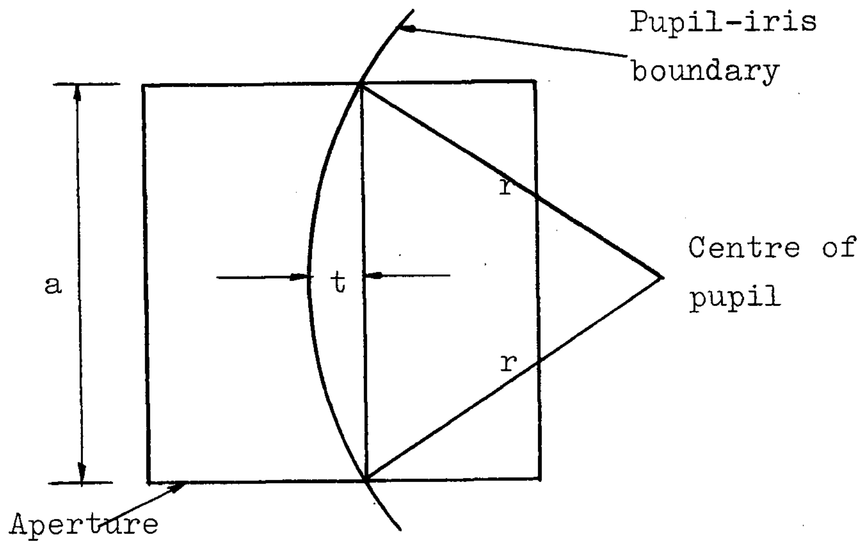

Figure 4.8
The limit on the aperture size

straight edge is t, and the pupil radius is r. The distance a is also the length of the chord in the circle, thus

$$a = \sqrt{4(2tr - r^2)} \qquad \ldots.4.3$$

The limit on t is arbitrarily set at $t \leqslant \frac{a}{10}$. Solving equation 4.3 for equality yields

$$a = \frac{80r}{104}.$$

The worst case is for the smallest pupil diameter. The smallest practical value is 3 mm. or r = 1.5 mm. Thus

$$a = 1.15 \text{ mm.} = 0.045 \text{ inch.}$$

This is the effective aperture size at the eye. The optical system (see section 4.2) performs a magnification of 0.432 so the actual maximum aperture size is 0.05 cm. or 0.02 inch.

The response of a photoemissive surface to a given light input is proportional to the area of the surface exposed to the light. It is therefore possible to compute the shape of the rising edge of the signal from an image dissector as the aperture crosses a light-dark boundary. Figure 4.9 shows the result for apertures of various shape and equal total area.

The results of section 4.3 indicate that best static resolution occurs with a slow sweep speed. This is equivalent to a low value of slope on the video signal at the boundary. Figure 4.9 shows that for a given aperture area (and hence a given maximum signal), the square aperture gives the lowest slope at the boundary.

4.5 Video band limiting

In section 4.3, it was pointed out that the noise on the video signal can cause multiple triggering at the threshold. It is possible to introduce hysteresis and thus trigger on the first crossing only. However, this provides no smoothing of the noise on the video signal. If instead, low-pass filtering is used, multiple triggering is prevented and also smoothing is provided. Various types of filters could be used (e.g. single- or multi-stage LC or RC). For simplicity, a single-stage RC filter was considered.

When sufficient filtering is performed to prevent multiple triggering at the threshold, there remains an uncertainty in the trigger time as shown in figure 4.5. This causes an uncertainty in the voltage which is loaded to represent the boundary, thus limiting system resolution. In the final system, the desired band limiting minimizes the uncertainty at a given speed of

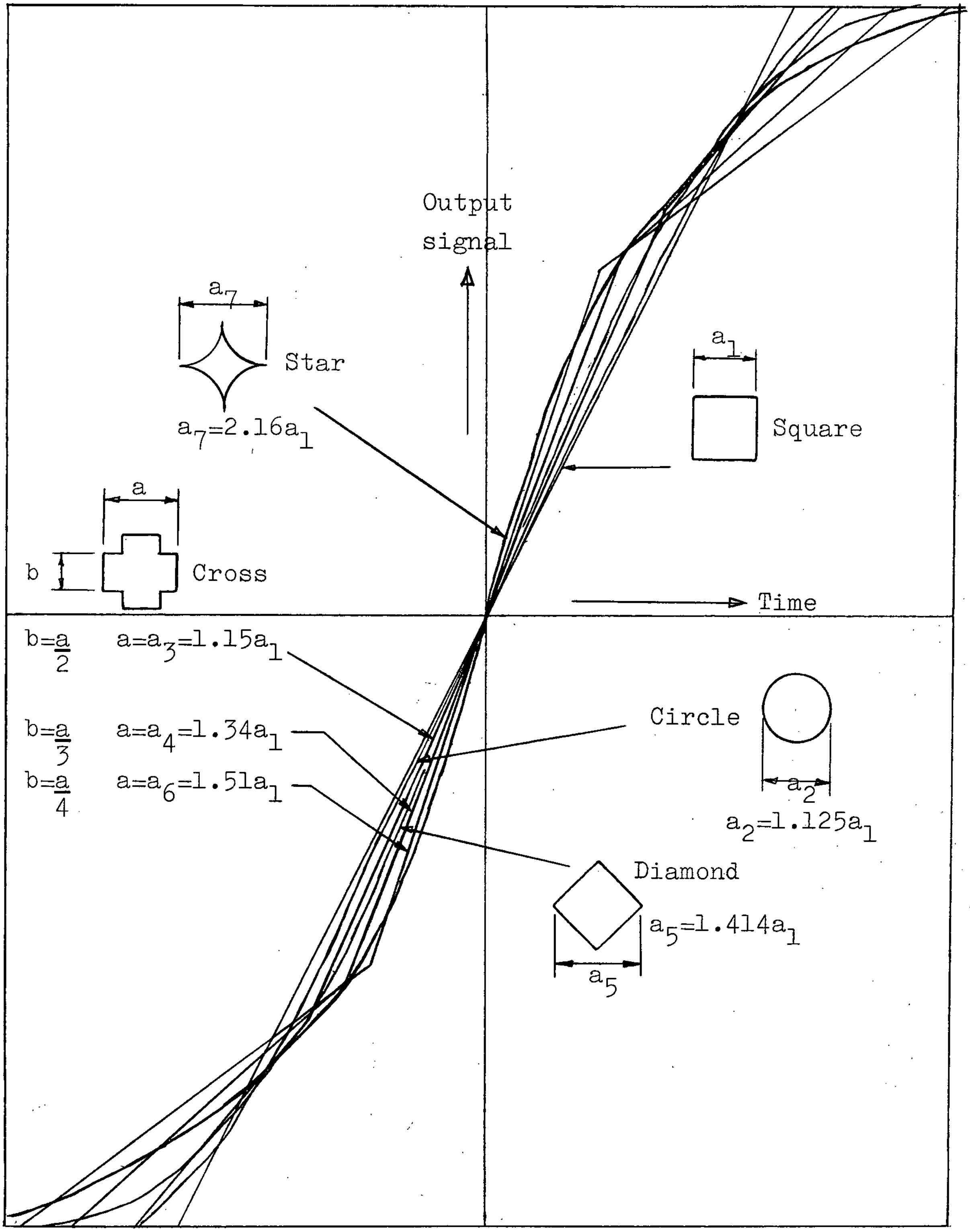

Figure 4.9
The effect of aperture shape on the video rising edge for apertures of equal total area

operation.

In order to determine the desired band limiting, measurements were performed on the flying-spot system. As a primary measurement, studies were made of the time of occurrence of the first boundary after a fixed point in the four-sweep scan cycle. The boundary is indicated by the triggering of the comparator in the video detection circuit. The fixed point is the occurrence of the X load pulse. This signal was used to trigger an oscilloscope* which then displayed the time of occurrence of the first video threshold after this pulse. The results are shown in the photographs of figure 4.10. The photographs were taken at identical exposure with the same intensity and sensitivity settings on the oscilloscope. The relevant data are in table 4.2.

It is possible to calculate the voltage resolution from these photographs as the product of the measured time uncertainty and the sweep speed. The results appear in table 4.3. The values of resolution show good agreement with those in table 4.1. (The trend was found to continue to poorer resolution at higher sample rates.) This shows again the trade-off between resolution and sweep speed.

Figure 4.10 shows that between 4 and 8 KHz., an increase in the RC time constant yields a decrease in the uncertainty. Table 4.3 shows that this also yields an improvement in resolution.

*The oscilloscope was a Tektronix type 545A. The delayed sweep was used to obtain a horizontal sensitivity of 0.1 μsec./div. The delay involved was less than 100 μsec. The specifications state a jitter of 1:20000 for the delayed sweep so this causes an error of 0.005 μsec. which is negligible on the 0.1 μsec./div. scale.

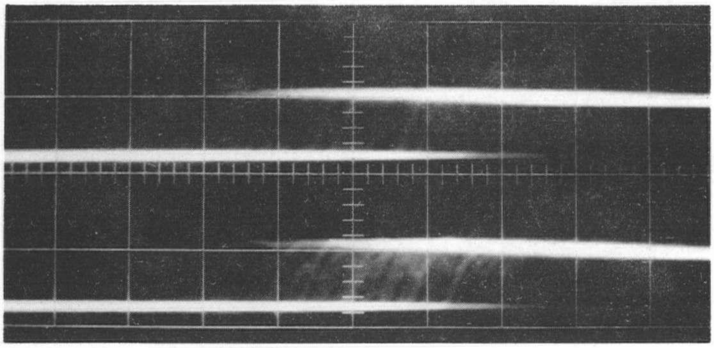

(a)

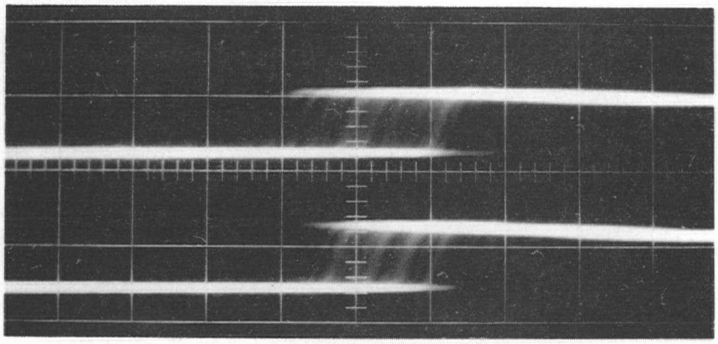

(b)

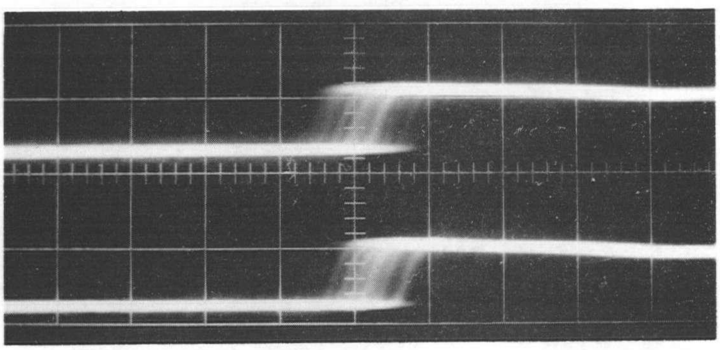

(c)

Figure 4.10

Photographs of the time uncertainty at the video threshold (see table 4.2)

Figure 4.10	Output sample rate KHz.	Sweep speed v./µsec.	RC filter sec.	Vert. sens. v./div.	Horiz. sens. nsec./div.
(a) upper	4	0.0235	$2.2x10^{-7}$	2	100
lower	4	0.0235	$1.0x10^{-6}$	2	100
(b) upper	6	0.0495	$6.8x10^{-8}$	2	100
lower	6	0.0495	$1.0x10^{-6}$	2	100
(c) upper	8	0.12	$1.5x10^{-9}$	2	100
lower	8	0.12	$1.0x10^{-6}$	2	100

Table 4.2

Sample rate KHz.	RC filter sec.	Time uncertainty µsec.	Resolution mv.
4	$2.2x10^{-7}$	0.5	11.8
	$1.0x10^{-6}$	0.45	10.6
6	$6.8x10^{-8}$	0.3	14.8
	$1.0x10^{-6}$	0.25	12.4
8	$1.5x10^{-9}$	0.14	16.8
	$1.0x10^{-6}$	0.12	14.4

Table 4.3

In order to determine the extent of the filtering being performed in each case, the theoretical transient response must be computed. The degree of decay of the exponential term at the threshold can then be determined.

The transient response is determined as follows. The input (V_i) to the filter during the time that the aperture (or

CRT spot in this case) is crossing the boundary is a ramp of slope k. As shown in figure 4.11, the clipping levels are ground and V_m. The threshold level is $V_t = \frac{V_m}{2}$. Also, "a" is the equivalent aperture or spot size in volts, v_s is the sweep speed in volts/μsec. Thus, the time of crossing the edge or the video risetime is $\frac{a}{v_s}$ and the slope $k = V_m/(a/v_s)$. After the spot has crossed the edge, the input is a constant V_m. Thus, the net input can be represented as a positive ramp starting at t=0 followed

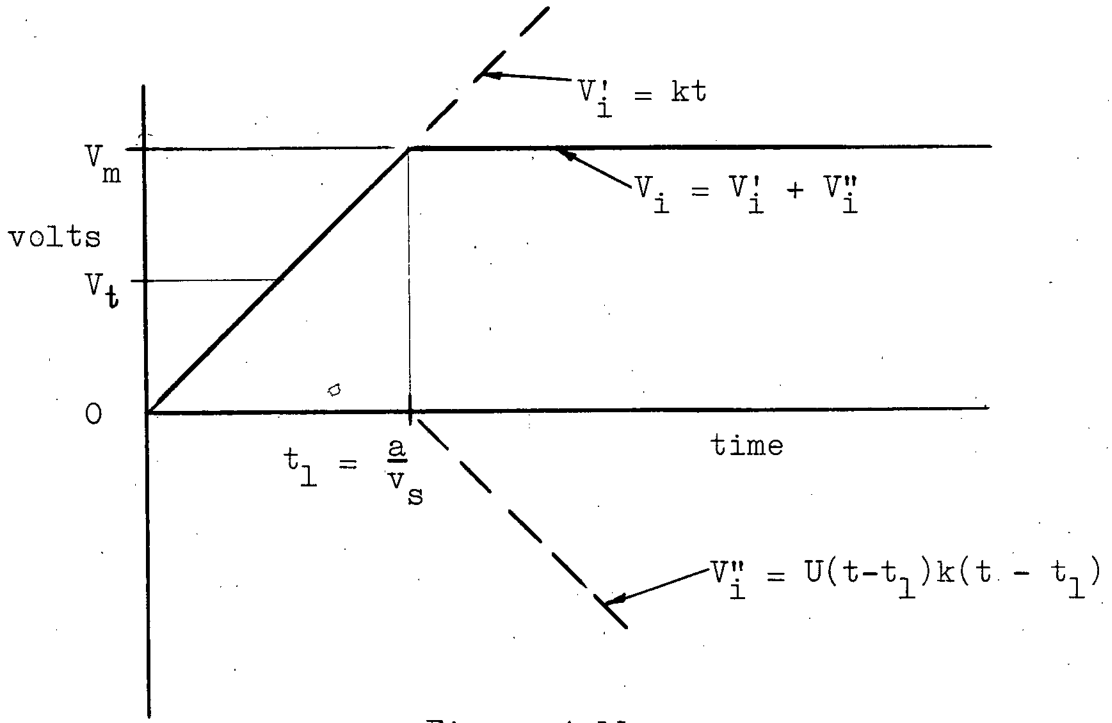

Figure 4.11
Mathematical representation of a transition on the video signal

by a negative ramp starting at $t = \frac{a}{v_s}$ as shown in figure 4.11. For this input, the output V_o (see figure 4.12) can be shown to be

$$V_o = k(t + RC(\exp(-t/RC) - 1)) - kU(t-t_1)(t - t_1 + RC(\exp(-(t-t_1)/RC) - 1)) \qquad \ldots 4.5$$

where $U(t-t_1)$ is a unit step function delayed by t_1. In all cases, V_m=6 volts and V_t=3 volts (see figure E.2).

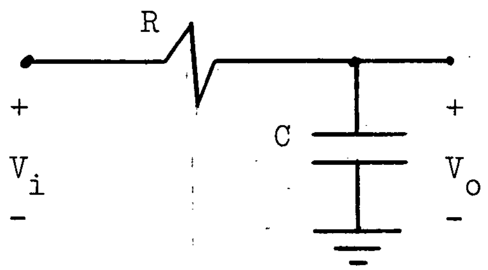

Figure 4.12
The video filter

Using equation 4.5, it is possible to determine (by trial and error) the time t_t at which $V_o=V_t$ for the system operating conditions shown in figure 4.10. For the CRT, the spot size is about 1 mm. so a=0.125 volt. The values of RC and v_s appear in table 4.2. The results are shown in table 4.4. For sample rates of 6 and 8 KHz., it is apparent that the exponential term at the threshold is not always negligible compared to unity. However, in both cases a reduction in uncertainty is achieved for these filters. Thus the filter is effective even if the decaying term is not negligible at the threshold level.

On the basis of these data, it is assumed that the requirement is simply that the exponential term at the threshold level be constant. This means that at the beginning of each boundary transition, the exponential due to the previous boundary should be negligible. If this is satisfied, then the video at each boundary starts from the same initial value (zero or V_m) so the transient response in each case is identical, as required.

This criterion requires detailed knowledge of the video signal. The main components of this signal are the transitions

Sample rate KHz.	RC filter sec.	$\frac{t_t}{RC}$	$\exp(-t_t/RC)$
4	2.2×10^{-7}	13	$<10^{-4}$
	1.0×10^{-6}	3.6	0.0273
6	6.8×10^{-8}	17	$<10^{-4}$
	1.0×10^{-6}	2.1	0.122
8	1.5×10^{-9}	346	-
	1.0×10^{-6}	1.2	0.301

Table 4.4

between the dark and the light levels caused by the pupil boundaries. The two possible forms of this signal are sketched in figure 4.13. The transitions marked x_1, x_2, etc. are those caused by the crossing of the respective pupil boundaries. The reason for the extra pulses marked A is as follows. The first edge (from light to dark) occurs because after the x_2 and y_2 edges are located, the track sweep is zeroed before the counter is advanced (see figure 3.2). Thus,the spot moves back onto the pupil. This is permissible since video blanking is also performed. The second edge of A (from dark to light) is produced when the counter is advanced and the spot is moved to its next position which is outside the pupil. Since these are both high-speed transitions, A is considered to have vertical sides.

The reason for the two forms of the video signal shown in figure 4.13 is the amount of filtering performed relative to the risetime $\frac{a}{v_s}$. In (a), a relatively large time constant is

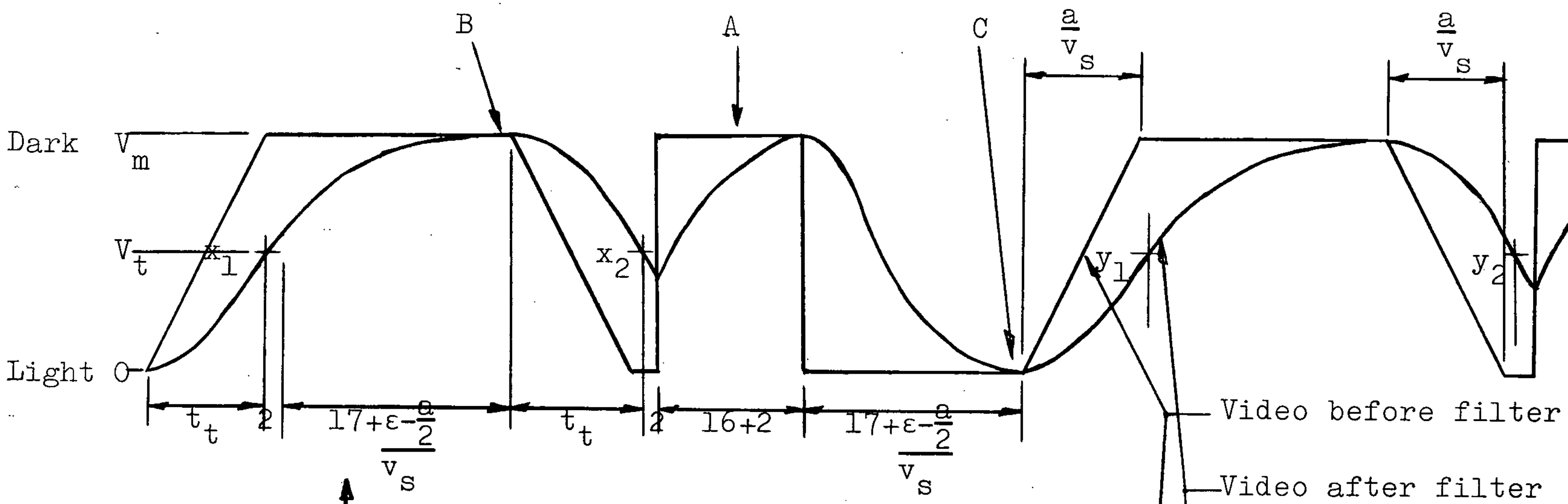

Figure 4.13 (a) The video signal for $t_t+2>\frac{a}{v_s}$

Figure 4.13 (b) The video signal for $t_t+2<\frac{a}{v_s}$

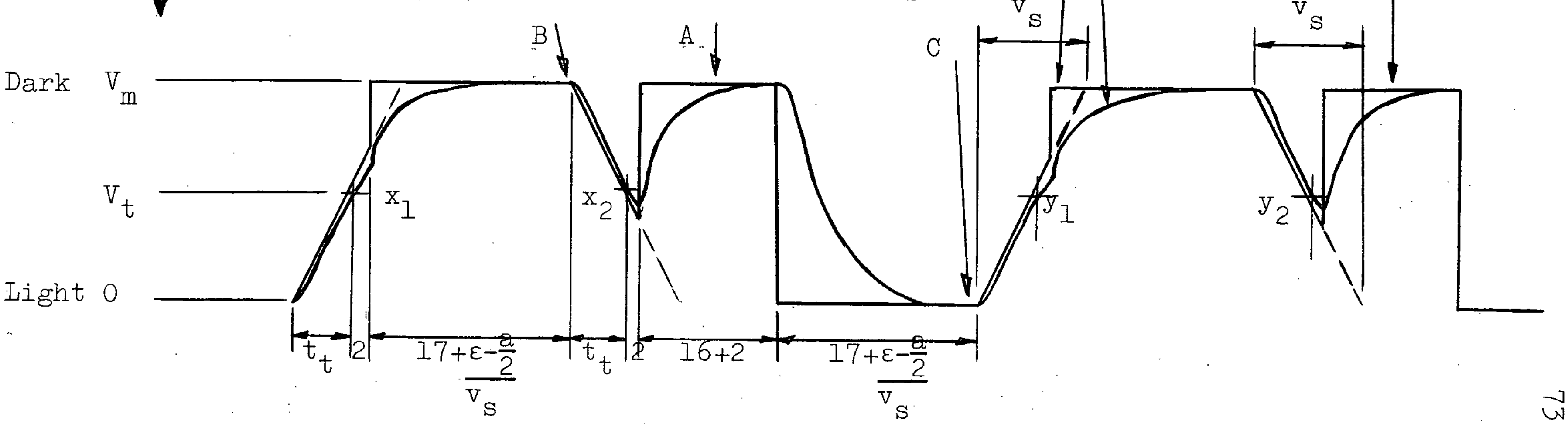

used so that $t_t+2 > \frac{a}{v_s}$. In (b) however, $t_t+2 < \frac{a}{v_s}$ and thus the spot has not fully crossed the boundary before the end of the 2 μsec. pulse. In the first case (x_1 or y_1), this is a "load number 1" pulse (see figure 3.2) and immediately after it, the track sweep is zeroed and the counter is advanced. This means that the spot is moved to its next position which is within the pupil, so the video suddenly changes to the dark level as shown. In the second case (x_2 or y_2), this is a "load number 2" pulse, so immediately after it, the track sweep is zeroed. This moves the spot back onto the pupil and the first edge of the A pulse is created before the video reaches the light level.

The criterion for negligible exponential terms must be satisfied at B and C on figure 4.13 since these points are the beginning of the boundary transitions (the other transitions at x_1 and y_2 are identical to these two). It is possible that the filtered video may not reach the dark level by the end of the pulse A, but to provide for the worst case, it is assumed that it does. In all cases, the video at C is a simple exponential decay of V_m volts in time $T' = 17 + \frac{\varepsilon - \frac{a}{2}}{v_s}$ μsec. For ease of comparison with B, this is inverted and treated as an exponential approach to V_m from zero. This can be expressed as

$$V_{oC} = V_m(1 - \exp(-t/RC))$$

and at C this is

$$V_{oC}(T') = V_m(1 - \exp(-T'/RC)). \qquad \ldots 4.6$$

The situation at B can be in two forms, corresponding to figure 4.13 (a) or (b). Case (a) is shown in figure 4.14. After the video input has reached V_m (i.e. after $t = \frac{a}{v_s}$), this

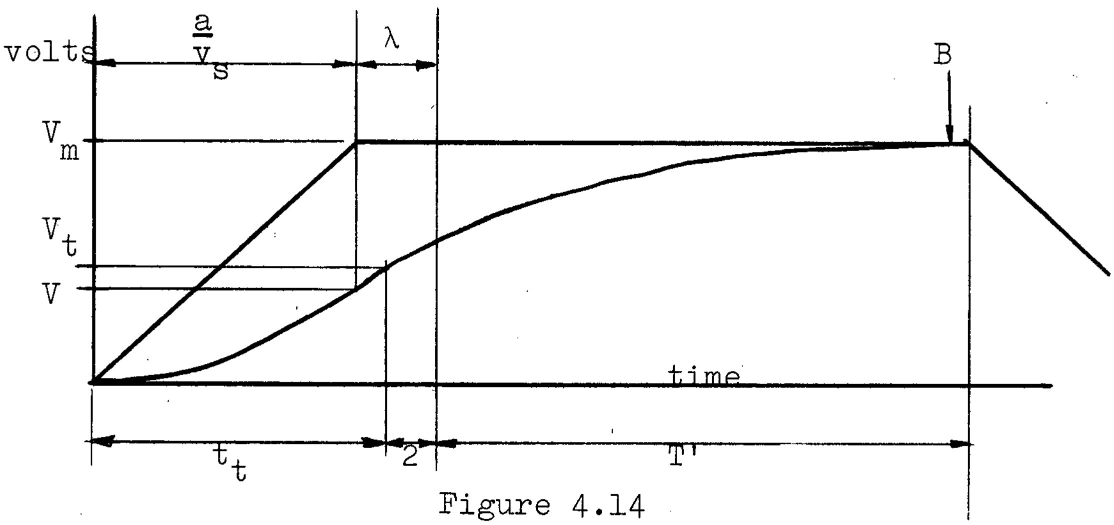

Figure 4.14
A video transition for $t_t+2 > \frac{a}{v_s}$

case can be treated as an exponential approach to V_m from some initial voltage V. This can be expressed as

$$V_{oB} = V_m(1 - \exp(-t/RC)) + V \exp(-t/RC))$$

where t starts at $\frac{a}{v_s}$. Then at B this is

$$V_{oB}(T'+\lambda) = V_m(1 - \exp(-(T'+\lambda)/RC)) + V \exp(-(T'+\lambda)/RC). \quad \ldots 4.7$$

Since $t_t+2 > \frac{a}{v_s}$, $\lambda > 0$. Thus at B, the first term in this expression is closer than equation 4.6 is to the terminal voltage V_m. Equation 4.7 has an additional positive term $V \exp(-(T'+\lambda)/RC)$. In this case then, the extent of the exponential decay is greater at B than it is at C.

The case (b) in figure 4.13 is shown in figure 4.15. Again, this can be treated as an exponential approach to V_m from some initial voltage V (after $t=t_t+2$ in this case). Thus, for case (b), the situation at B is

$$V_{oB}(T') = V_m(1 - \exp(-T'/RC)) + V \exp(-T'/RC). \quad \ldots 4.8$$

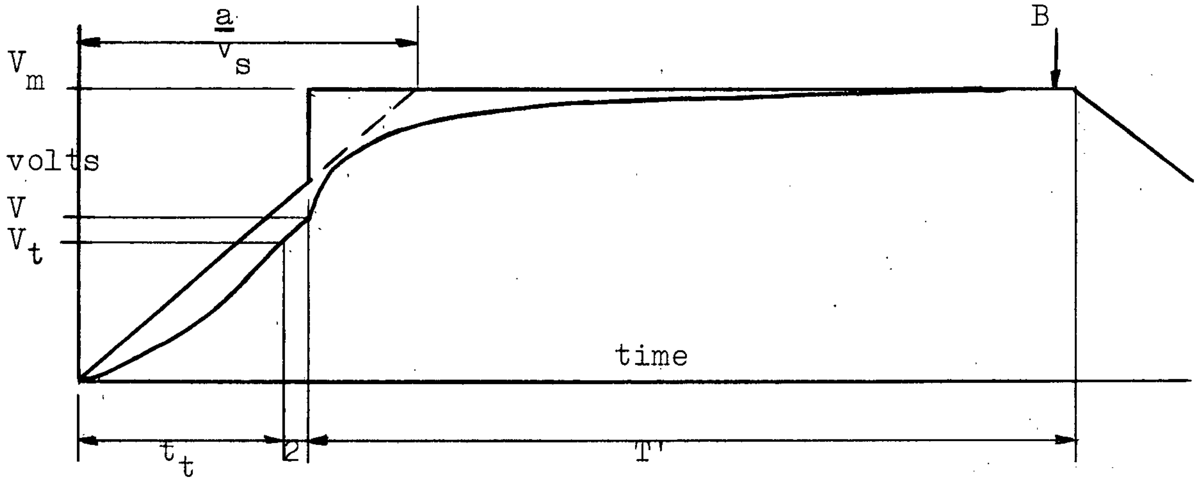

Figure 4.15
A video transition for $t_t + 2 < \frac{a}{v_s}$

In this case, the first term is identical to equation 4.6 so the presence of the second term in equation 4.8 means that the video signal is nearer to V_m at B than it is at C.

Thus, in both cases, the most stringent requirement is that the exponential term at C be negligible. To examine this requirement, equation 4.6 is solved for RC:

$$\exp(-t/RC) = \frac{V_m - V_{oC}}{V_m}$$

and $$-t/RC = \ln\left(\frac{V_m - V_{oC}}{V_m}\right).$$

When t=T', the error $\frac{V_m - V_{oC}(T')}{V_m}$ is set to some small value d (in section 4.6, d is set to 1% and 0.1%). Then the maximum filter time constant is given as

$$RC \simeq \frac{T'}{-\ln(d)} = \frac{17 + \frac{\varepsilon - \frac{a}{2}}{v_s}}{-\ln(d)} \ \mu\text{sec.} \qquad \ldots\ 4.9$$

and the corresponding video bandwidth is

$$\Delta f = \frac{-\ln(d)}{17 + \frac{\varepsilon - \frac{a}{2}}{v_s}} \quad \text{MHz.} \qquad \ldots\ 4.10$$

This bandwidth gives optimum filtering at a given sweep speed v_s. However, it is apparent from figure 4.13 that as the time constant RC is increased, the time to the threshold t_t will increase. This increases the total period T directly and yields a reduced output sample rate. If this change is more important than the reduction in resolution, then a larger minimum bandwidth than that set by equation 4.10 must be used. This new limit will be set experimentally according to the sample rate required. The extent of the change in sample rate can be computed as follows.

For a given set of system parameters (ε, a, and v_s), the minimum bandwidth is calculated from equation 4.10. Using the corresponding value of RC in equation 4.5 (k and t_1 computed as before), the value of t for V_o=3 volts is calculated (by trial and error). This is the time t_t on figure 4.13. For system operation at very large bandwidths, $t_t \approx \frac{a}{2v_s}$. Thus, at finite bandwidths, the filter adds a delay $t_t - \frac{a}{2v_s}$ at each boundary. Then the period of the four-sweep scan is increased by $4(t_t - \frac{a}{2v_s})$.

Table 4.5 shows the results with d=0.1% for 4, 6, and 8 KHz. with ε = 0.8 volt and a = 0.125 volt (the parameter values for figure 4.10 and table 4.2). In each case, the upper trace of figure 4.10 is taken as the large-bandwidth reference.

Table 4.5 also shows the change in sample rate for an intermediate bandwidth (from table 4.4).

Sample rate KHz.	RC filter sec.	Time to threshold µsec.	$t_t - \frac{a}{2v_s}$ µsec.	Change in sample period %
4	ref.	2.65	-	-
	1.0×10^{-6}	3.6	0.95	+1.5
	6.7×10^{-6} max	7	4.35	+ 7
6	ref.	1.26	-	-
	1.0×10^{-6}	2.1	0.84	+2.0
	4.4×10^{-6} max	4	2.74	+6.5
8	ref.	0.52	-	-
	1.0×10^{-6}	1.2	0.68	+2.2
	3.3×10^{-6} max	3	2.48	+8

Table 4.5

4.6 Noise considerations

In properly constructed photomultiplier tubes, there are three fundamental sources of noise: statistical fluctuations of (a) the dark current due to thermionic emission and cosmic rays; (b) the signal current; (c) the secondary emission process.

Although S1 photocathodes have quite high dark current (normally between 3×10^{-13} and 3×10^{-12} A/cm^2), it is usually several orders of magnitude below the usable signal current. Also, it may be reduced as much as one-hundred fold by cooling from room temperature to the temperature of liquid nitrogen[23]. If in addition, the dark current due to cosmic rays is assumed negligible, then only the other two sources of noise need be considered.

The signal current in a phototube contains shot noise. For a DC cathode current of I_k, the shot noise in this signal is $\overline{i_{nk}^2} = 2eI_k\Delta f$

where i_{nk} is the rms noise current in the signal,

e is the electronic charge $= 1.6\times10^{-19}$ coulomb,

I_k is the DC cathode current,

Δf is the bandwidth of the associated equipment (since the secondary emission multiplier in a photomultiplier is a very wide-band amplifier, this is usually the bandwidth of the circuits connected to the tube).

In the case of a photomultiplier, both the noise and the signal undergo tremendous amplification in the multiplier section. However, because shot noise is also associated with the secondary emission process, it can be shown[24] that this process causes a slight decrease in the signal-to-noise ratio.

Since the video detection system is a voltage threshold detector, a signal current-to-noise current ratio was considered in preference to a signal power-to-noise power ratio.

Appendix G shows that this signal-to-noise ratio for a photomultiplier is

$$\frac{S}{N} = \sqrt{\frac{(\omega - 1)I_k}{2e\Delta f\omega}} \, .$$

In an image dissector, the cathode signal I_k is that portion of the total current which enters the aperture. For dissectors with unity gain in the image section, this current is given by $I_k = J_kA$ where J_k is the cathode current density in amperes per cm^2 and A is the aperture area in cm^2. Substitution for I_k, e, and ω (see appendix G) yields

$$\frac{S}{N} = 1.53\text{x}10^{-9}\sqrt{\frac{J_kA}{\Delta f}} \, .$$

In the above, the noise current is an rms value. This is not a good measure of the noise on a signal being used for threshold detection. In this case, some estimate of a peak-to-peak value is more practical. While peak-to-peak noise is theoretically meaningless (because pulses of any amplitude can theoretically occur), reference 25 indicates that a value can be estimated from an oscilloscope presentation. The conclusion in reference 25 based on experimental as well as theoretical[26] considerations is i_n(peak-to-peak) = $7i_n$(rms). Then the effective signal-to-noise ratio using this approximation is

$$\frac{S}{N} = 2.2\text{x}10^{-8}\sqrt{\frac{J_kA}{\Delta f}} \, . \qquad \ldots\ 4.12$$

Figure 4.16 shows this signal-to-noise ratio plotted against image dissector cathode current density. The sample rates are the nominal values based on T = 125 and 250 μsec. Using these values and equation 3.1, values of v_s were obtained in each case for ε = 0.5, 1.0, and 1.5 volts. Then equation 4.10 gave the minimum bandwidth for the two conditions d = 1.0% and 0.1%.

Table 4.6 shows the bandwidths calculated by this procedure. Also shown is the change in sample period for each case. These are calculated in a similar manner to the results in table 4.5. The reduction in bandwidth caused by the use of d = 1.0% instead of 0.1% causes an additional 3% increase in the sample period. However, figure 4.16 shows that only a relatively small increase in signal-to-noise ratio is achieved by this change. The use of d = 0.1% appears more practical since it gives a smaller reduction in sample rate (i.e. a smaller increase in sample period).

T µsec.	ε volts	v_s v./µsec.	d %	Δf KHz.	Change in sample period %
125	0.5	0.154	0.1	362	6.7
			1.0	241	9.6
	1.0	0.308	0.1	350	6.7
			1.0	234	9.6
	1.5	0.462	0.1	347	6.7
			1.0	231	9.6
250	0.5	0.014	0.1	178	8.2
			1.0	119	11.5
	1.0	0.029	0.1	153	8.2
			1.0	102	11.5
	1.5	0.044	0.1	146	8.2
			1.0	99	11.5

Table 4.6

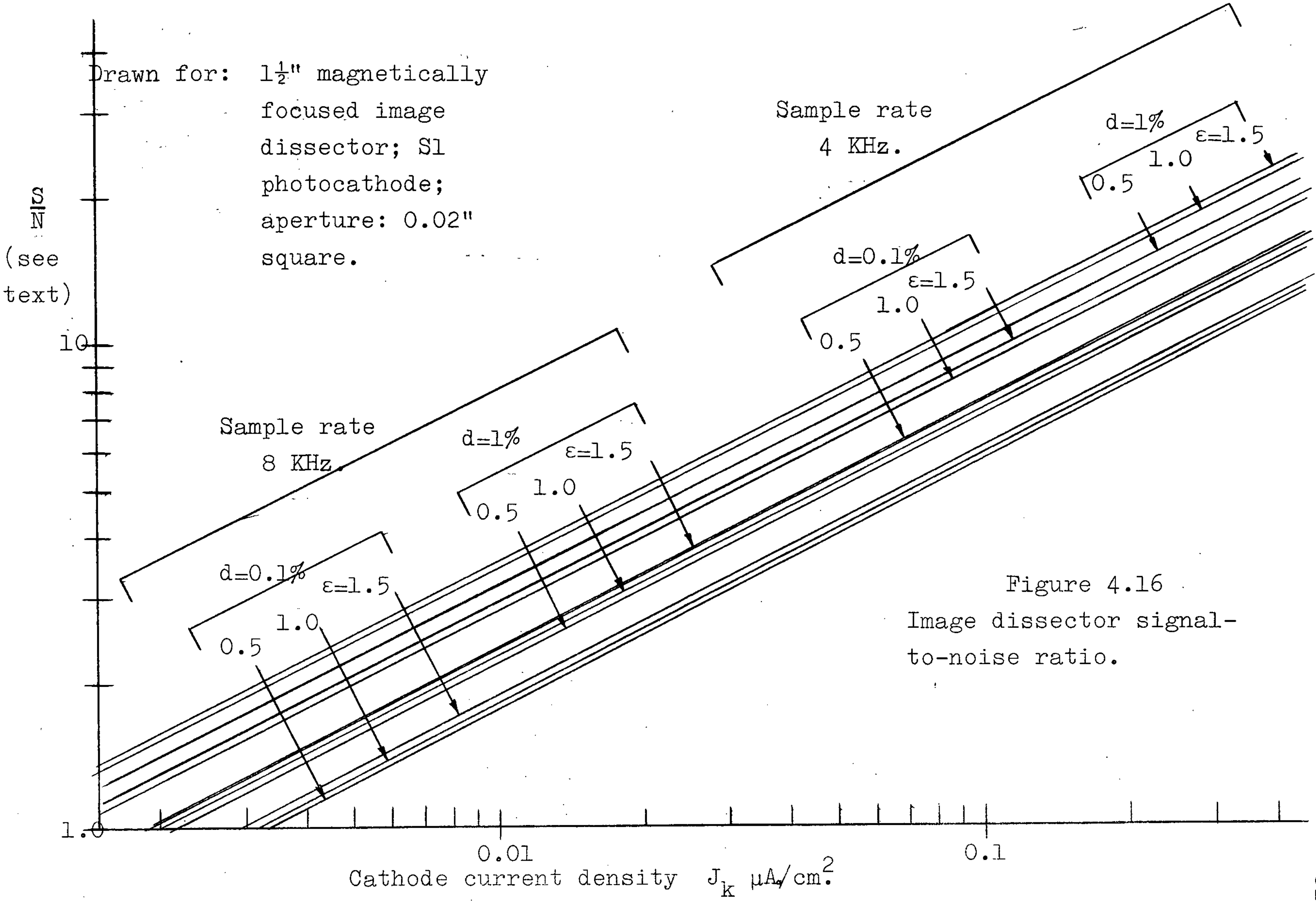

Figure 4.16
Image dissector signal-to-noise ratio.

Figure 4.16 also shows the trade-off between sample rate and signal-to-noise ratio. At the slower speeds, better resolution and signal-to-noise ratio are predicted, but the higher speeds are preferred for differentiation of the output.

At the slower sweep speeds, there is a wider spread in signal-to-noise ratio for variations in ε because at these speeds, the sweeps occupy a relatively larger portion of the sample period. However, even at 4 KHz. only a slight variation with ε is predicted.

The simulation performed in chapter 5 determines the approximate values of J_k that would be anticipated in system operation with an image dissector. In chapter 6, this information is used in conjunction with figure 4.16 to evaluate system performance.

CHAPTER 5

Image dissector evaluation

5.1 Purpose

The purpose of the evaluation experiments was to gain insight into the operation to be expected from the image dissector in the proposed final system. Since these tubes require high light levels for successful operation, it was necessary to ensure that this could be achieved in the proposed application. It was possible to use a simple photomultiplier and glass eyes to predict the approximate signals in the image dissector. Then a predicted signal-to-noise ratio was computed. In addition to this, considerable information was obtained about the illumination of the eye and its reflectivity to infra-red light.

5.2 Description of image dissector simulation

The simulation was performed by using a simple photomultiplier with a spectral response similar to the proposed image dissector. For light in the infra-red, the closest match is obtained with an S1 photocathode. The spectral response is shown in figure 5.1. By focusing an image of the eye onto the cathode of the simple photomultiplier and by using a mask with a small hole to expose only one area of this image to the photocathode at a time, it is possible to determine the relative signal levels at various points on the image. This is done by moving the hole in the mask to various positions on the image and noting the relative anode currents from the photomultiplier.

In addition, it is possible to form an expression which

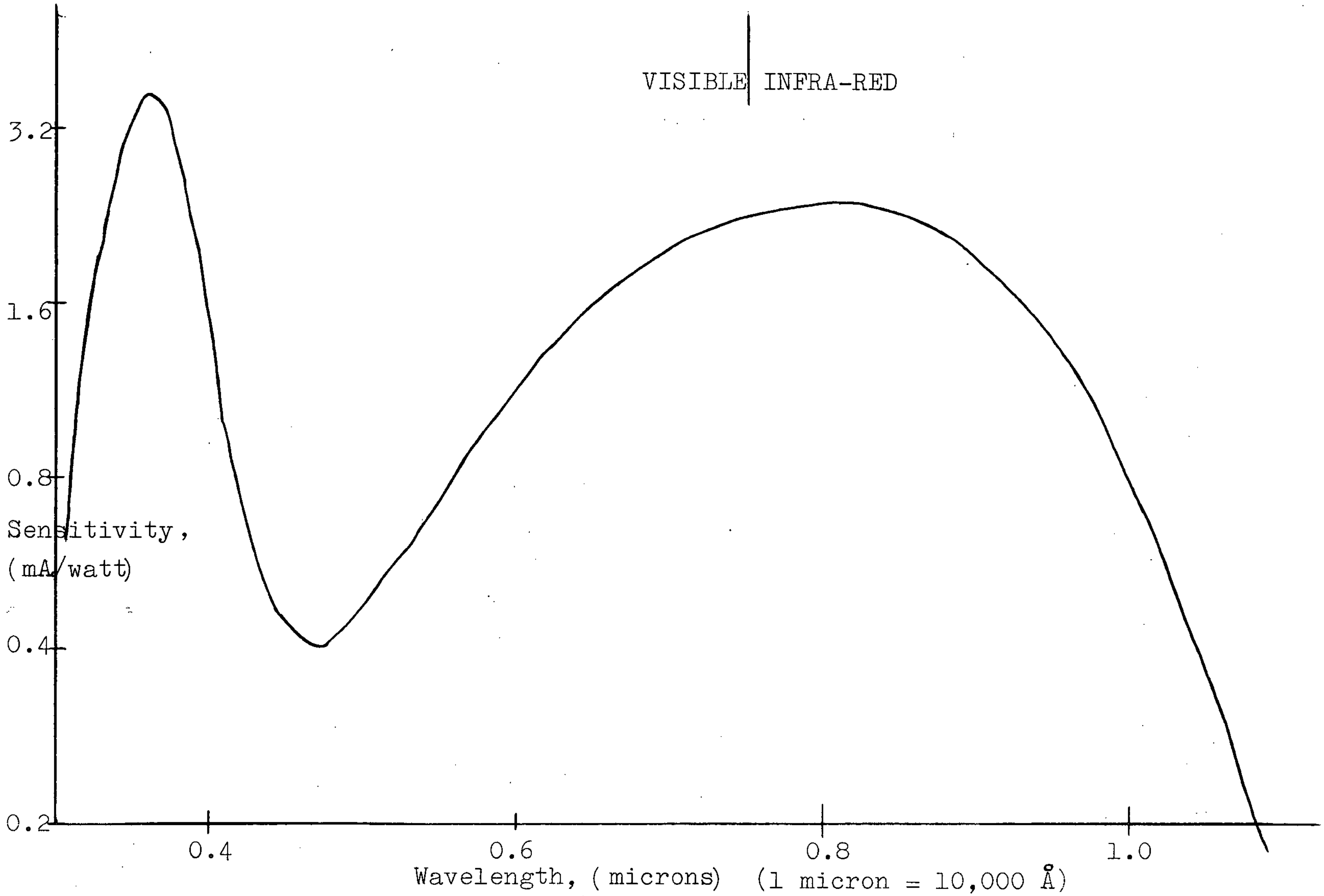

Figure 5.1 Spectral response of S1 photocathode

describes mathematically the differences between this experimental configuration and the proposed configuration using the image dissector (see section 5.3). With this expression plus the measured anode current from the simple photomultiplier, the absolute value of the cathode current density in the image dissector is computed. Using the curves in section 4.6, it is then possible to predict the system performance.

Since the actual method of illuminating the eye in the experiment is identical to that which will be used with the image dissector, this does not enter into the conversion expression. Thus, it is convenient to experiment with various illumination methods.

In the experiment, it was found that it was not practical to focus the image directly onto the photomultiplier cathode. The relative response of the various portions of the cathode surface was highly non-uniform, creating differences in the tube output which interfered with the differences in radiant energy in the various portions of the image. For this reason, the Köhler illumination system was used instead of direct focusing onto the photocathode. The system essentially defocuses the light from the aperture so that the whole photocathode is used for all positions of the mask (see figure 5.3).

5.3 Calculations for image dissector simulation

Figures 5.2 and 5.3 show the image dissector configuration and the experimental configuration respectively. It can be seen that the illumination method is common to both. It is assumed that the luminance of the eye is B watts/cm.^{2} This will be a function of position on the eye.

Consider first figure 5.2. The following symbols are used: r is the fraction of the incident light that is reflected from the mirror (assumed independent of wavelength) = 0.7,

$t(\lambda)$ is the transmission function of the infra-red filter,

n_I is the standard f number of the lens = 2.8,

m_I is the magnification of the system = 0.432,

t_p is the transmittance of the lens,

$S_I(\lambda)$ is the spectral sensitivity of the S1 photocathode in amperes/watt.

Then the illuminance of the image on the photocathode of the image dissector as a function of wavelength is (see appendix H)

$$E_I = \frac{\pi r B t_p t(\lambda)}{4 n_I^2 (1 + m_I)^2} \quad \text{watts/cm.}^2$$

Then the total cathode current density is

$$J_{kI} = \frac{\pi r B t_p}{4 n_I^2 (1 + m_I)^2} \int t(\lambda) S_I(\lambda) d\lambda \quad \text{amps./cm.}^2 \qquad \ldots.5.1$$

The integration is performed over all wavelengths in the incident light.

Next consider figure 5.3. This development follows reference 27. The eye is imaged onto the plane of the mask

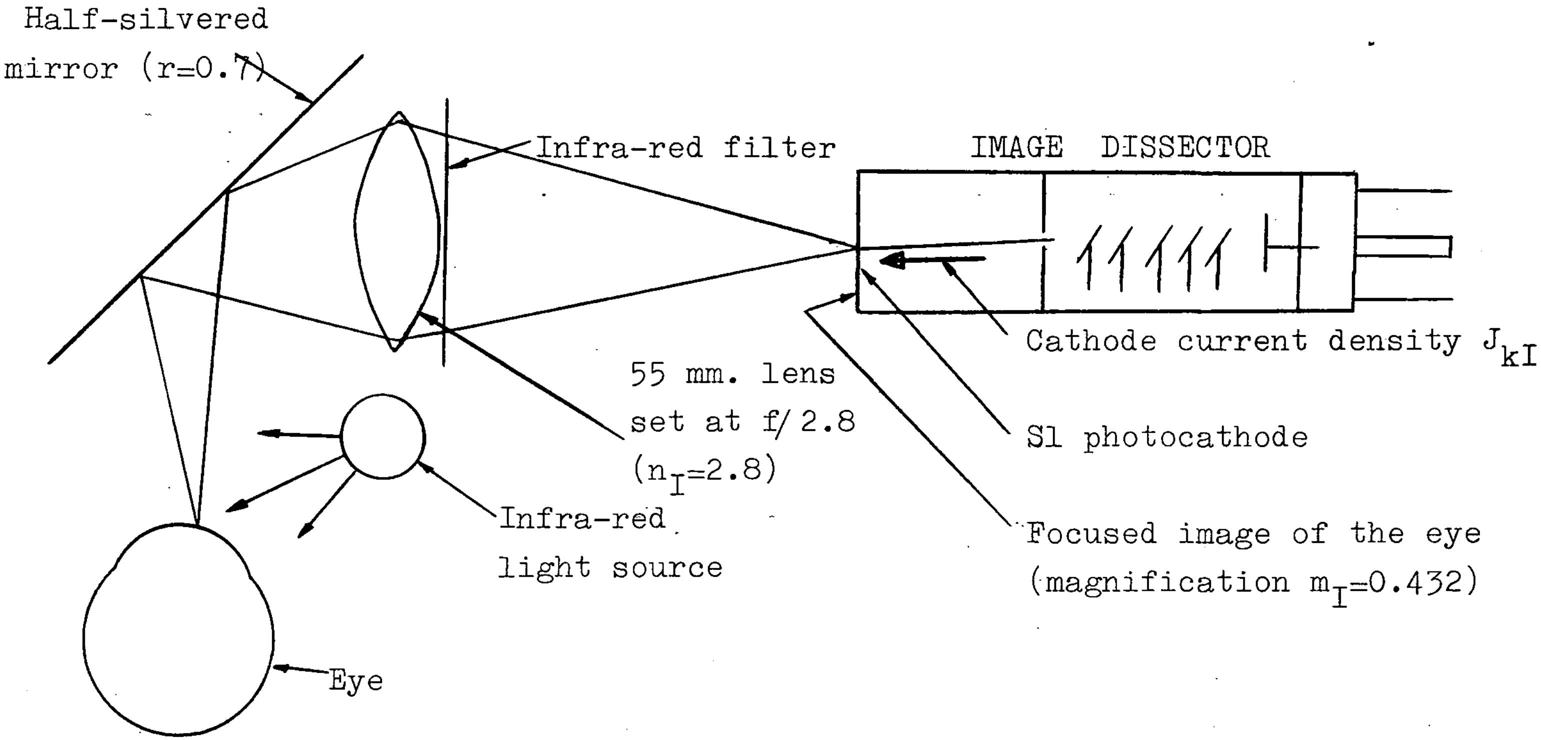

Figure 5.2
Image dissector optical configuration

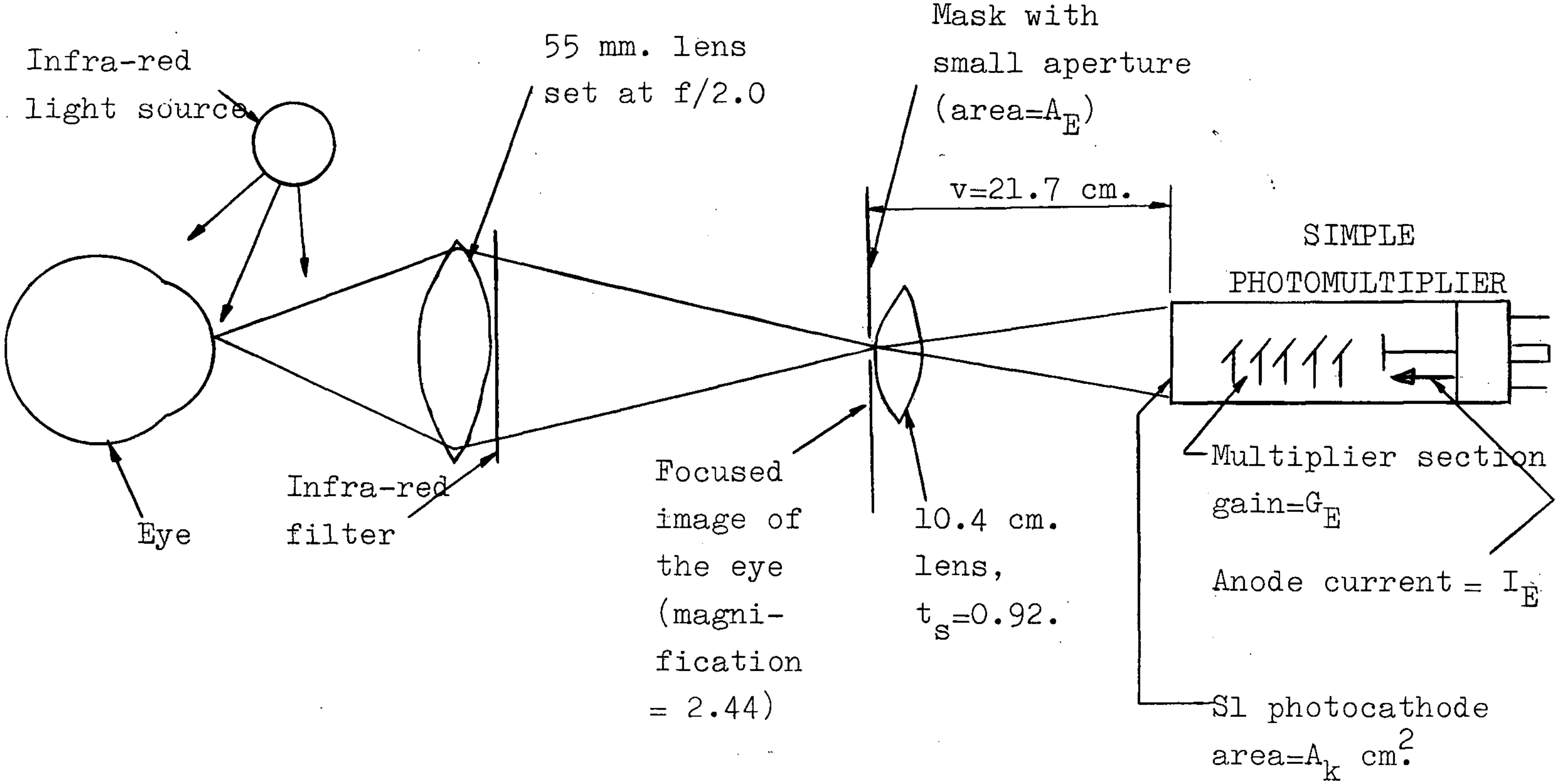

Figure 5.3
Experimental optical configuration

with the 55 mm. lens. The diaphragm of this lens is imaged onto the photocathode with the second lens. In this way the light passing through the aperture in the mask fills the whole of the photocathode independent of the position of the aperture.

The image of the eye on the mask has the same average luminance as the eye itself except for the lens transmittance t_p and filter transmittance $t(\lambda)$[28]. Image luminance then is $Bt_p t(\lambda)$ watts/cm.^{2} The small hole in the mask (area A_E) acts as a light source to illuminate the cathode. The intensity of this source seen from the cathode is $Bt_p t(\lambda) t_s A_E$ watts (where t_s is the transmittance of the simple lens). Thus the illuminance of the cathode at distance v (see figure 5.3) is

$$E_E = \frac{Bt_p t(\lambda) t_s A_E}{v^2} \text{ watts/cm.}^2 \qquad \ldots.5.2$$

Finally, for a cathode of area A_k cm.^{2}, a spectral sensitivity of $S_E(\lambda)$ amperes/watt, and a multiplier section of gain G_E, the photomultiplier anode current is

$$I_E = \frac{Bt_p t_s A_E A_k G_E}{v^2} \int t(\lambda) S_E(\lambda) d\lambda \text{ amperes} \qquad \ldots.5.3$$

where the integration limits are as before.

Combining equations 5.1 and 5.3 and noting that $S_E(\lambda)$ and $S_I(\lambda)$ are both JEDEC S1 response curves (i.e. $S_E(\lambda) = S_I(\lambda)$) yields

$$\frac{J_{kI}}{I_E} = \frac{\pi r v^2}{4n_I^2(1 + m_I)^2 t_s A_E A_k G_E} \qquad \ldots.5.4$$

Only t_s and G_E are not known at this point. An estimate of t_s is 0.92 based on the assumption that 4% of the incident light is lost at each lens surface. The gain of the secondary emission multiplier was measured as described in appendix I.

The results of the gain measurement on the tube used appear in appendix I and the average gains appear in table 5.1.

V_b (over-all voltage)	1200	1300	1400	1450
G_E	$0.5\text{x}10^6$	$1.05\text{x}10^6$	$1.85\text{x}10^6$	$2.45\text{x}10^6$

Table 5.1

5.4 Comparison of direct and diffuse illumination

As stated earlier, it was felt that if practicable, diffuse illumination was preferable to direct illumination because under diffuse light there is no highlight formed on the eye.

Initially, diffuse <u>transmission</u> was considered using ground glass and certain plastics. In most cases the diffusion was insufficient to prevent the formation of a highlight. The reason for this was that although the illumination was diffused to a larger area than the light itself, this area was bright enough to cause a highlight. A more uniform distribution could be achieved with greater distance between the source and the diffuser but then less light is being used. Reflecting or focusing the light onto the diffuse transmitter again creates a relatively small, bright area.

Probably the best diffuse transmitting medium was polyethylene $\frac{1}{4}$ to $\frac{1}{2}$ inch thick. In this case the light source could be very close behind the medium without causing a highlight to be formed. However it was obvious that the transmittance of this material was very low. Studying the data in table 6-18 of reference 29, it is apparent that materials with good diffusing properties have transmittances in the range from 5% to 65%. However diffuse <u>reflecting</u> surfaces reflect 75% to 92%. This range is obtainable with such simple materials as flat white paint or white plaster.

Tests indicated that very uniform lighting could be obtained with no corneal reflection using the theory of the Ulbricht sphere[30]. The theory is based on a complete sphere whose inner surface is perfectly diffusing and which contains a light source. The photometric brightness of any point on the wall due to reflected light only, is proportional to the total light flux from the source[29]. A small hemisphere (3 inches diameter) was obtained and the inner surface painted white. A hole was cut for the subject's eye as shown in figure 5.4 and a light was shone into the hemisphere. Even this partial sphere yielded uniform fairly strong light with no corneal reflection. However as the intensity was increased to obtain higher signal levels, the eye took on a washed-out appearance. The reason for this is the integrating effect of the sphere. The brightness of all points on the inner surface is proportional to the total flux in the sphere. Thus the contrast of the pupil-iris boundary is lost. This was

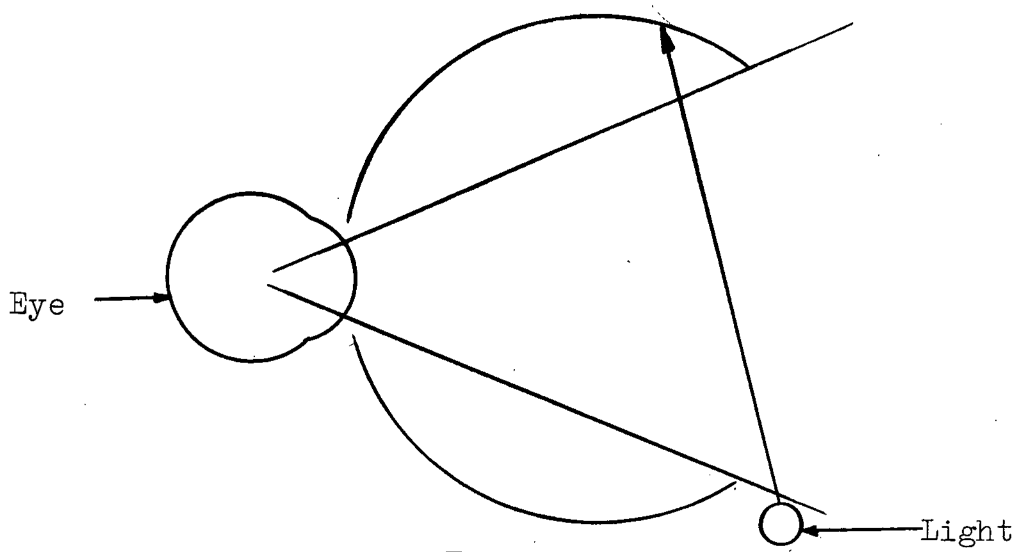

Figure 5.4
Ulbricht sphere illumination of the eye

confirmed when the simulation tests were performed since no clear transition was evident in the photomultiplier signal (see figure 5.10 configuration "g").

It was thus necessary to consider direct illumination of the eye. This is permissible if the light is positioned so that the corneal reflection never obscures the pupil. For a maximum pupil diameter of 1 cm., computer analysis of the corneal reflection indicates that the above requirement is satisfied if the line of sight is never less than 45 degrees from the position of the light source. This does not represent a severe limitation if the illumination can be performed with a single light source (for example configurations d, e, f, or h in section 5.5). If a multi-light source is used, careful positioning and limitation of eye movements will be required.

5.5 Lighting configurations

In choosing the source of light to illuminate the eye, the principal consideration is the spectral distribution compared to the spectral response of the S1 photocathode. Figure 5.5 shows these data for several sources[29]. This forcibly demonstrates that very little of the infra-red spectrum is actually useful with an S1 photocathode. A good source is one which also has energy in the visible portion of the spectrum.

One system requirement however, is that the subject should not be disturbed by the light. This means that filtering must be performed to remove some of the visible light. Figure 5.6 shows some suitable filters. It is evident that the 87 or 88A filters would provide practically "invisible illumination" of the eye by filtering out all the visible region. However these also remove a rather large portion of the S1 response curve.

Medically it is known that light of wavelength 6500 Å or greater does not affect the process of dark adaption. For these purposes then, either filter number 70 or 92 would be suitable. The tests were performed using four filters: 87, 70, 92, and 25.

On the basis of the above information, several arbitrary lighting configurations were constructed. Following are descriptions of these configurations:

a. three indicator lamps (GE 1477) mounted in a circle about 2" from the eye, each with a reflector directing the

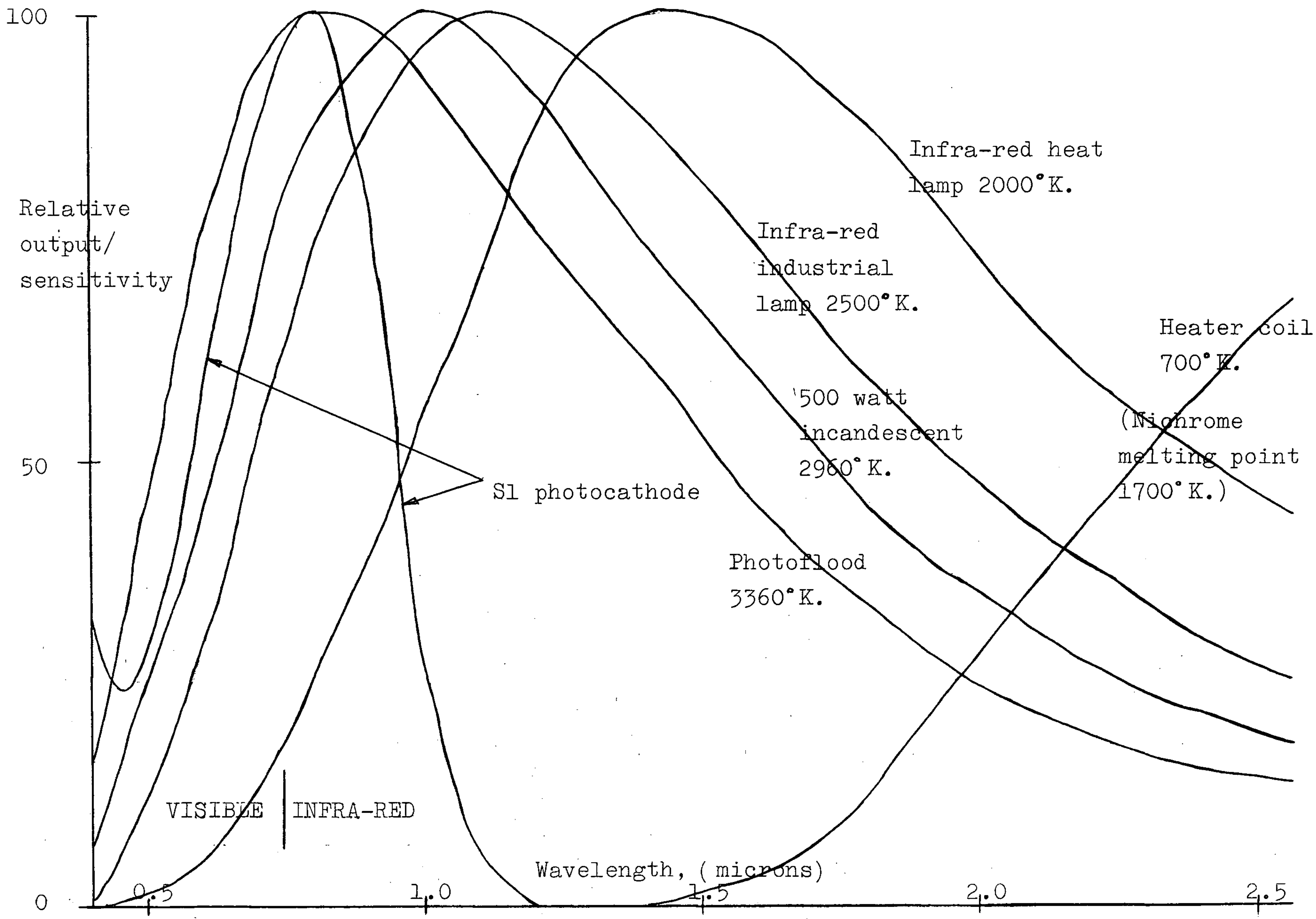

Figure 5.5 Comparison of light sources for use with S1 photocathode

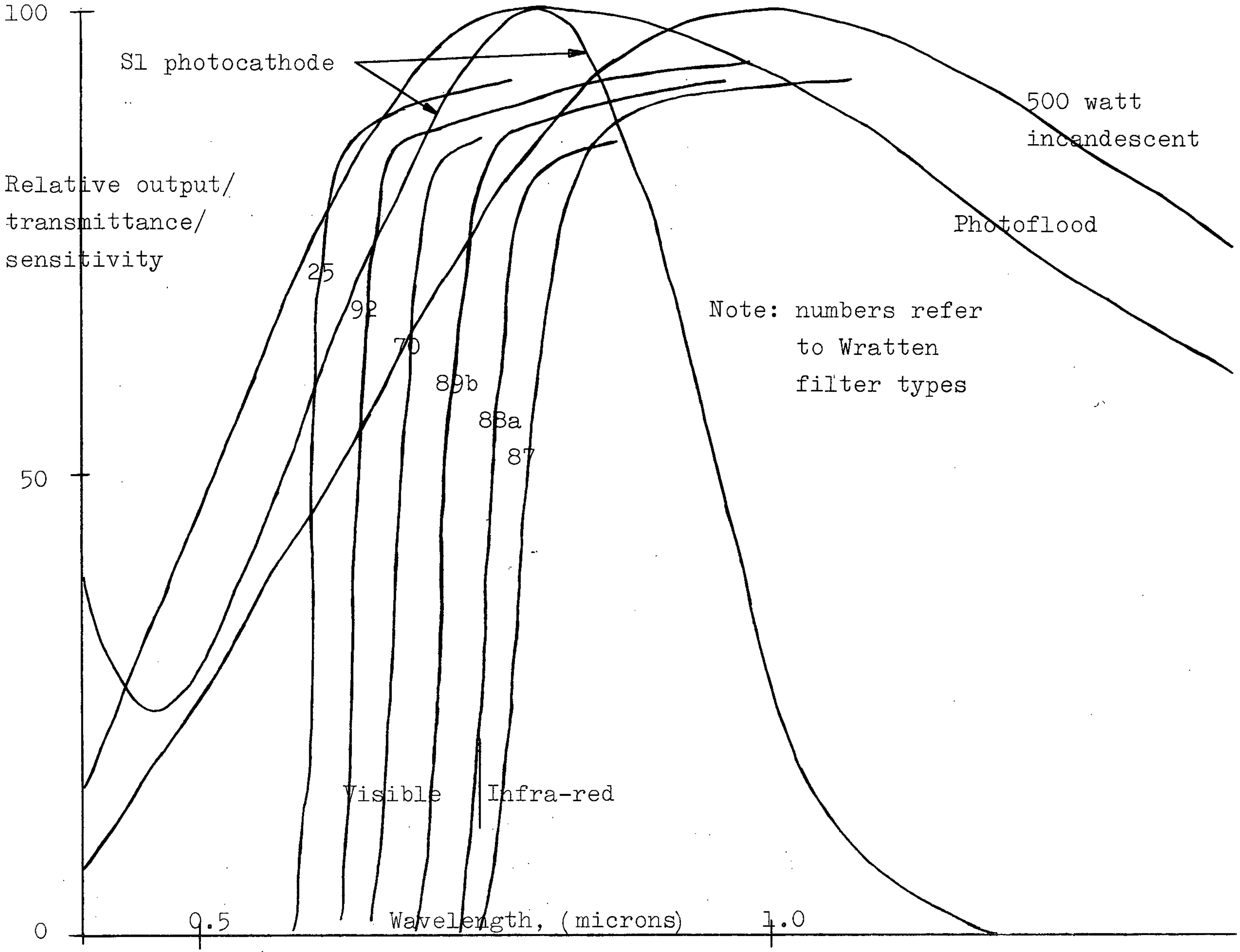

Figure 5.6 Comparison of filters for use with S1 photocathode

light onto the eye. In this case they are operated at rated voltage (25 volts).

b. identical configuration to "a" only run at 35 volts.

c. four indicator lamps (GE 6S6) mounted in a similar manner to the three 1477's in "a". They are operated at rated voltage (145 volts).

d. a 300 watt slide projector with the focusing lens fully extended and positioned about 3 inches from the eye. This concentrates the light onto the eye and a small area around it. This is run at 145 volts.

e. a 500 watt projector with condenser optics only, positioned in a similar manner to the projector in "d". This is run at 145 volts.

f. identical configuration to "d" except that a good diffuse reflector is placed on the opposite side of the eye from the projector. It is positioned so as to improve the uniformity of the illumination.

g. the integrating hemisphere described in section 5.4 illuminated with the 300 watt projector (run at 145 volts).

h. the 300 watt projector with condenser optics only, positioned as in "d". In addition, a diffusing surface is positioned for uniformity of illumination as in "f". This is run at 145 volts.

The diffusing surface used in configurations "f" and "h" did not affect the pupil-iris boundary, but did improve the uniformity of illumination on the eye without creating an additional corneal reflection. Spectral distribution data were not available for the small indicator lights used in configurations "a" and "c", but they were included in the experiments because they are relatively small and thus would be convenient if the results were favourable.

5.6 Reflectivity of the eye to infra-red light

As a preliminary indication of the usefulness of infra-red light, photographs of real eyes were taken using infra-red light and infra-red film. The film is sensitive in the region from 6700 Å to 8700 Å, so it is not identical to the S1 photocathode. Figure 5.7 (a), (b) and (c) show three such photographs. Subject (a) had brown eyes, subject (b) had blue and subject (c) had dark brown. Subject (c) is especially interesting since the whole of the iris and the pupil appeared dark brown under visible light. The pupil was barely distinguishable from the iris. These results indicate good contrast exists between the iris and the pupil when using infra-red light.

Figure 5.7 (d) and (e) are photographs of the two artificial eyes used in the experiment. It is apparent that the differences in the amount of reflected light between false eyes and real eyes are comparable to the differences between individual real eyes. Since the equipment necessary to perform the simulation experiment on real eyes was not available, the artificial eyes were used. The equipment required consists mainly of a head rest with a skull strap, a fixation point for the subject, and a means of mounting and adjusting the equipment to enable accurate focusing to be performed.

In the course of the simulation experiments, both the

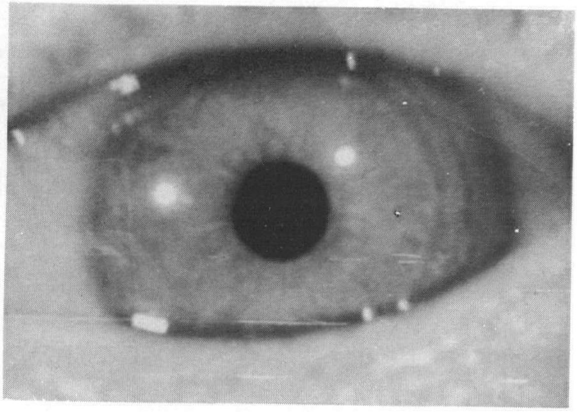

(a)
Brown eye (real)

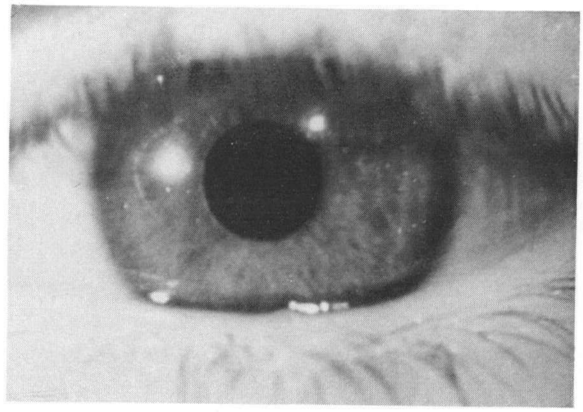

(b)
Blue eye (real)

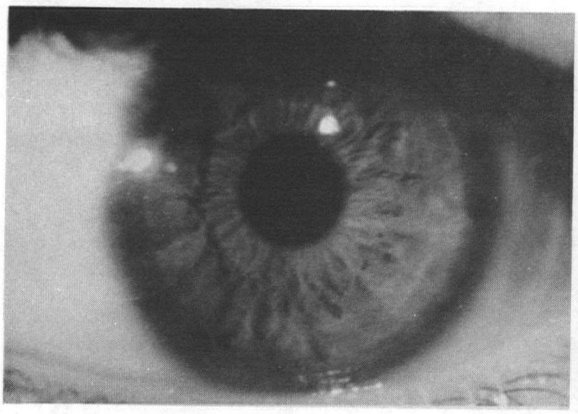

(c)
Dark brown eye (real)

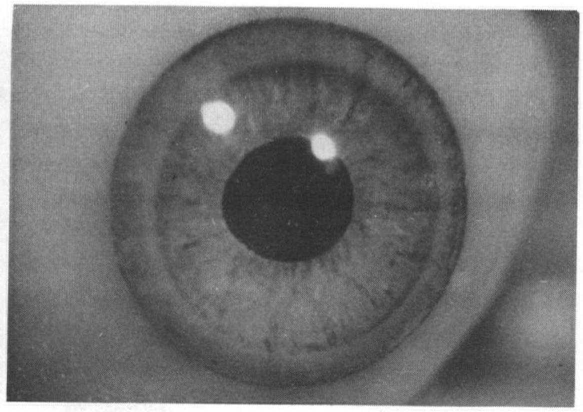

(d)
Blue eye (artificial)

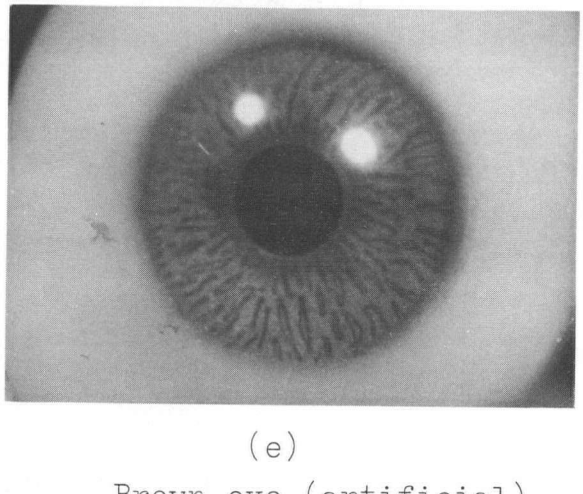

(e)
Brown eye (artificial)

Figure 5.7

Infra-red photographs of eyes

blue and the brown artificial eye were used for part of the work. This provided comparative information about blue and brown irises under infra-red light. The results appear in figure 5.8. The conclusion is that in all cases the brown iris has the higher reflectivity.

In determining the contrast between the pupil and the iris, the following procedure was used. By moving the aperture and observing the photomultiplier output, it was possible to locate the pupil. When the aperture was moved from the pupil to the iris in either direction, the current increased at first quite quickly as the actual boundary was crossed, and then slowly and to a lesser extent due to variations in the illumination on the iris. The general shape of the signal is shown in figure 5.9. The value used as the "iris current" was the lowest value beyond the

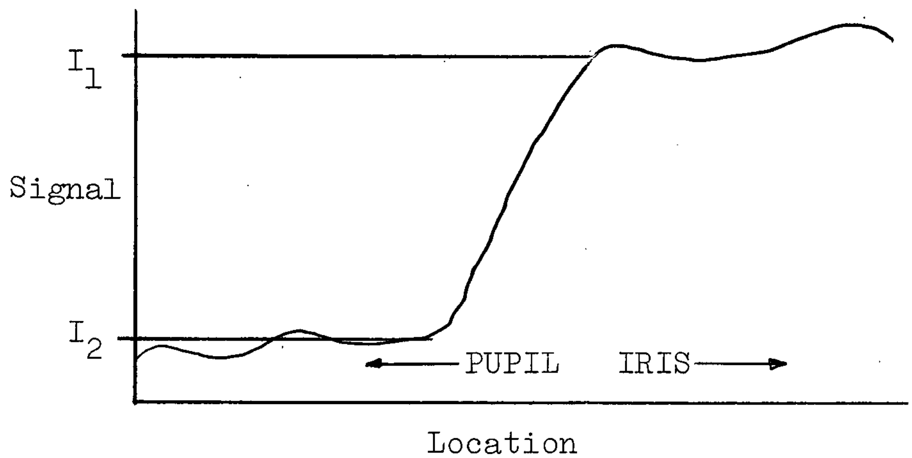

Figure 5.9
Determination of pupil-iris contrast

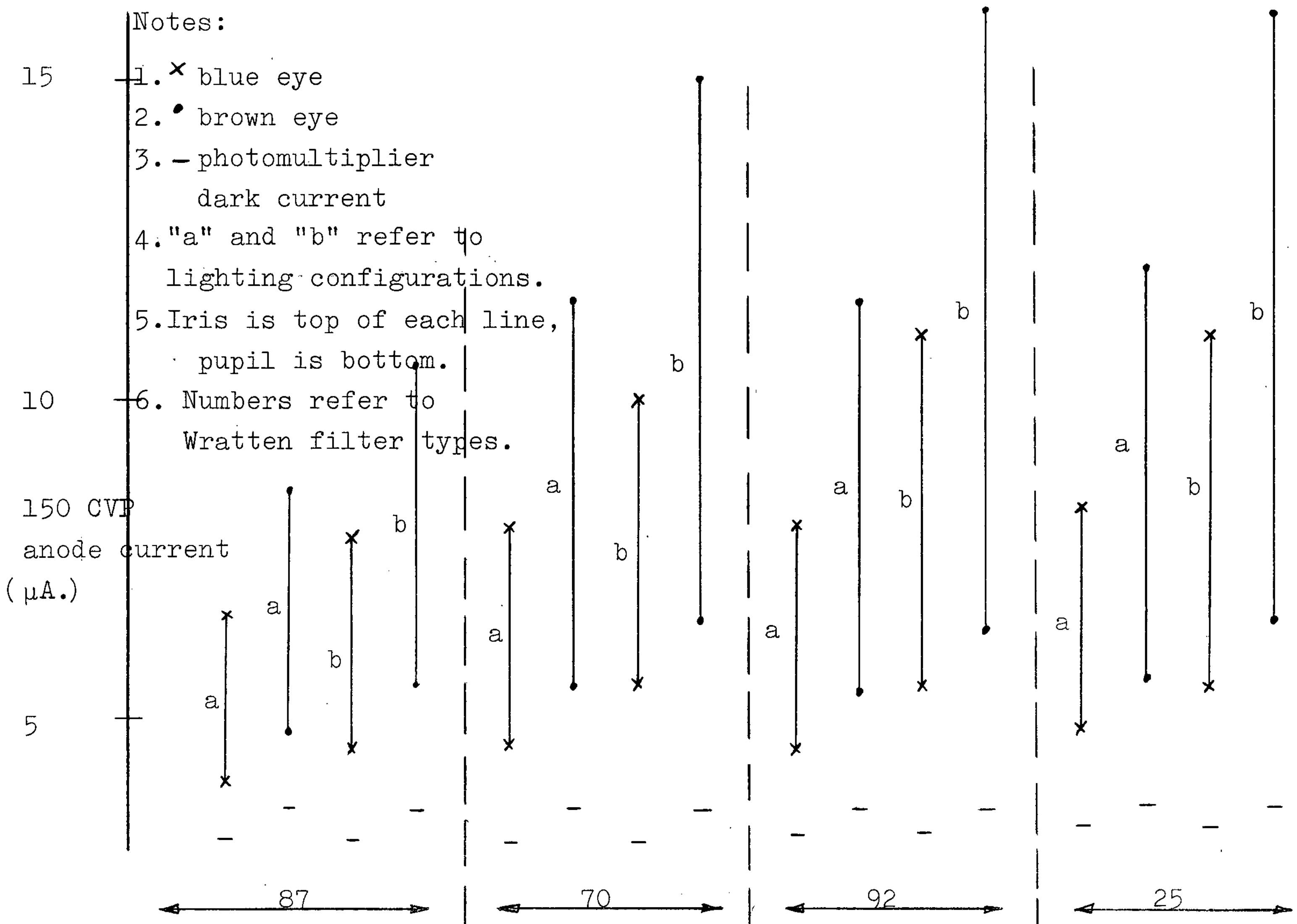

Figure 5.8 Relative reflectivity of blue and brown eye under infra-red light.

boundary - I_1 in the figure. The pupil was fairly flat so the average value I_2 was used.

5.7 Simulation results

Performing the experiments as described above yielded values for pupil current and iris current for the various configurations used. In this case however, the quantities of interest are the pupil and iris signals. These are defined as the pupil current less the dark current and the iris current less the dark current respectively. The values thus obtained for the pupil signal and the iris signal are successively used as I_E in equation 5.4 to obtain the corresponding values of predicted image dissector cathode current density. These are plotted in figure 5.10 where the top of each line represents the iris signal and the bottom represents the pupil signal.

The parameters in equation 5.4 are as follows:

$G_E = 10^6$ (see $V_b = 1300$ table 5.1)

$A_k = 2.25\pi$ cm.^{2} (full area of 150CVP photocathode)

$A_E = 9.23 \times 10^{-4}$ cm.^{2} (number 80 drill).

The remaining values are given on figures 5.2 and 5.3.

Each reading was performed first with two of the appropriate filters and then repeated with only one. This required a shutdown for each change and thus a double-check of each reading. By subsequently checking that the two readings differed by a small amount, this ensured repeatability of the readings. The dark current was checked before and after each reading. Because

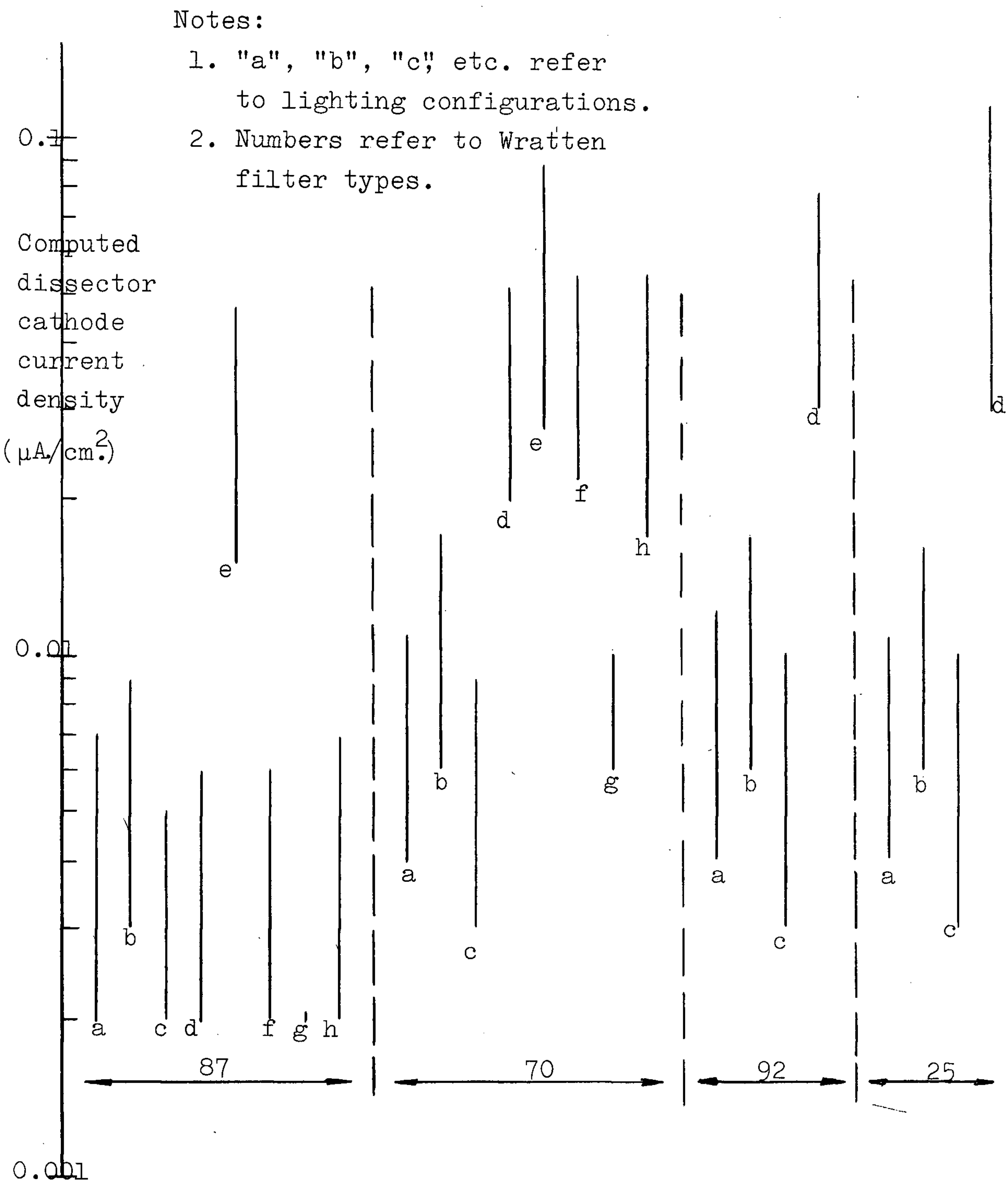

Figure 5.10
Image dissector evaluation for various infra-red lighting configurations

the small indicator lamps (GE 1477) were being run over-voltage, they tended to blacken in use. New bulbs were used for the final readings.

CHAPTER 6

Conclusion

The purpose of this research was to study the various methods for measuring eye movements and to attempt to design a better method. It is believed that the system described here achieves this. Although the complete system has not been constructed, extensive testing of the electronic circuitry and careful simulation of the photoelectric interface enable the system's performance to be accurately predicted. The following improvements over other methods have been achieved : (1) very large eye movements can be tracked ($\pm$ 45 degrees); (2) both vertical and horizontal movements are measured; (3) continuous tracking of all eye movements is assured including the fastest saccades; (4) the system causes very little interference with the subject's normal vision (one eye looks through a half-silvered mirror, the other has normal vision); (5) since there are no attachments to the subject's eye or face, a large number of subjects can be easily examined with the system; (6) when the output is interrupted by eye blinks, it is re-attained automatically in approximately 10 msec.; (7) the output of the system is in real time; (8) in addition to the eyeball position, the system measures pupil diameter (up to 10 mm.).

The only apparent short-comings of the system are: (a) the subject must wear a head cap on which some of the system components are mounted and (b) the resolution of the system is not quite sufficient to measure accurately the miniature eye movements.

The former limitation is not too serious and its effect can be minimized by carefully designing the cap for light weight, comfort, and balance. With regard to the latter limitation, the actual resolution of the final system cannot be accurately predicted because it is affected by the movements of the head relative to the measuring apparatus (caused by the subject's pulse). It is easy to limit these movements so that they cause apparent eye movements no greater than $\frac{1}{2}$ degree. The resolution of the electronics is currently better than this and can be improved, if necessitated by even better limitation of the head movements.

The electronics section of the system has been constructed and tested (see chapter 3). Its performance is completely satisfactory. The remaining section of the system is the photoelectric interface (image dissector and optics). This section was not constructed but a careful simulation of it (see chapter 5) shows that the image dissector should operate with effective signal-to-noise ratios (see section 4.6) of the order of 5 to 10 (see figures 4.16 and 5.10). Improvements are suggested in appendix J which further increase the predicted signal-to-noise ratio.

It is thus predicted that the proposed complete system will operate successfully and will more than satisfy the requirements of section 1.4. It is recommended that the specified image dissector (see chapter 4) be purchased and the lighting and optical sections of the system be constructed.

Appendix A

Characteristics of the human eye

It is convenient to assemble in one place a concise description of the eye as used in this work.

Figure A.1 shows the main internal features of the right eye from above.

A simplified model of the eye has been constructed using data from various sources (chiefly references 31 and 6). The dimensions shown in figure A.2 vary from person to person; thus the values shown are approximate only. Biologically the eye has no single point which is its centre of rotation. Likewise, the eye and cornea are not parts of perfect spheres nor is the pupil actually a circular opening on a flat iris. However, the deviations are minor and the model shown in figure A.2 is useful in this case.

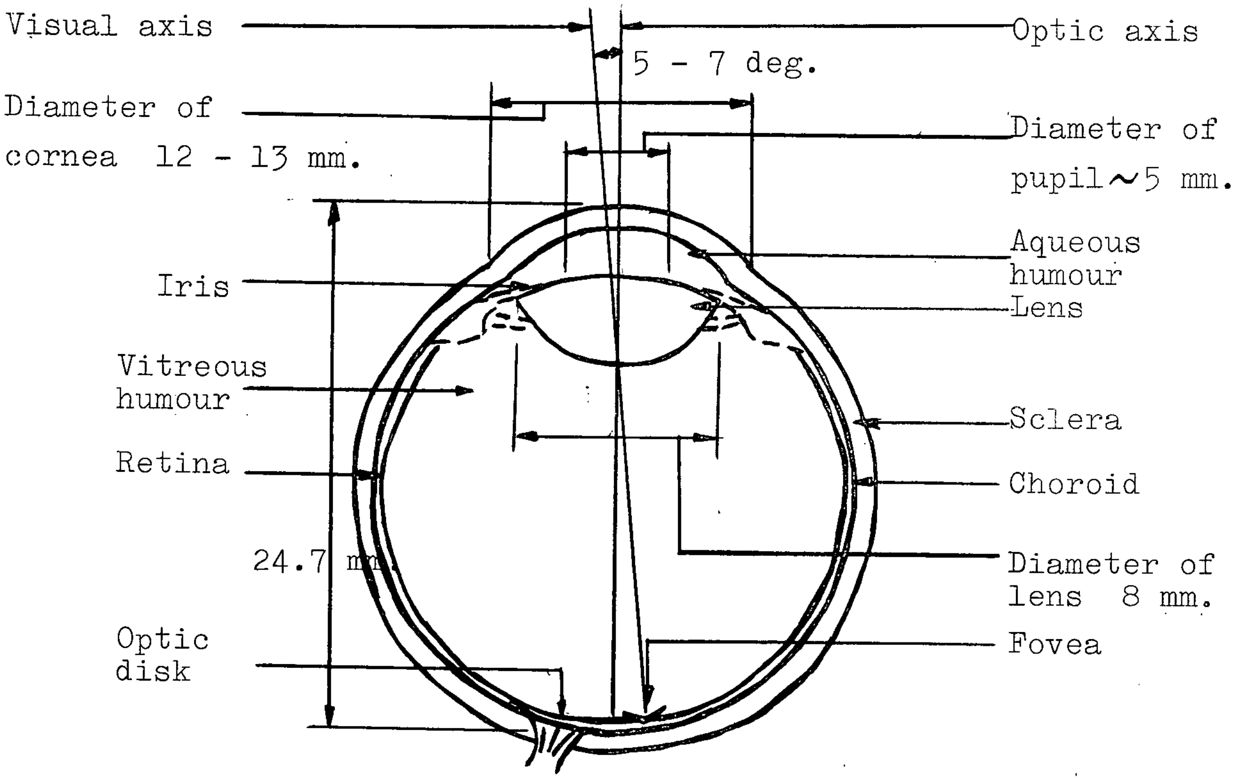

Figure A.1
Main features of the eye.

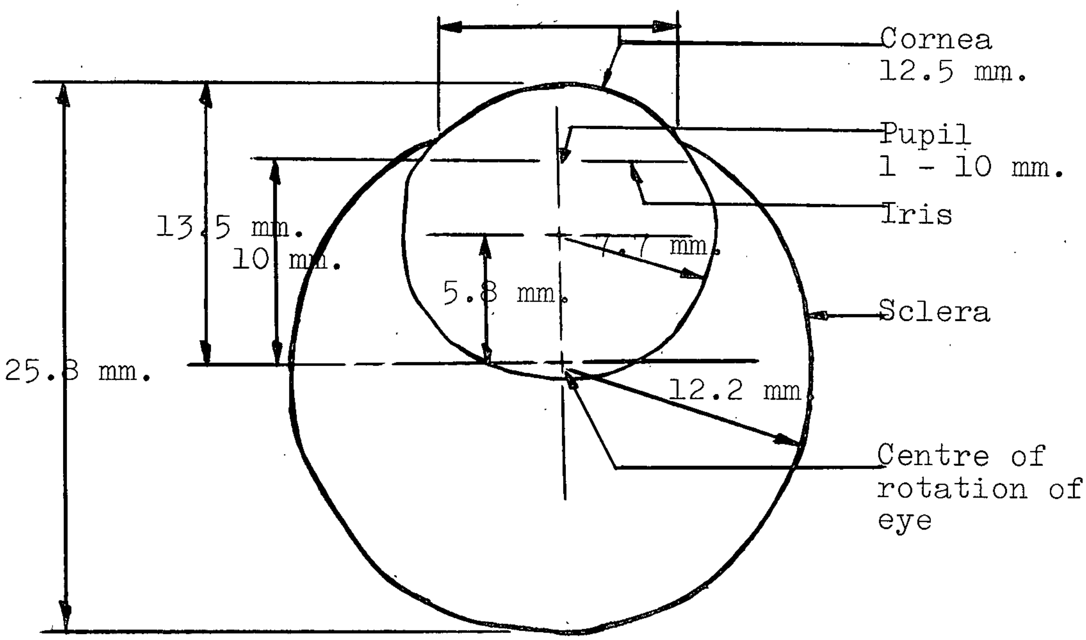

Figure A.2
Model of the eye.

Appendix B

Sample and Hold

The sample and hold circuit (after reference 32) shown in figure B.1 is the basic element of the analog buffer and the memory. The voltage waveform appearing at the input is sampled during the load signal and the latest sample is held until the next such signal. For inputs between $\pm$ 5 volts, the DC accuracy is approximately 10 mv. for a 2 μsec. load pulse.

The load signal is a 3.6 volt pulse to ground which turns on Q8. This turns on the current source Q9, thus activating the comparator Q3 and Q4. Since the comparator operates with respect to the output level rather than the capacitor (C3) level, offset and drift in the output buffer are cancelled. The comparator controls the two constant-current charging sources Q5 (charge up) and Q10 (charge down) thus controlling the charge on the storage capacitor C3. Q6 is a source follower (FET) providing high-impedance readout of the capacitor and Q7 is the output buffer.

The sample and hold number 9 in the system required a zeroing capability as part of the system initialization (zero pupil-diameter signal). Figure B.2 shows how this was performed. Signal 88 is a short monostable pulse which occurs during the initialize period. It sets the flip flop shown in figure B.2 which grounds the input to sample and hold number 9. This signal is also used as a load signal for this sample and hold so zero volts is loaded into this sample and hold. Thus the diameter signal is zeroed. Signal 89 is an inverted version of 88; thus a short time after 88 falls to zero (thus ending the load interval for the sample and hold), the flip flop is reset. Then the regular input is applied to the sample and hold through the FET switch (more detail about these switches is found in appendix C).

The resolution of these circuits when sampling a constant input is less than 10 mv. However, the error varies with the voltage being sampled. Thus, as the eye moves to different positions, a variable voltage offset is introduced creating a slight non-linearity.

It is very difficult to measure the system performance of this circuit to any accuracy. The reason for this is that during the load pulse, the sample and hold output contains oscillations which are larger than the offset. It is clean after this pulse, but then the input is being switched to another value (maximum delay before this switching begins is 600 nsec.). Thus, measurement of the error with an oscilloscope differential amplifier is impossible. Less accurate measurements can be made by carefully calibrating a dual-trace amplifier. Measuring the error in this manner for voltages near zero is successful but it is required that these measurements be made over the whole working range of the sample and hold. However, amplifier saturation and insufficient zero suppression limit the sensitivity that can be used. Also, since two amplifiers are being used, drift introduces another error. Using this method, it can only be said that the error is less than 0.1 volt over the whole range (± 5 volts). If the error were 0.1 volt, the limit on the system resolution would be 1.8 degrees of eye movement (see section 3.7).

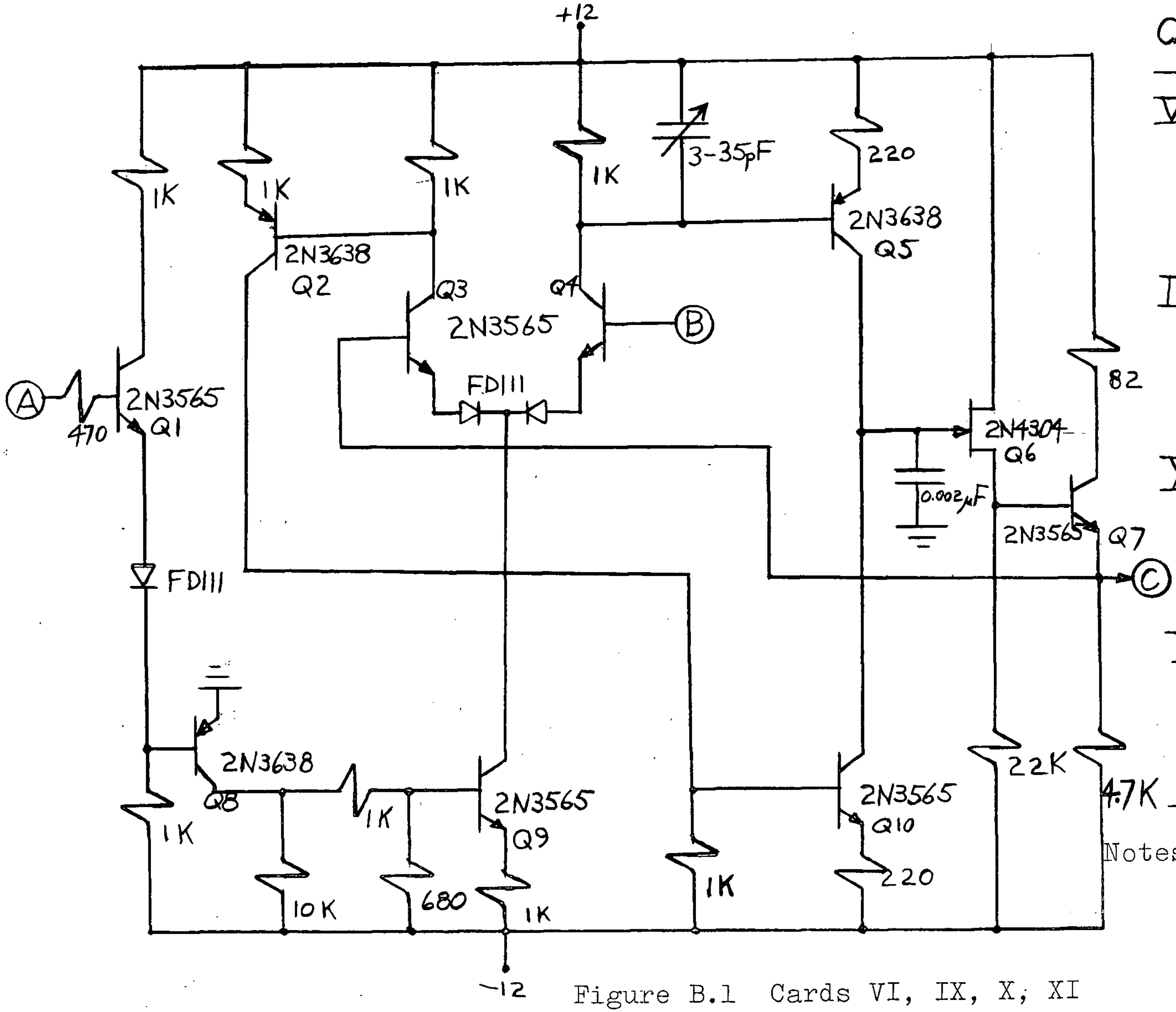

Figure B.1 Cards VI, IX, X, XI

CARD	SAMPLE & HOLD No.	A	B	C
VI	1	15 I	50 VIII	71 VII
	2	16 I	50 VIII	72 VII
IX	3	19 I	46 VIII	59 XIII
	4	20 I	47 VIII	60 XIII
X	5	19 I	52 VIII	61 XIII
	6	20 I	53 VIII	62 XIII
XI	7	19 I	55 VIII	63 XIII
	8	20 I	56 VIII	64 XIII

Notes: 1. Signal 63 is system X output.
2. Signal 64 is system Y output.
3. See notes 2 and 3, figure B.2.

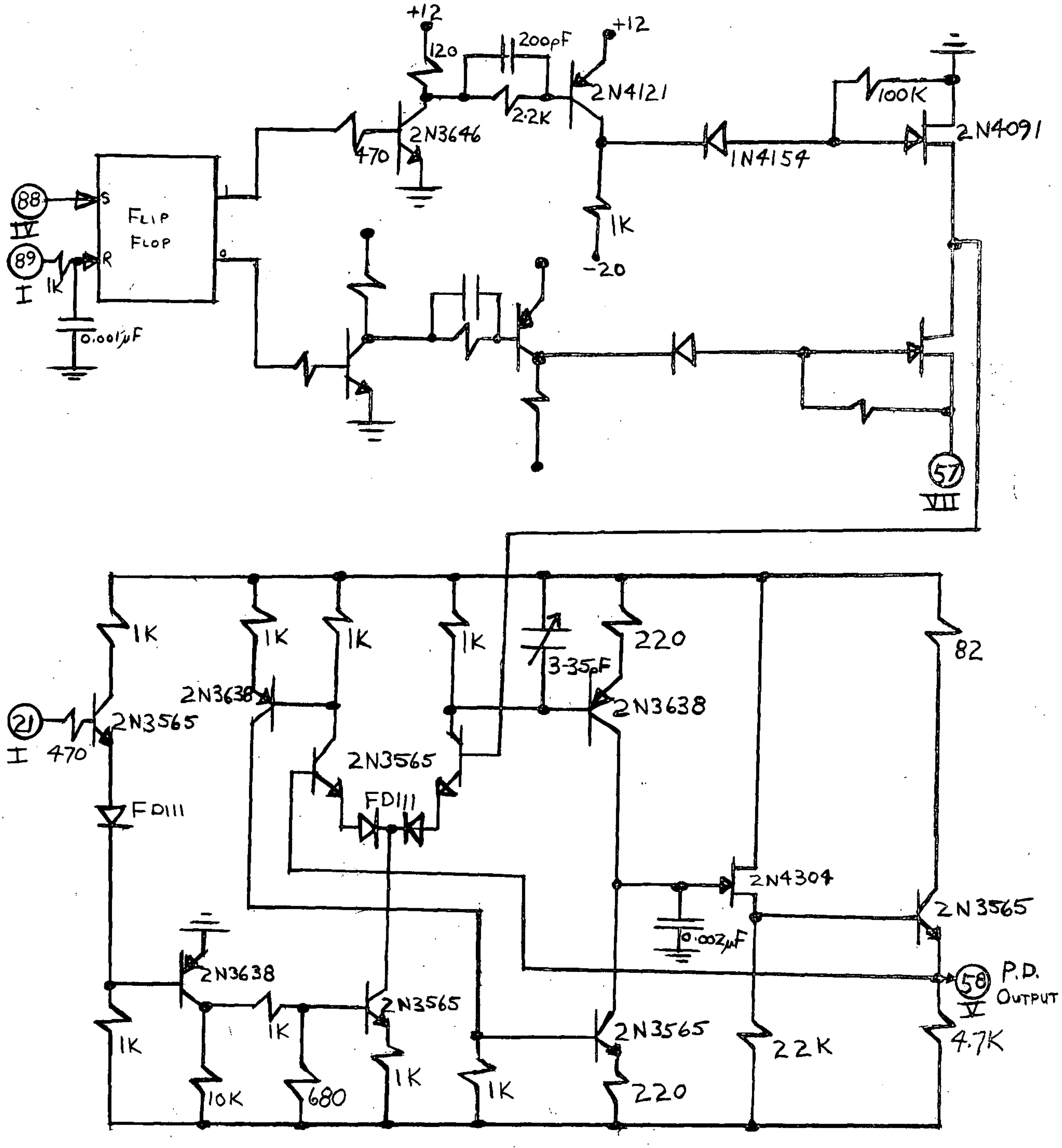

Notes: 1. Signal 58 is pupil dia. output from system.
2. Circled numbers are inputs or outputs for each card.
3. Roman numerals indicate the card to which the respective signal is connected.

Figure B.2 Card XII

Appendix C

Switching

This includes the analog switch and the various counter-controlled switches (see figure 3.2). The switching is performed with field-effect transistors with a specified "on" channel resistance of 30 ohms. The gate-drive circuits were designed for switch input levels between ±5 volts. The gate drives operate as saturated switches which supply +12 or -20 volts to the diode on the FET gate. The +12 is sufficient to keep the diode off for all voltage levels at the FET source so the gate-source voltage is zero and the switch is on. For -20 the diode is on so the gate is held at -20. Thus the pinch-off voltage of 10 volts is maintained for signal levels down to -10 volts at the source (5 volts more than necessary).

The analog switch is on card XIV (figure C.1). The gate drives for this switch are on cards III and IV (figures E.5 and E.6 respectively).

The counter-controlled switches in the output section appear on card VIII (figure C2.). The gate drives are on card III (figure E.5).

The counter-controlled switches in the scan-computation and feedback section appear on card XIII (figure C.3).

A switch was also necessary to preset sample and hold number 9 to zero volts. The switch and the gate drives appear on card XII (figure B.2).

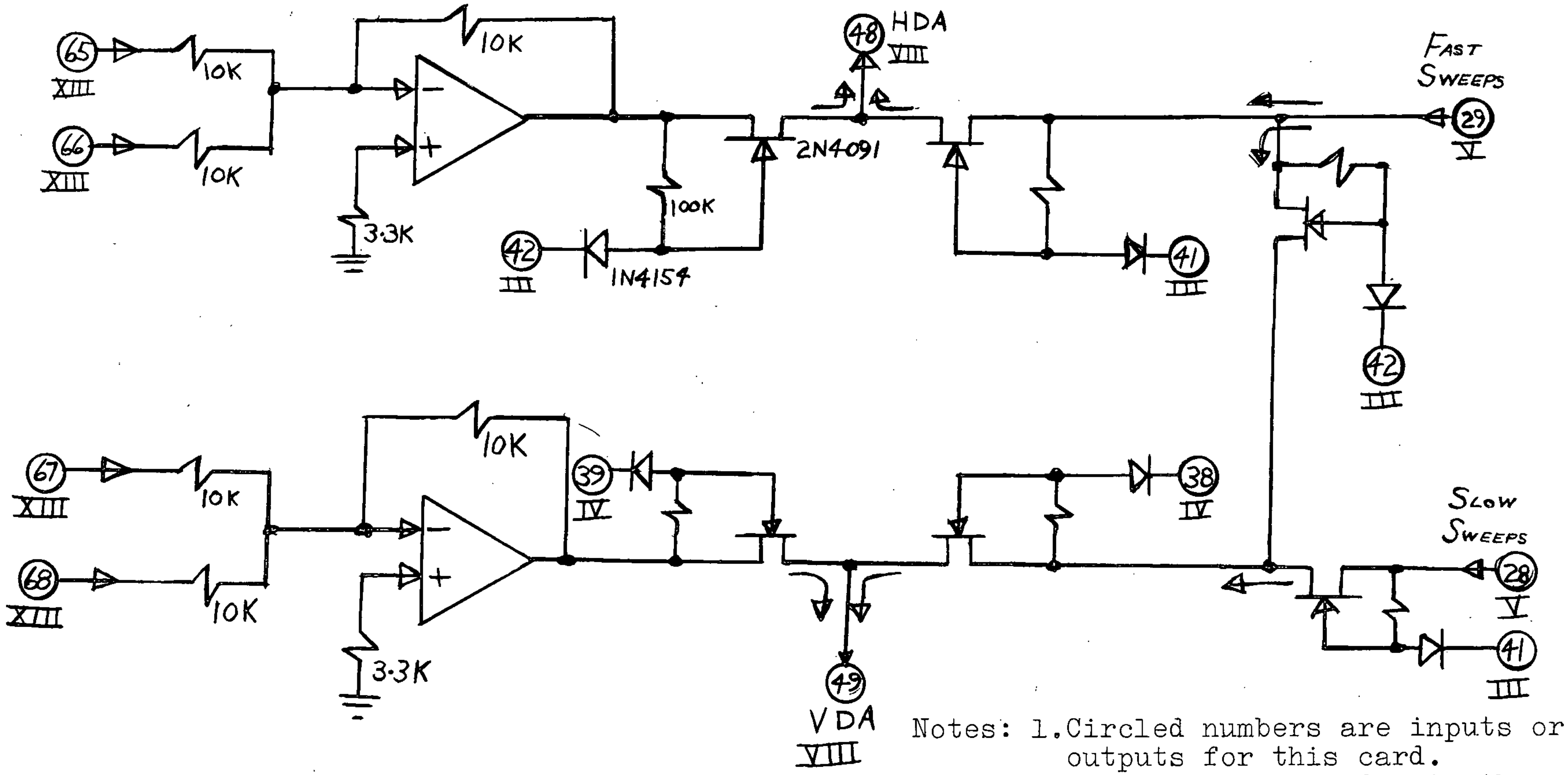

Figure C.1 Card XIV

Notes: 1. Circled numbers are inputs or outputs for this card.
2. Roman numerals indicate the card to which the signal is connected.
3. "HDA" and "VDA" are also connected to the horizontal and vertical deflection amplifiers respectively.

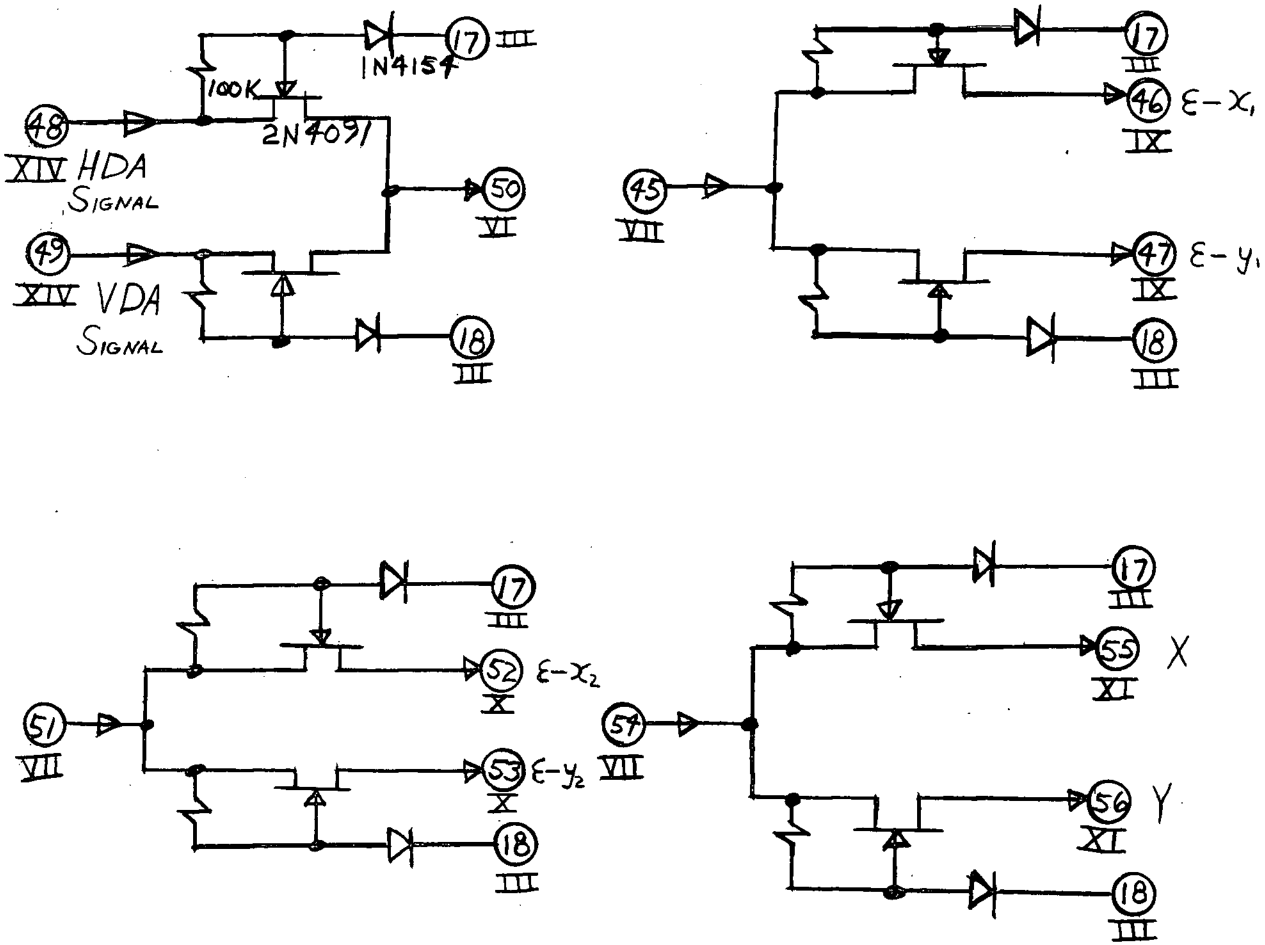

Figure C.2 Card VIII

Notes: 1. Circled numbers represent input or output signals for this card.
2. Roman numerals indicate the card to which the respective signal is connected.

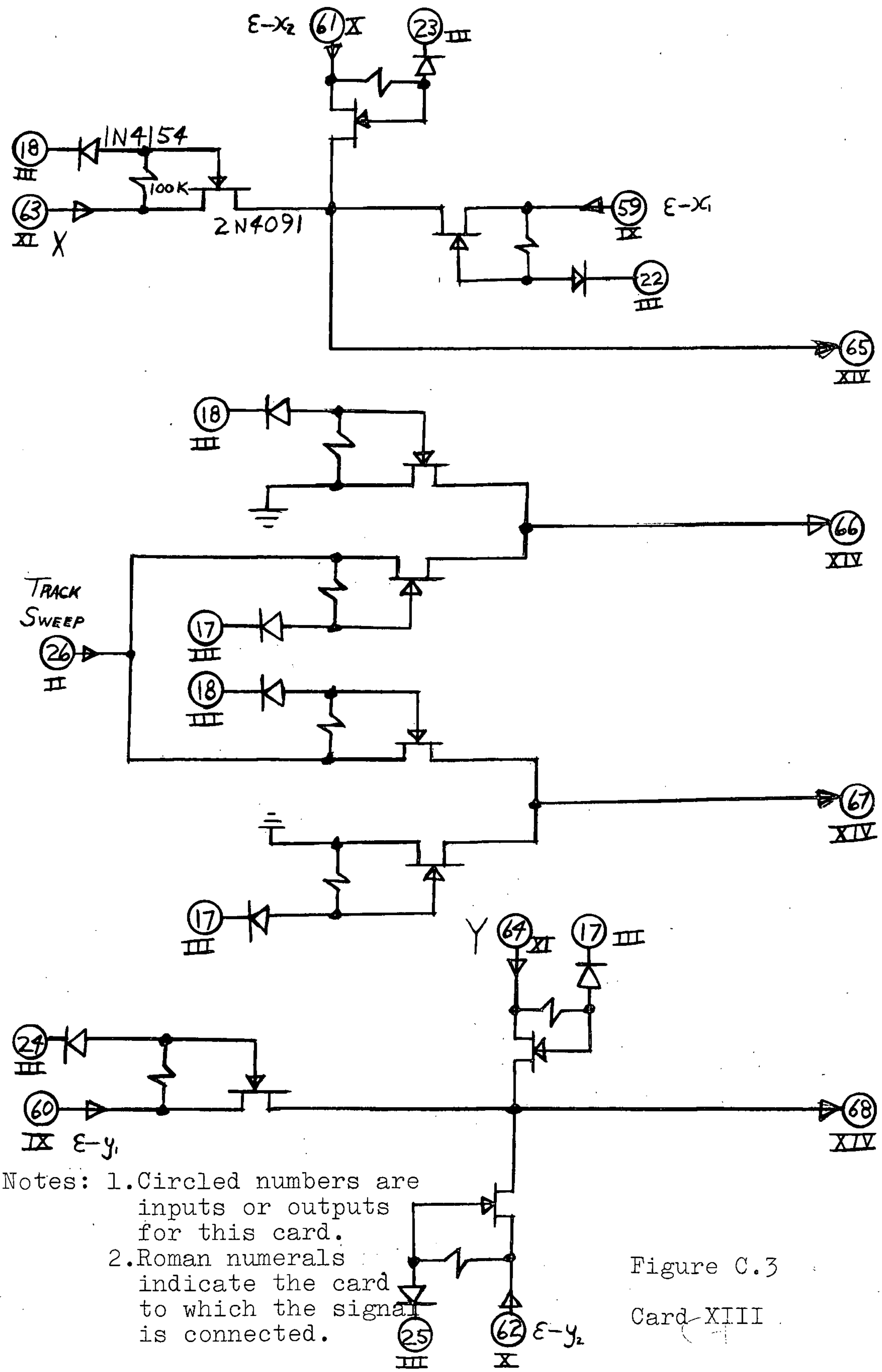

Notes: 1. Circled numbers are inputs or outputs for this card.
2. Roman numerals indicate the card to which the signal is connected.

Figure C.3

Card XIII

Appendix D

Analog Computation

The various computational requirements were performed in the standard manner using Nexus SQ 10a operational amplifiers. Output computation is shown on card VII (figure D.1). Scan computation is shown on card XIV (figure C.1).

The specified minimum slewing rate for these amplifiers (for full output) is 1.1 volts/μsec. Thus it was necessary to allow several μsec. for slewing the maximum possible in this application. Experimentally the maximum time required for -5 to +5 volts slewing was approximately 13 μsec. In the system, 16 μsec. delays were allowed.

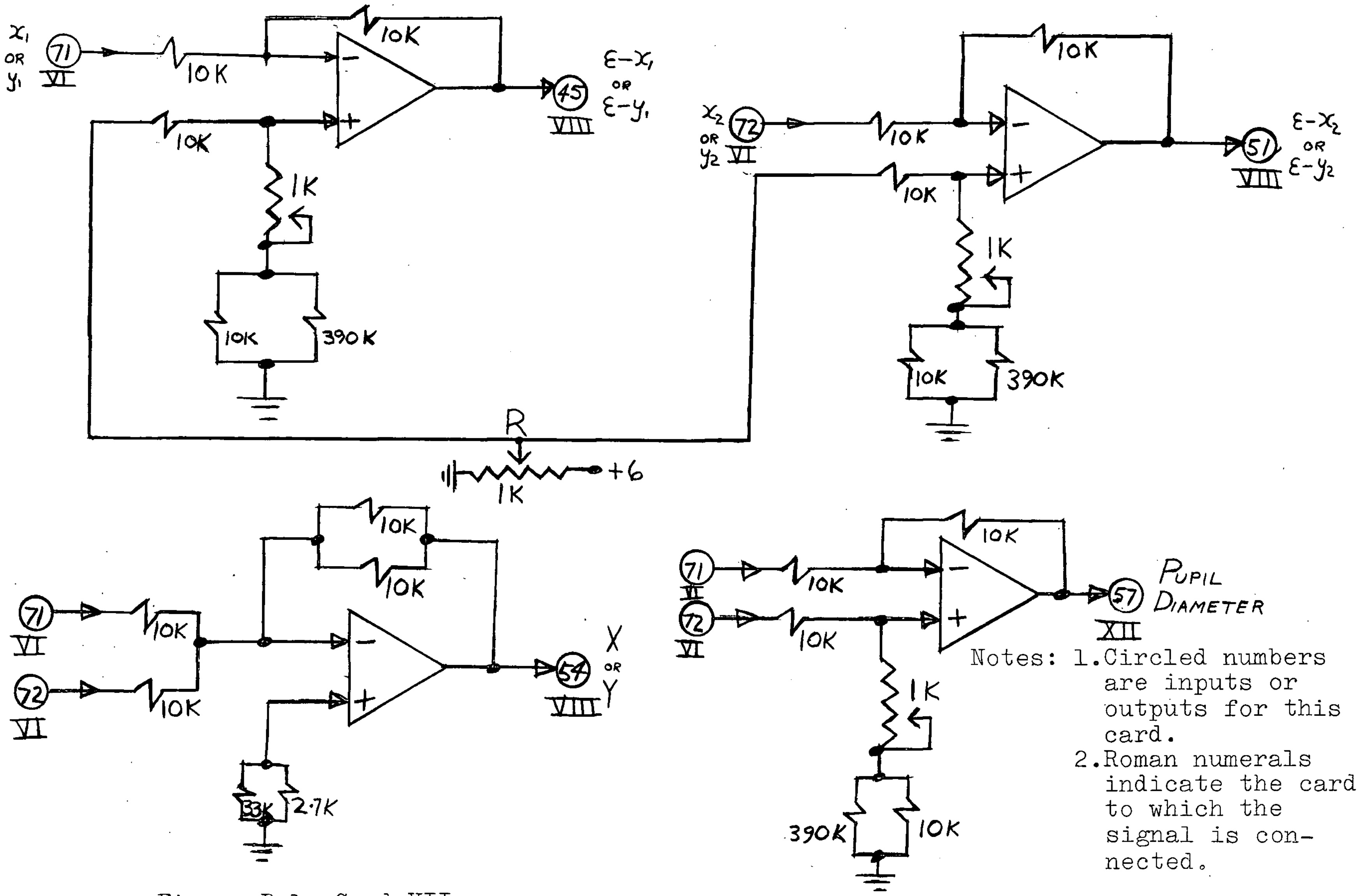

Notes: 1. Circled numbers are inputs or outputs for this card.
2. Roman numerals indicate the card to which the signal is connected.

Figure D.1 Card VII

Appendix E
Control section

The logic was performed using Fairchild medium-power micrologic components. The inversions and the various NAND and NOR gates were performed in the normal manner with μL914; the set-reset flip flops and the monostables were also realized with μL914; the JK flip flops for the two-bit counter were μL923; buffers were μL900. The wiring diagram to make a monostable is shown in figure E.1.

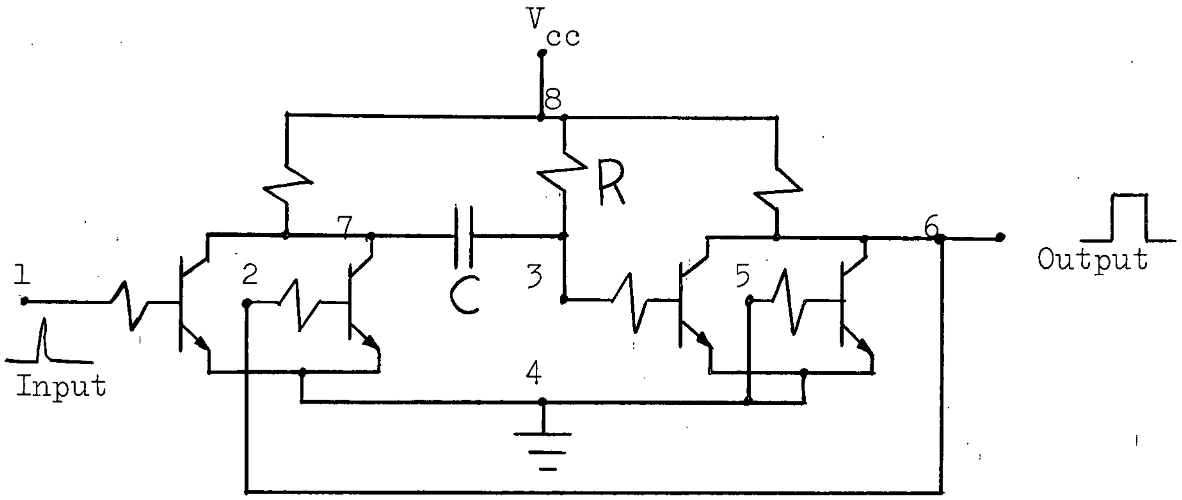

Figure E.1
Wiring diagram for a monostable multivibrator

Figure E.2 shows the photomultiplier voltage divider, the video detection circuits (μA710 is the voltage comparator) and the video blanking.

Figure E.3 shows the first section of the control logic.

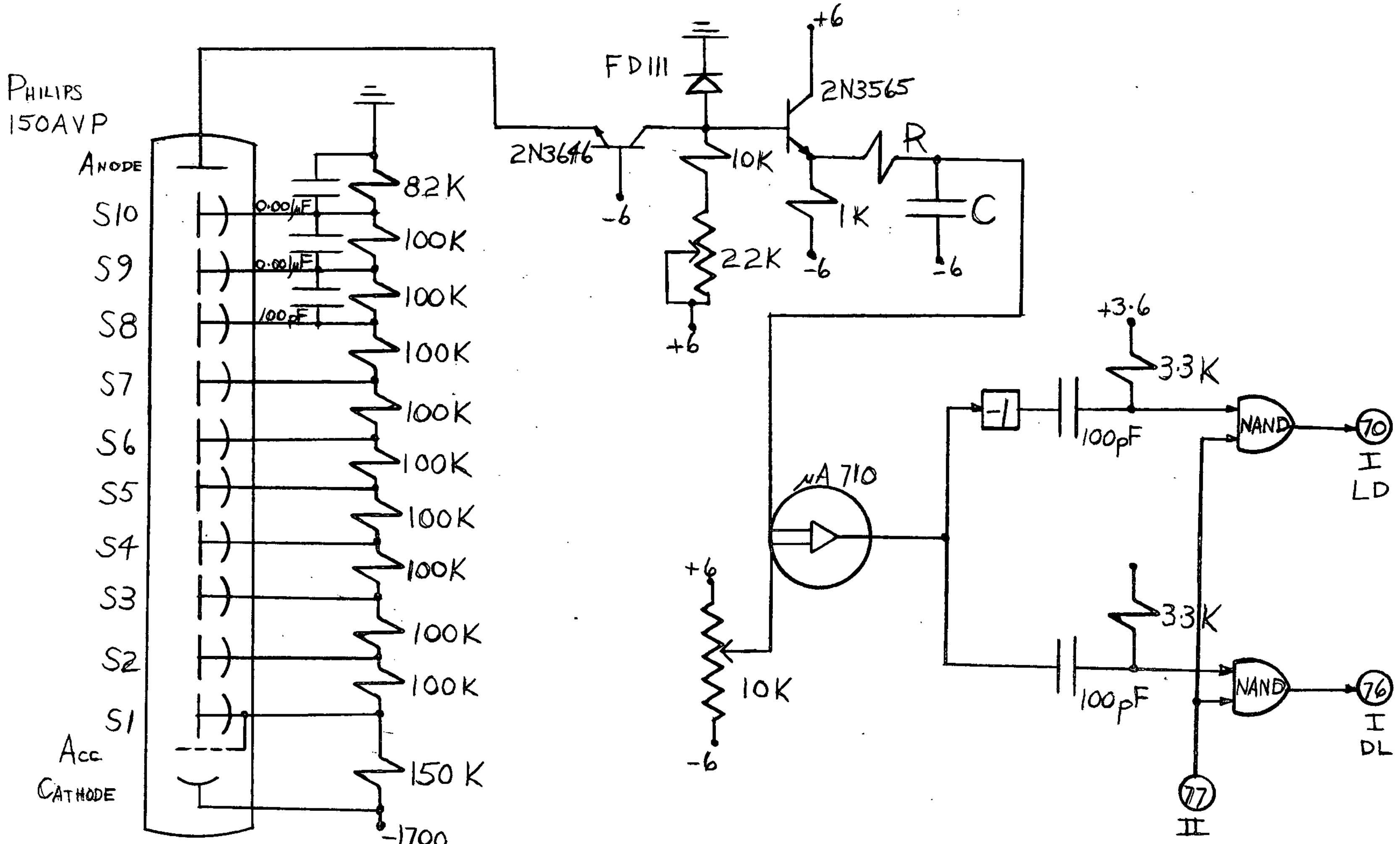

Figure E.2 Video

Notes: 1. Circled numbers represent input or output signals for this card.
2. Roman numerals indicate the card to which the respective signal is connected.

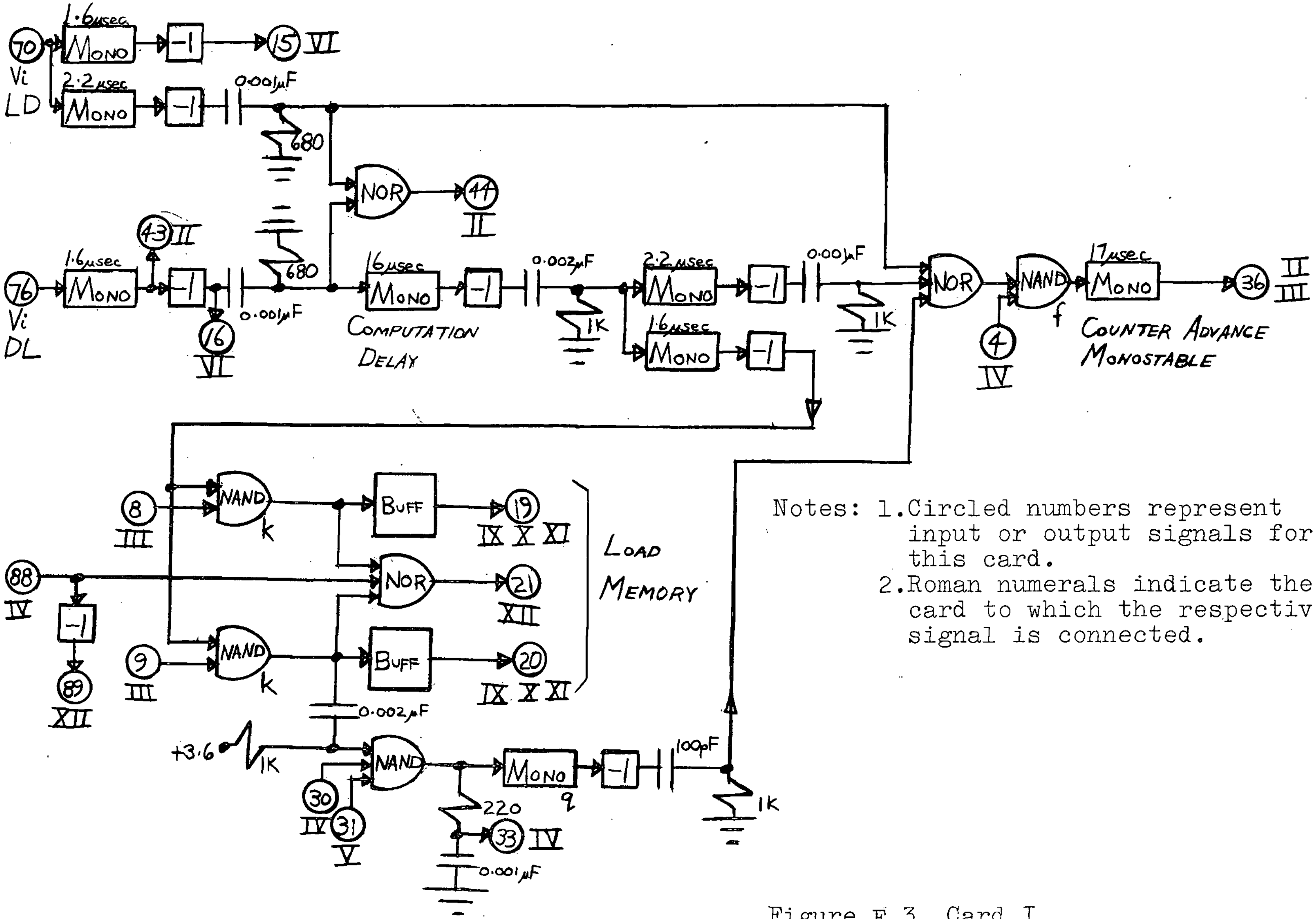

Notes: 1. Circled numbers represent input or output signals for this card.
2. Roman numerals indicate the card to which the respective signal is connected.

Figure E.3 Card I

The two NAND gates marked "k" are controlled by the counter. Their function is to steer the load pulse to the proper section of the memory according to the counter setting. For a counter setting of 00 or 01, the pulse is steered to 19 thus loading sample and hold numbers 3, 5, and 7. For a counter setting of 10 or 11, the load pulse goes to 20 so sample and hold numbers 4, 6, and 8 are loaded.

The "search mode B only" signals on figure 3.2 are performed by 43, 33, and the monostable "q".

The input 88 provides a load pulse to the pupil diameter (load memory 21) as part of the "preset sample and hold number 9 to zero volts".

The NAND gate "f" performs the function "track mode only".

Figure E.4 shows the track mode flip flop, the track sweep generator, and the generation of the video blanking signal.

The NAND gate 1 performs the function "track mode only".

The NAND gate 6 allows video blanking from other sources than the track mode flip flop during search mode. Signal 85 provides line-flyback blanking during the normal search raster. Signal 84 provides blanking between search mode A and mode B. Signal 86 provides blanking while the system is initializing.

The value of 2ε is set by the potentiometer R. When the sweep reaches the value necessary to turn on this transistor, a pulse is generated (signal 10) which initiates search.

Figure E.5 shows the two-bit counter and the gate drives to the counter-controlled switches. Signal 5 initially sets the counter to 00 for search. During search mode, 2 is "high" so that the pulse which appears on 6 loads the counter to 11 for

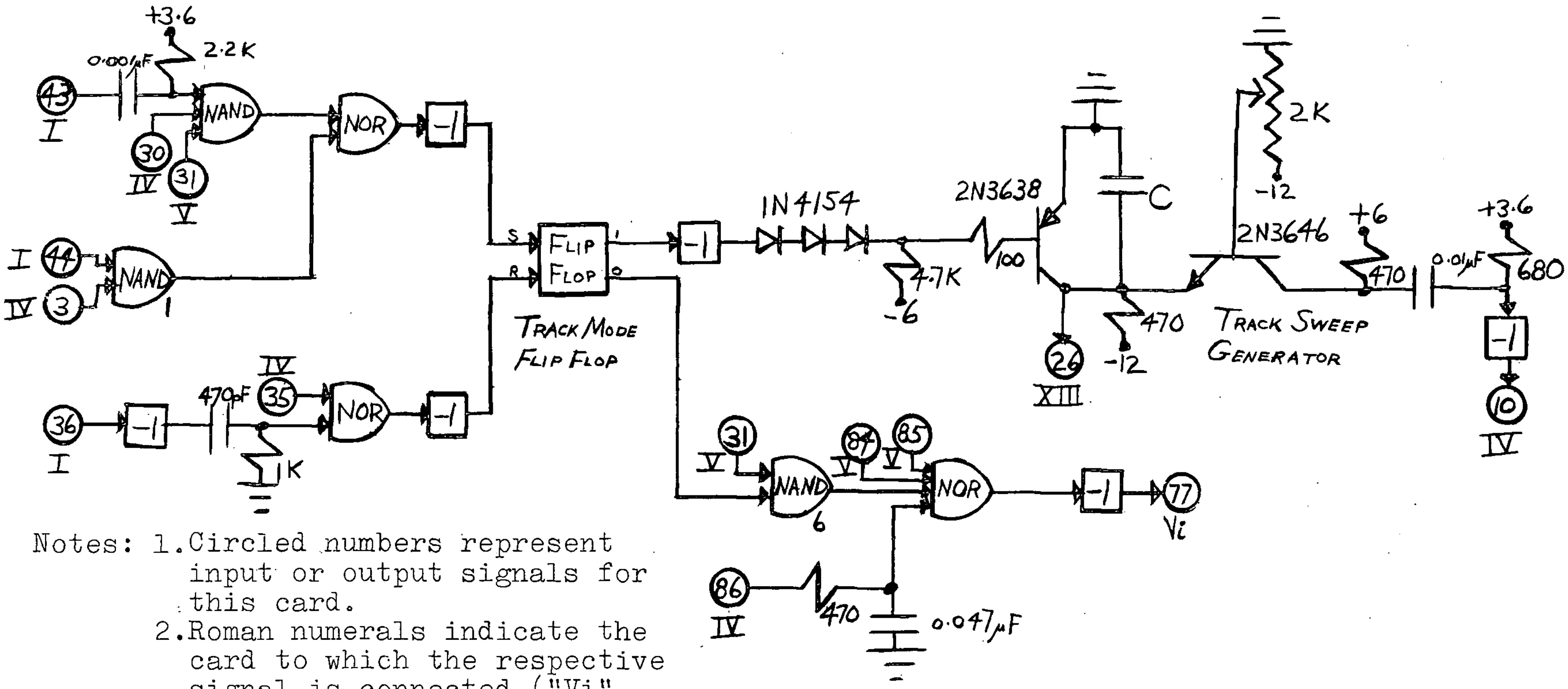

Notes: 1. Circled numbers represent input or output signals for this card.

2. Roman numerals indicate the card to which the respective signal is connected ("Vi" refers to the video section - see figure E.2).

Figure E.4 Card II

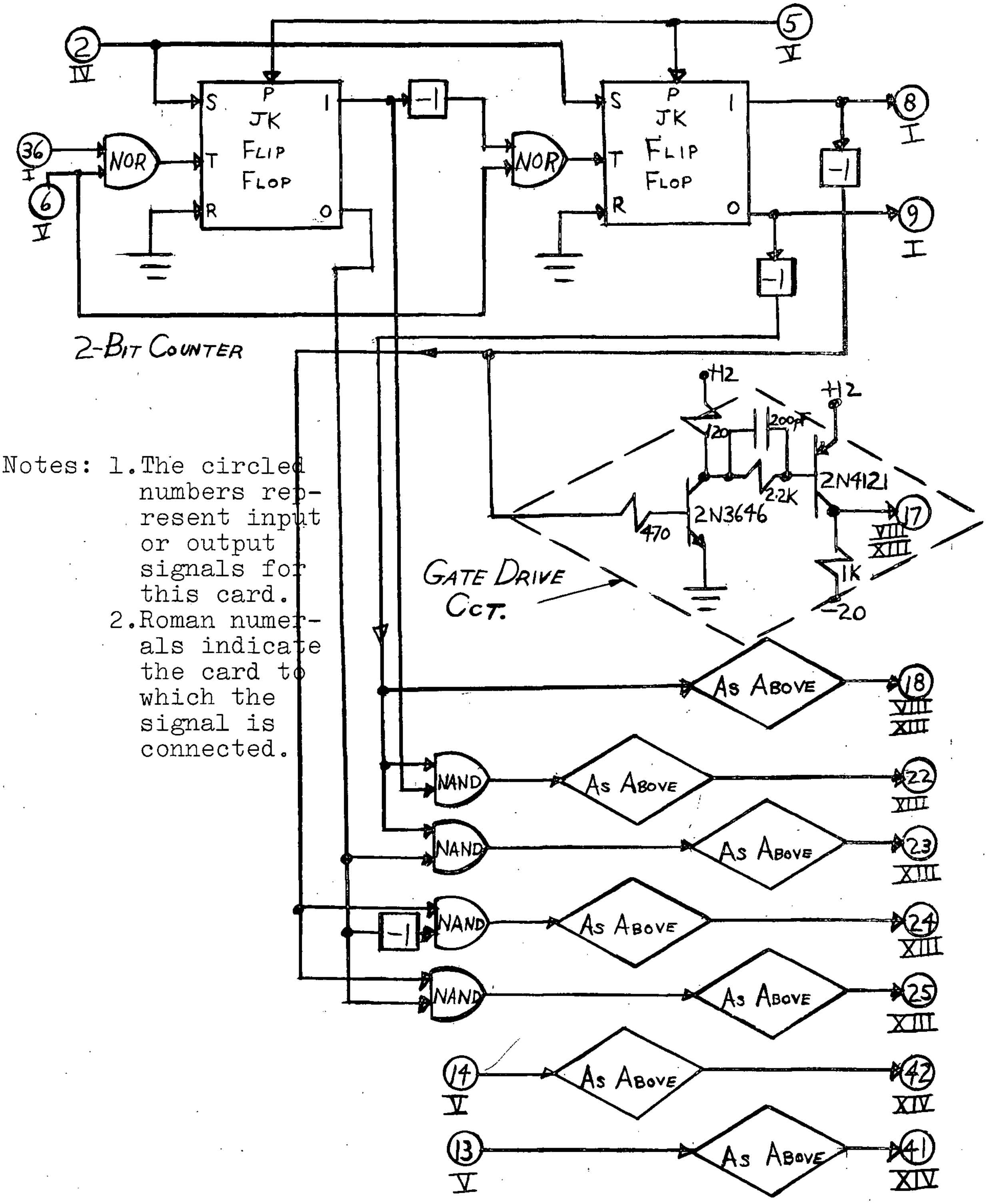

Notes: 1. The circled numbers represent input or output signals for this card.
2. Roman numerals indicate the card to which the signal is connected.

Figure E.5 Card III

the search mode B. During track mode, 2 is "low" so the counter is a normal complementing counter.

Figure E.6 shows the search mode B flip flop and the generation of the initialize signals. Signals 88 and 86 are used to preset sample and hold number 9 to zero volts. Signals 34, 35, and 37 are used to initialize the three flip flops.

Figure E.7 shows the search mode A flip flop and the search sweep generators. The derivation of the video blanking signals 85 and 84 also appears on this figure. The two monostables on the 1 output of the flip flop produce the delay, video blanking, and single sweep of search mode B. To ensure that a pulse appears on 5 when the flip flop is set (by 37), signal 34 first resets the flip flop. Signal 58 is the pupil diameter signal. When this signal increases by a sufficient amount, the 2.1 μsec. monostable is triggered. After this delay (which allows for completion of the final load pulse in search mode A), the search mode A flip flop is reset.

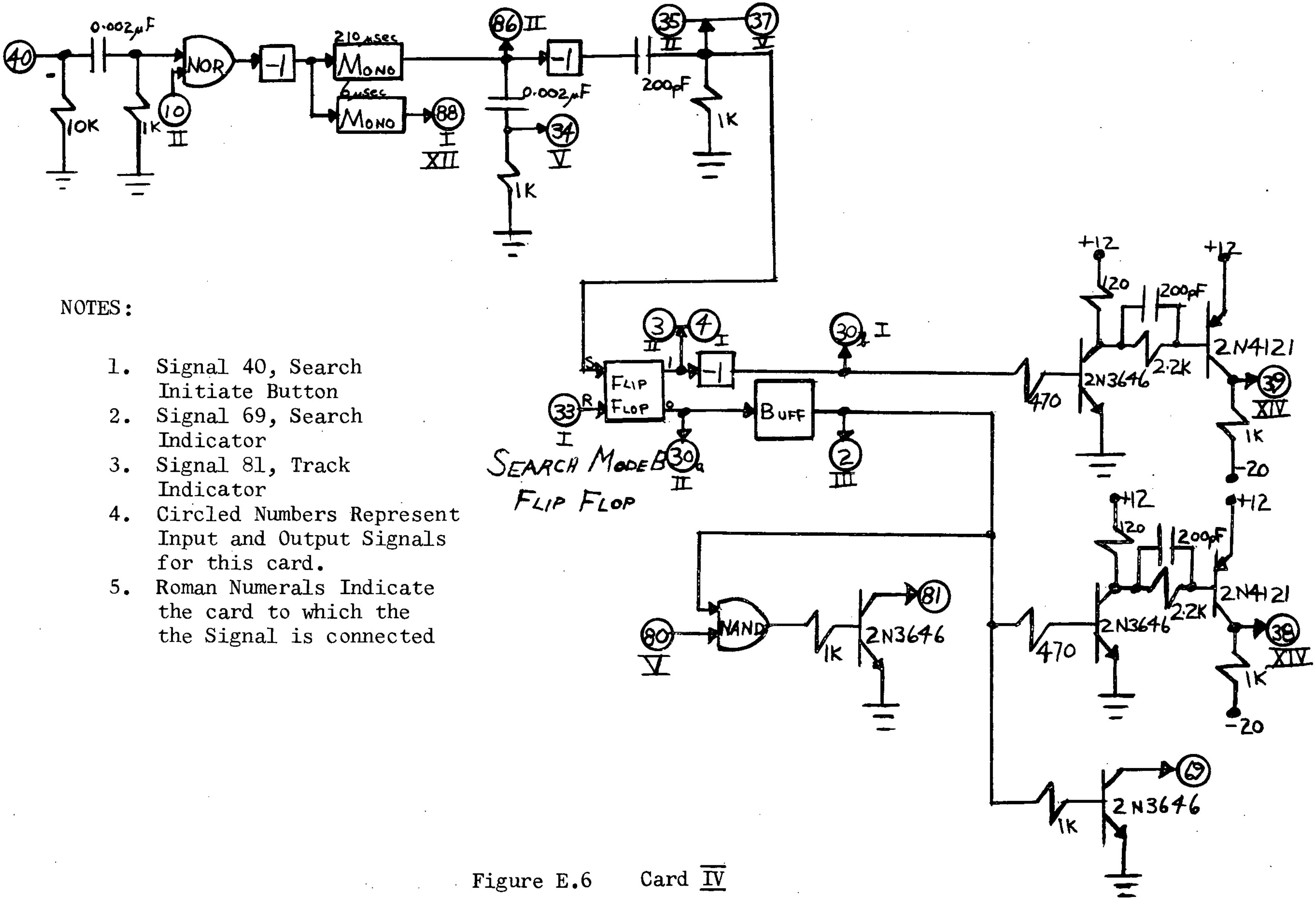

NOTES:

1. Signal 40, Search Initiate Button
2. Signal 69, Search Indicator
3. Signal 81, Track Indicator
4. Circled Numbers Represent Input and Output Signals for this card.
5. Roman Numerals Indicate the card to which the the Signal is connected

Figure E.6 Card IV

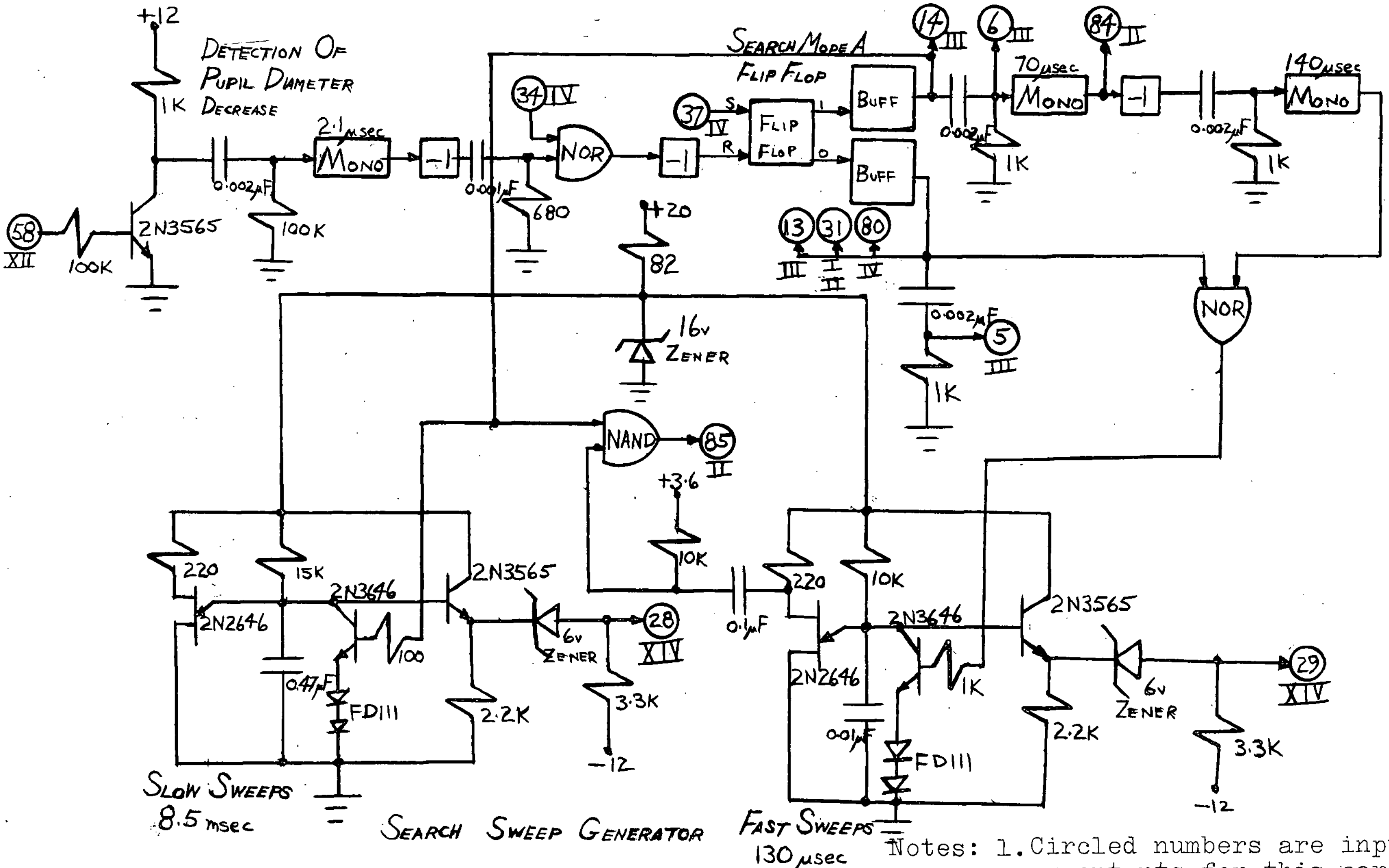

Notes: 1. Circled numbers are inputs or outputs for this card.
2. Roman numerals indicate the card to which the signal is connected.

Figure E.7 Card V

Appendix F

Variation in sample rate due to pupil velocity

It is assumed in section 3.8 that the output sample rate is constant when the system is tracking a pupil moving at constant velocity. To determine the error this introduces, consider figure F.1. This shows the output of the track sweep generator (sweep speed v_s volts/sec.) when the system is in track mode. The x_1, x_2, etc. indicate which boundary the sweep is approaching and the periods CA and D are identical to those indicated on figure 3.6.

It is assumed that previous to t = 0, the pupil was at rest and, that at t = 0, it begins moving at a constant velocity

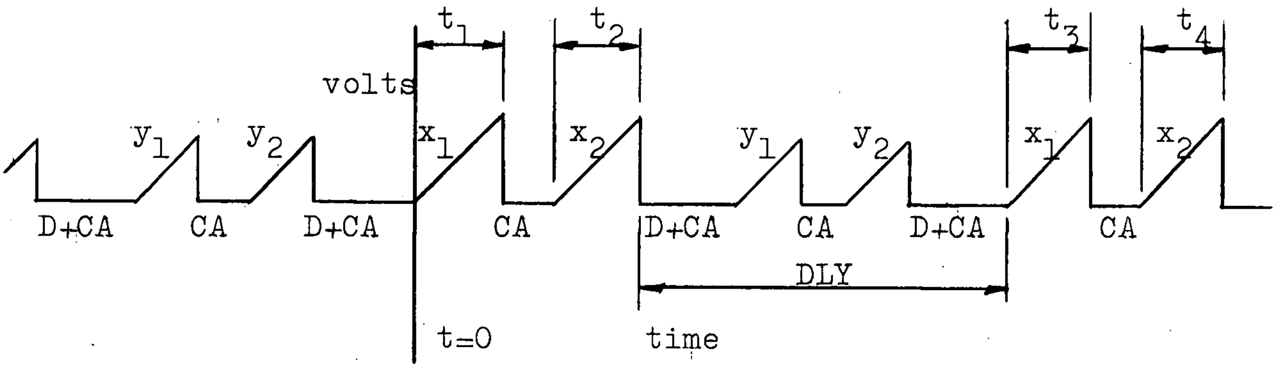

Figure F.1
Track sweep generator output (inverted)

v volts per second in the x direction. Thus the length of the x_1 and x_2 sweeps will depend upon the speed and direction of this movement after t = 0. The first x_1 boundary is encountered after t_1 sec. thus, equating distances:

$$v_s t_1 = v t_1 + \varepsilon \; .$$

Similarly the second boundary is encountered after $t_1 + CA + t_2$ sec. Thus

$$v_s t_2 = v(t_1 + CA + t_2) + \varepsilon.$$

The y_1 and y_2 sweeps are unaffected by the movement in the x direction so the next point of interest occurs at the second x_1 boundary. In this case

$$v_s t_3 = v(CA + t_2 + DLY + t_3) + \varepsilon,$$

and

$$t_3 = \frac{v(t_2 + CA + DLY) + \varepsilon}{v_s - v}.$$

Then at the second x_2 boundary

$$v_s t_4 = v(DLY + t_3 + CA + t_4) + \varepsilon$$

and

$$t_4 = \frac{v(t_3 + CA + DLY) + \varepsilon}{v_s - v}.$$

In general for each cycle of the four-sweep scan after the first:

$$v_s t_n = v(CA + t_{n-1} + DLY + t_n) + \varepsilon \qquad \text{....F.1}$$

thus

$$t_n = \frac{v(t_{n-1} + CA + DLY) + \varepsilon}{v_s - v}, \qquad \text{....F.2}$$

and

$$v_s t_{n-1} = v(CA + t_{n-2} + DLY + t_{n-1}) + \varepsilon$$

thus

$$t_{n-1} = \frac{v(t_{n-2} + CA + DLY) + \varepsilon}{v_s - v}.$$

In order that the sample rate be a constant for constant pupil velocity, $t_n = t_{n-1}$. In equation F.2, the term $(t_{n-1}+CA+DLY)$

is the sample period of the system less the time of one sweep. The sample period is in the range 125 to 250 μsec. In operation ε is of the order of 1 volt. Using the maximum value of 33.6 v./sec. for v, equation F.2 becomes

$$t_n \approx \frac{33.6(200\mathrm{x}10^{-6}) + 1}{v_s - v}$$

$$\approx \frac{1}{v_s - v} .$$

Thus $t_n \approx t_{n-1}$. This introduces a maximum error of about 0.6% and the simple development of section 3.8 is justified.

The resolution of the system does not permit operation with ε of the order of millivolts but if this were possible, this development shows that the system sample rate would then be time varying.

Appendix G

Photomultiplier signal-to-noise ratio

For a cathode signal current of I_k, the anode current in an n-stage photomultiplier is $\omega^n I_k$ (where ω is the gain per stage of the multiplier - for an over-all gain of 10^6 in 10 stages as in the F 4011, $\omega = 4$). For an effective load resistor R, the signal voltage is $\omega^n I_k R$. Reference 24 states that for such an n-stage multiplier,

$$\frac{\text{noise power out}}{\text{noise power in}} = \frac{\omega^n(\omega^{n+1} - 1)}{\omega - 1} .$$

Thus for a cathode noise current of i_{nk}, the rms anode noise voltage is

$$\sqrt{\frac{i_{nk}^2 \omega^n(\omega^{n+1} - 1)}{\omega - 1}} \; R ,$$

or

$$\sqrt{\frac{2eI_k\Delta f \; \omega^n(\omega^{n+1} - 1)}{\omega - 1}} \; R .$$

For a resistor at temperature T, the rms thermal-agitation noise voltage is

$$\sqrt{\overline{e^2}} = \sqrt{4kTR\Delta f}$$

where k is Boltzman's constant. Then the video signal-to-noise ratio is

$$\frac{S}{N} = \frac{\omega^n I_k R}{\sqrt{2eI_k\Delta f \; \frac{\omega^n(\omega^{n+1} - 1)}{\omega-1}} \; R + \sqrt{4kTR\Delta f}} .$$

Because of the amplification of the noise (first term in the denominator), the term $\sqrt{4kTR\Delta f}$ is negligible. Then the expression becomes

$$\frac{S}{N} = \sqrt{\frac{\omega^{2n}(\omega - 1)I_k}{2e\Delta f\omega^n(\omega^{n+1} - 1)}}.$$

Dividing by ω^{n+1} and noting that for $\omega = 4$, then $1 - \frac{1}{\omega^{n+1}} \approx 1$ yields

$$\frac{S}{N} = \sqrt{\frac{(\omega - I)I_k}{2e\Delta f\omega}}.$$

Appendix H

The illumination of an image in an optical system

The situation is that shown in figure H.1. The object "ds" has luminance B perpendicular to the axis of the system. EP is the entrance pupil and EP' the exit pupil of the optical system. The image formed by the system is "ds'". For object

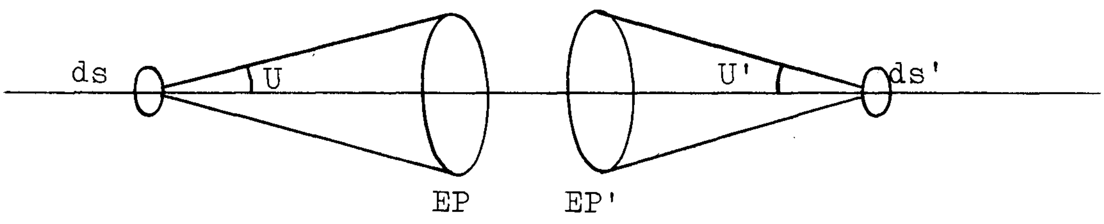

Figure H.1
A general optical system

and image in media of the same refractive index, it can be shown[28] that the flux leaving the optics (of transmission factor t) is

$$F' = \pi B\ t\ ds'\ \sin^2 U'$$

and thus the illumination of the image is

$$E = \pi B\ t\ \sin^2 U'.$$

An expression for $\sin^2 U'$ is now derived. For a system of magnification m, the image distance v and the object distance u are related by $v = mu$. For a lens of focal length F, this becomes

$$v = (1 + m)F.$$

This is the distance of the image from the second principal point. The situation is shown in figure H.2. The extreme marginal ray that

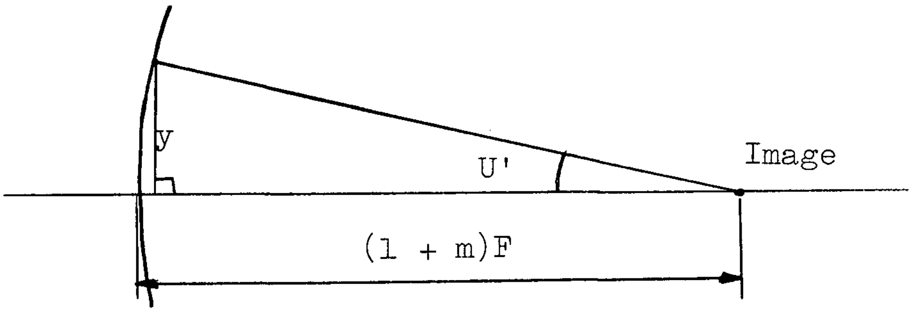

Figure H.2

Derivation of an expression for U'

can pass through the lens is at height y above the axis. From the figure, $\sin U' = \dfrac{y}{(1 + m)F}$ so the illumination of ds' can be expressed as

$$E = \frac{\pi B\ t\ y^2}{(1 + m)F} .$$

But the usual definition of f number for a lens focused on infinity is $f = \frac{F}{D} = \frac{F}{2y}$. For a lens at finite magnification m, the effective f number is $f' = f(1 + m)$. Finally then the illumination is

$$E = \frac{\pi\ B\ t}{4\ f'^2} = \frac{\pi\ B\ t}{4\ f^2(1 + m)^2} .$$

Appendix I

Photomultiplier gain measurement

The gain of a photomultiplier is the ratio of the anode current to the cathode current. However, because of the large gain of the photomultiplier, it is not possible to measure both these under the same conditions. In fact the anode current represents the most efficient measure of the cathode current. Since the currents involved are proportional to the incident radiant energy, the following procedure is customary. First, all the dynodes are connected together so the tube operates as a diode. The diode current I_d is measured under relatively strong illumination. Then, the illumination is reduced by a known amount a_1 and the tube is connected as a multiplier. The anode current I_a produced by the reduced illumination is measured. The gain then is

$$G = \frac{I_a}{a_1 I_d}.$$

Care must be taken to ensure that the diode current is above the knee of the I_k vs. V_{kS1} characteristics and thus is in the linear range, but does not approach the maximum. In this case, the maximum current density is about 100 nA/cm^2 which for the tube used (150 CVP) corresponds to a cathode current of about 0.8 μA. Except for currents approaching this maximum, the response is linear for an applied voltage of 100 volts. Normally, currents of the order of 0.1 μA. are practical.

The tube was set up in the experimental configuration of figure 5.3 except that the eye was replaced by a diffuse reflecting surface. A 300 watt projector illuminated this surface and the infra-red filter was a Wratten 70 (see figure 5.6) so the infra-red portion of the cathode response was being used. Equation 5.2 shows that the illuminance of the cathode is proportional to the area of the aperture in the mask. Since the mask is evenly illuminated by the diffuse surface, the reduction in light a_1 is equal to the change in area of the mask.

In the multiplier connection, the aperture area was 5×10^{-4} cm^2. In the diode connection, two series of readings were taken, one with an aperture area of 7.06×10^{-2} cm^2 and the other with an area of 1.13 cm^2. Thus, in the first case,

$$a_1 = 7.1 \times 10^{-3}$$

while in the second case,

$$a_1 = 4.42 \times 10^{-4}.$$

The dark current in the diode connection was between 1.1×10^{-10} and 1.5×10^{-10} A., while in the multiplier connection it varied from 1.6 to 8 μA. according to the over-all voltage (V_b) applied. In all cases, the current used for the calculation was the observed current less the dark current. The circuit connections are shown in figure I.1. The current meter was an electrometer.

The over-all voltages applied in the multiplier connection were 1200, 1300, 1400, and 1450 volts. Since the light source was run from a variable-voltage transformer, several readings were taken for each of these values of V_b. Each of the results shown in table I.1 is the average of five or more readings.

Table I.1

V_b	1200v.	1300v.	1400v.	1450v.
Gain G_E for $A_E=$				
7.06×10^{-2} cm^2.	0.5×10^6	1.1×10^6	2.0×10^6	2.6×10^6
1.13 cm^2.	0.5×10^6	1.0×10^6	1.7×10^6	2.3×10^6

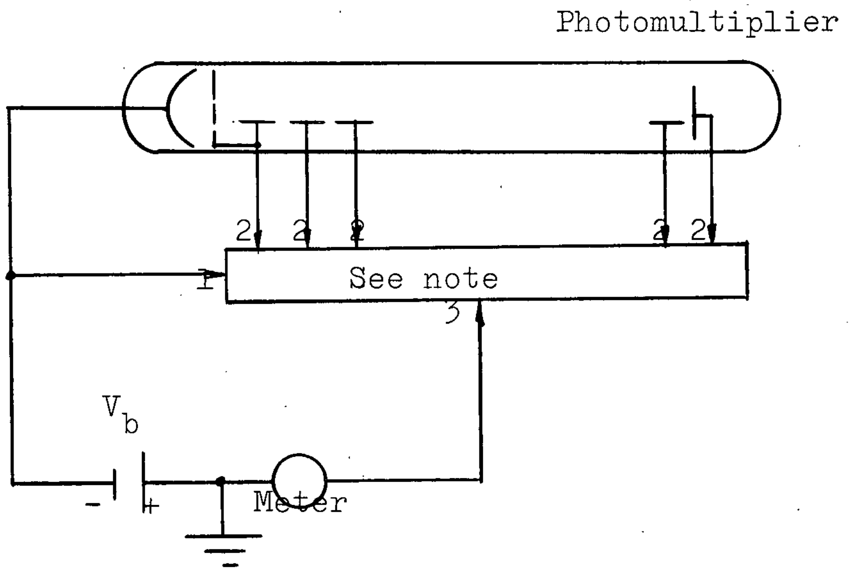

Note: For multiplier connection, terminals marked 1, 2, and 3 are interconnected as a voltage divider.
For diode connection, short terminals marked 2 to 3, and leave 1 open.

Figure I.1
Photomultiplier gain measurement

Appendix J

Suggested improvements

When the system was designed, inexpensive operational amplifiers were selected for use during the development stage. However, their slow slew-rate (1.1 v./μsec.) necessitated the insertion of fairly long delays in the four-sweep scan cycle. The scan system was designed to provide fast information output at the slowest possible sweep speed (and hence at the maximum signal-to-noise ratio). However, the delays introduced somewhat offset the efficiency of the scan scheme.

To avoid this problem in the final system, operational amplifiers with high slewing rates should be substituted. At present, amplifiers with slew rates from 100v./μsec. to 250 v./μsec. are available. If any one of these is used, the delays become negligible compared to the sample and hold load pulse. If this too is reduced, equation 3.1 becomes

$$T \approx \frac{2\varepsilon}{v_s}(k_1 + k_2). \qquad \text{... J.1}$$

At T = 250 μsec. and ε = 1.0 v., equation J.1 yields v_s = 0.016 v./μsec. instead of the previous value of 0.029 v./μsec. (from table 4.6). This increases the signal-to-noise ratio (due to the change in Δf - see equations 4.10 and 4.12) by a factor of 1.22.

Furthermore, it is possible to double the sample rate at a given sweep speed if the better operational amplifiers are used. This is achieved by computing the output after every edge encounter instead of after every pair. Previously, the system used the values of x_1 and x_2 from each cycle to compute X. The suggestion here is to use each x-edge with the x-edge immediately preceeding it to compute X. Thus, x_1 is used in conjunction with the previous x_2 to compute X. Then the next x_2 is used in conjunction with this x_1 to compute another X. A similar procedure is followed for the Y output. Since the system currently performs the sweeps in the order x_1, x_2, y_1, y_2, x_1, x_2, etc., this scheme will produce two X outputs followed by two Y outputs. If this is undesirable, the sweeps can be changed to the order x_1, y_1, x_2, y_2, x_1, y_1, etc., thus producing alternate X and Y outputs.

With the faster amplifiers, the delays necessary for the additional computations introduced by this scheme are negligible when compared to the period of the four-sweep scan. Thus when $T = 250$ μsec., the system computes two samples of X and two of Y for each cycle i.e. the sample rate is 8 KHz. Since this can be achieved at the same sweep speed of 0.016 v./μsec., the signal-to-noise ratio in this case retains the improvement of 1.22 over that shown in figure 4.16 for 4 KHz.

A further increase in signal-to-noise ratio will be achieved when this modified system is set to yield samples at 4 KHz. (i.e. $T = 500$ μsec.). Then the sweep speed will be 0.008 v./μsec. and the signal-to-noise ratio is increased by 1.62 over that shown in figure 4.16 for 4 KHz.

REFERENCES

1. L.R. Young, "Measuring eye movements," Medical research engineering, vol. 2, no. 4 (October-December, 1963), p. 300.

2. L.A. Riggs, J.C. Armington, & F. Ratliff, "Motions of the retinal image during fixation," Journal of the optical society of America, vol. 44, no. 4 (April, 1954), p. 315.

3. T.N. Cornsweet, "Determination of the stimuli for involuntary drifts and saccadic movements," Journal of the optical society of America, vol. 46, no. 11 (November, 1956), p. 987.

4. F. Ratliff & L.A. Riggs, "Motions of the eye during fixation," Journal of experimental psychology, vol. 40, (1950), p. 697.

5. M.P. Lord & W.D. Wright, "Eye movements during monocular fixation," Nature (London), vol. 162, no. 4105 (3 July, 1948), p. 25.

6. R. Dodge, "An experimental study of visual fixation," Psychological monographs of the Psychological review, vol. VIII, no. 4, whole no. 35 (November, 1907), p. 1.

7. J.F. Mackworth & N.H. Mackworth, "Eye fixations recorded on changing visual scenes by the television eye-marker," Journal of the optical society of America, vol. 48, no. 7 (July, 1958), p. 439.

8. E.L. Thomas, N.H. Mackworth, & M.R. Mowat, "The television eye marker as a recording and control mechanism," IRE transactions on medical electronics, vol. ME-7, no. 3 (July, 1960), p. 196.

9. R.W. Ditchburn & B.L. Ginsborg, "Involuntary eye movements during fixation," Journal of physiology, vol. 119, no. 1 (January, 1953), p. 1.

10. T.N. Cornsweet, "New technique for the measurement of small eye movements," Journal of the optical society of America, vol. 48, no. 11 (November, 1958), p. 808.

11. C. Rashbass, "New method for recording eye movements," Journal of the optical society of America, vol. 50, no. 7 (July, 1960), p. 642.

12. C. Rashbass & G. Westheimer, "Disjunctive eye movements," Journal of physiology, vol. 159, no. 2 (December, 1961), p. 339.

13. W.M. Smith & P.J. Warter Jr., "Eye movement and stimulus movement; new photoelectric electromechanical system for recording and measuring tracking motions of the eye," Journal of the optical society of America, vol. 50, no. 3 (March, 1960), p. 245.

14. Hs.R. Richter & C.R. Pfaltz, "A propos de l'electro-oculographie (rapport preliminaire sur une nouvelle method)," Confina neurologica, vol. 16 (1956), p. 279.

15. L. Stark & A. Sandberg, "A simple instrument for measuring eye movements," in Quarterly progress report number 62, Research laboratory of electronics, MIT, (1961), p. 268.

16. D. O'Meara, "Photo-electric eye movement detector," Engineering in biology, proceedings of the 19 th annual conference, (1966), p. 34.3.

17. J. Merchant, Interim technical report — oculometer (Boston: Honeywell radiation centre, 31 January 1966).

18. J. Merchant, Oculometry - a technique for visual control (Boston: Honeywell radiation centre, September 1965).

19. G.W. King, "An improved electronic pupillograph for clinical use," Electronics, vol. 32, no. 39 (25 September, 1959), p. 67.

20. L. Stark, "Stability, oscillations, and noise in the human pupil servomechanism," Proceedings of the IRE, vol. 47, no. 11 (November, 1959), p. 1925.

21. N.H. Mackworth & E.L. Thomas, "Head-mounted eye-marker camera," Journal of the optical society of America, vol. 52, no. 6 (June, 1962), p. 713.

22. Kodak lenses (5 th ed.; "Kodak data book"; Rochester, N.Y.: Eastman Kodak Co., 1955).

23. Dumont multiplier phototubes (3 rd ed.; Clifton, N.J.: Fairchild Camera and Instrument Corp., March, 1963).

24. K.R. Spangenberg, Vacuum tubes (New York: McGraw Hill Book Co. Inc., 1948).

25. E.H. Eberhardt, "Signal-to-noise ratio in image dissectors," _ITTIL research memo,_ number 386 (Revised 7/9/64).

26. S.O. Rice, "Mathematical analysis of random noise, part II," _Bell system technical journal_, vol. 24, no. 1 (January, 1945), p. 74.

27. _The detection of light and infra-red radiation_, ed. R. Kingslake (5 vols.; "Applied optics and optical engineering"; New York: Academic Press, 1965), vol. II.

28. R.S. Longhurst, _Geometrical and physical optics_ (London: Longmans, Green and Co. Ltd., 1964).

29. _IES lighting handbook_ (3 rd ed.; New York: Illumination Engineering Society, 1959).

30. E.B. Rosa & A.H. Taylor, "Thoery, construction, and use of the photometric integrating sphere," Scientific paper number 447, _Bulletin of the U.S. bureau of standards_ (28 August, 1957).

31. _Bioastronautics data book_, ed. P. Webb (Washington D.C.: Scientific and technical information division, National Aeronautics and Space Administration, 1964).

32. P.E. Harris & B.E. Simmons, "DC accuracy in a fast boxcar circuit via a comparator," _IEEE transactions on electronic computers_, vol. EC-13, no. 3 (June, 1964), p. 285.